METAMORPHIC STRETCHABLE ELECTRONICS

SHANTONU BISWAS

Shantonu Biswas was born on 10 June, 1986 at Chitalmari, Bagerhat, Bangladesh, where he spent his childhood. He obtained his secondary school certificate (SSC) from Chitalmari S. M. High School in 2001. He moved to Dhaka and obtained his higher secondary certificate (HSC) from BCIC College, Mirpur in 2003.

Later, he went to Sylhet to attend for his bachelor degree at Shahjalal University of Science and Technology (SUST) which is the first science and technology university in the country. There he accomplished his BSc (hons') degree in Physics in April 2010.

Mr. Biswas moved to Sweden in 2011 for higher studies. He successfully accomplished his MSc degree in Physics (focusing Nanoscience) from the Lund University in May 2013. Then, he moved to Germany for his doctoral degree. He joined to the Nanotechnology group at the Technische Universität Ilmenau in May 2013 and started his research. He initiated the stretchable electronics project and established the stretchable electronics laboratory at TU Ilmenau from scratch. He achieved his doctoral degree in May 28, 2018.

Mr. Biswas is the youngest child of his parents (Nirendra Nath Biswas and Shyamoli Biswas) and has another four siblings (three sisters and one brother).

urn:nbn:de:gbv:ilm1-2018000172

©ShantonuBiswas

METAMORPHIC STRETCHABLE ELECTRONICS SHANTONU BISWAS

TECHNISCHE UNIVERSITÄT
ILMENAU

METAMORPHIC STRETCHABLE ELECTRONICS

SHANTONU BISWAS

PhD Dissertation

urn:nbn:de:gbv:ilm1-2018000172

Metamorphic Stretchable Electronics

Shantonu Biswas

Nanotechnology, Technical University of Ilmenau, Germany

May 28, 2018

Doctoral Thesis

©Shantonu Biswas

urn:nbn:de:gbv:ilm1-2018000172

Metamorphic Stretchable Electronics

by

Shantonu Biswas

Supervisor

Heiko O. Jacobs, Professor, TU Ilmenau

Defense date: May 28, 2018

Reviewers

Prof. Heiko O. Jacobs, Department of Nanotechnology, TU Ilmenau, Germany

Prof. Andreas Dietzel, Institute of Microtechnolgy, TU Braunschweig, Germany

Dr. Sukhdeep Singh, Department of Nano-biosystem Technology, TU Ilmenau, Germany

A dissertation submitted to the
Department of Electrical Engineering and Information Technology,
Technische Universität Ilmenau, Ilmenau, Germany
in partial fulfilment of the requirements for the degree of
DOCTOR OF ENGINEER (Dr.-Ing.).
©Shantonu Biswas

urn:nbn:de:gbv:ilm1-2018000172

Promotionsordnung der Technischen Universität Ilmenau – Allgemeine Bestimmungen –

Anlage 1

Erklärung

Ich versichere, dass ich die vorliegende Arbeit ohne unzulässige Hilfe Dritter und ohne Benutzung anderer als der angegebenen Hilfsmittel angefertigt habe. Die aus anderen Quellen direkt oder indirekt übernommenen Daten und Konzepte sind unter Angabe der Quelle gekennzeichnet.

Weitere Personen waren an der inhaltlich-materiellen Erstellung der vorliegenden Arbeit nicht beteiligt. Insbesondere habe ich hierfür nicht die entgeltliche Hilfe von Vermittlungsbzw. Beratungsdiensten (Promotionsberater oder anderer Personen) in Anspruch genommen. Niemand hat von mir unmittelbar oder mittelbar geldwerte Leistungen für Arbeiten erhalten, die im Zusammenhang mit dem Inhalt der vorgelegten Dissertation stehen.

Die Arbeit wurde bisher weder im In- noch im Ausland in gleicher oder ähnlicher Form einer Prüfungsbehörde vorgelegt.

Ich bin darauf hingewiesen worden, dass die Unrichtigkeit der vorstehenden Erklärung als Täuschungsversuch bewertet wird und gemäß § 7 Abs. 10 der Promotionsordnung den Abbruch des Promotionsverfahrens zur Folge hat.

(Shantonu Biswas)

Ilmenau, ____________

Declaration

I, Shantonu Biswas, hereby confirm that this dissertation entitled

"**Metamorphic Stretchable Electronics**"

represents my own research and results for the degree of Doctor of Engineer (Dr.-Ing.) under supervision of Prof. Heiko O. Jacobs at Technische Universität Ilmenau, Ilmenau, Germany.

All the results, images and data presented here are obtained or illustrated during this thesis by or under supervision of the author. I have acknowledged all the sources of help.

This dissertation has not been submitted, in part or in whole, for the award of any other degree or examination in any other university or other tertiary institution. Most of the results have been or will be published in scientific journals or elsewhere. Large portions of the texts have been taken from previously published articles by the author.

I am aware that the falsity of this declaration will be regarded as an attempt of deception and will cause the derogation of the doctoral procedure.

(Shantonu Biswas)

Ilmenau, ________________

To

My family!

Preface

This dissertation represents a culmination of research work and learning that has taken place over the past few years (2013-2017). The experimental works of this dissertation have been initiated at the FG Nanotechnologie, Technische Universität Ilmenau, Ilmenau, Germany in May 2013. The research on this dissertation has been carried out under the supervision of Professor Heiko O. Jacobs.

The dissertation is organized as short summaries both in English and Deutsch and followed by the main body. The main body consists of two parts; the first part contains an introduction and reviews on current state-of-the-art of the related field, and the second part gives insight into the experiments performed with achieved results and ends with conclusions. The experiments and results portions are arranged in different chapters where each chapter presents an individual device type. Note that the processing method and design vary slightly from each device to the other. Thus, the method and design have been briefly discussed individually with each demonstrator.

This dissertation has been submitted for assessment in partial fulfilment of the PhD degree at Technische Universität Ilmenau, Ilmenau, Germany. The content of this dissertation as its current state has not been submitted or not intent to be submitted anywhere else for publication purposes. However, part of the content and results of the thesis have been, or will be published in scientific journals. All the results, images, and graphics are obtained or produced during the thesis by or under the supervision of the author.

Shantonu Biswas

Ilmenau, Germany

shantonu.biswas@tu-ilmenau.de

Acknowledgement

The submission of this dissertation brings to an end of a wonderful journey filled with many joyous moments, as well as hurdles. I was very fortunate to work with a bunch of extraordinary people from the Institut für Mikro- und Nanotechnologien (IMN) MacroNano and at the FG Nanotechnologie, Technische Universität Ilmenau, Ilmenau, Germany. The dissertation would not have been possible without the help of so many people in so many ways. I sincerely thank all of you who helped directly or indirectly in this study.

I am deeply indebted to my supervisor Professor Heiko O. Jacobs for his guidance and the opportunity. As many are aware, initially the project was not well defined and the laboratories were also not equipped. Despite all this reasons, his persistent faith on me encouraged the initiation of this project and to establish the stretchable lab in TU Ilmenau from scratch. His mentorship is paramount in providing a well-rounded experience consistent with my long term career goals.

My deepest acknowledgment is for my co-supervisor Dr. Thomas Stauden, without his help my years in TU Ilmenau would have been difficult and certainly this thesis would have been unmanageable. I am also deeply thankful to Dr. Jörg Pezoldt for his inspirations, thoughtful discussions, assistance with manuscripts, and guidance. There are many more things about science and life that I could learn from him.

I would also like to take this opportunity to thank all my colleagues from ZMN, whom I never managed to thank properly due to the lack of my language skill for their life saving help. Dankeschön! In particular, Birgitt Hartmann for her great help in wet-chemistry, Jutta Uziel, David Venier, Ilona Marquardt, Joachim Döll, Manuela Breiter, Uwe Genatis, Dietmar Schäfer and everyone else who directly or indirectly helped me in the past four years.

A bunch of special thanks goes to my colleagues and friends for assisting me in the lab or in the office, for the comfort they provided and well-behaviour throughout the whole period. A special thanks to Johannes for his support during the past years. I also appreciate the significant contributions of my graduate and undergraduate students: Felix Krug, Andreas Schöberl and David T. Arboleda.

Finally, my deepest gratitude goes to my parents, sisters, and brother for their unflagging love, inspiration and strong support

throughout my life. Their inspirations always guide me even when I am far away from them. At last but not least, many thanks to my wife for her tremendous support throughout my PhD. Without her love, life in Ilmenau or anywhere else in the world would be meaningless.

Shantonu Biswas

_______________, Ilmenau, Germany

List of publications

Journal articles

Directly related to the thesis:

1. **S. Biswas**, J. Reiprich, T. Cohrs, D. T. Arboleda, A. Schöberl, M. Mozafari, L. Schlag, T. Stauden, J. Pezoldt, H. O. Jacobs, *3D Metamorphic Stretchable Microphone Arrays*, Advanced Materials Technologies, 2, 10, (2017).

2. **S. Biswas**, J. Reiprich, T. Cohrs, T. Stauden, J. Pezoldt, H. O. Jacobs, *Metamorphic Hemispherical Microphone Array for Three-Dimensional Acoustics*, Applied Physics Letters, 111, 4, (2017).

3. **S. Biswas**, A. Schöberl, M. Mozafari, J. Pezoldt, T. Stauden, H. O. Jacobs, *Deformable Printed Circuit Boards that Enable Metamorphic Electronics*, NPG Asia Materials, 8, e336, (2016).

4. **S. Biswas**, M. Mozafari, T. Stauden, H. O. Jacobs, *Surface Tension Directed Fluidic Self-Assembly of Semiconductor Chips across Length Scales and Material Boundaries,* Micromachines, 7, 4, (2016).

5. S. C. Park, **S. Biswas**, J. Fang, M. Mozafari, T. Stauden, H. O. Jacobs, *Millimeter Thin and Rubber-Like Solid-State Lighting Modules Fabricated Using Roll-to-Roll Fluidic Self-Assembly and Lamination,* Advanced Materials, 27, 3661, (2015).

6. **S. Biswas**, M. Mozafari, J. Reiprich, L. Schlag, Nishchay A. Isaac**,** T. Stauden, J. Pezoldt, H. O. Jacobs, *Metamorphic and Stretchable Electronic Systems – A Materials, Assembly, and Interconnection Challenge*, Microsystem Technology in Germany, (2018).

Manuscript under preparation

7. **S. Biswas**, T. Stauden, J. Pezoldt, H. O. Jacobs, *Stress-Adaptive Meander Metal for Stretchable Electronics*, Submitted, (2018).

8. **S. Biswas**, A. Schöberl, J. Reiprich, T. Stauden, J. Pezoldt, H. O. Jacobs, *Heterogeneous Integration of Multilayer Metamorphic Optoelectronic System*, manuscript in preparation, (2018).

9. **S. Biswas**, T. Stauden, J. Pezoldt, H. O. Jacobs, *Materials, Methods, and Devices for Stretchable Electronics*, manuscript in preparation, (2018).

10. **S. Biswas**, T. Stauden, J. Pezoldt, H. O. Jacobs, *Metamorphic Touchpad*, manuscript in preparation, (2018).

11. **S. Biswas**, T. Stauden, J. Pezoldt, H. O. Jacobs, *Mounting Methods of Conformal Wearable Electronics*, manuscript in preparation, (2018).

Talks

1. **S. Biswas**, *Metamorphic Electronics*, MRS Spring meeting 2017, Phoenix, USA.
2. **S. Biswas**, *Metamorphic Stretchable Electronics*, E-MRS Fall meeting 2016, Warsaw, Poland.

Indirectly related to the thesis:

1. S. C. Park, J. Fang, **S. Biswas**, M. Mozafari, T. Stauden, H. O. Jacobs, *A First Implementation of an Automated Reel-to-Reel Fluidic Self-Assembly Machine*, Advanced Materials, 26, 34, (2014) 5942-5949.

2. S. C. Park, J. Fang, **S. Biswas**, M. Mozafari, T. Stauden, H. O. Jacobs, *Automated Reel-to-Reel Fluidic Self-Assembly for the Production of Solid State Lighting Modules*, MRS Proceedings, 1761, (2015).

3. S. C. Park, J. Fang, **S. Biswas**, M. Mozafari, T. Stauden, H. O. Jacobs, *Approaching Roll-to-Roll Fluidic Self-Assembly: Relevant Parameters, Machine Design, and Applications*, JMEMS, 24, 6, (2015).

4. S. C. Park, J. Fang, **S. Biswas**, M. Mozafari, T. Stauden, H. O. Jacobs, *Automated Reel-to-Reel Fluidic Self-Assembly Enabling the Production of Solid State Lighting Panels*, GMM-Fachbericht-Mikro-Nano-Integration, (2014).

News

1. Metamorphic Electronics: Stretching into Complex Forms: *https://www.advancedsciencenews.com/metamorphic-electronics-stretching-complex-forms/*
2. Metamorphic Electronics For 3D Acoustics: *https://sciencetrends.com/metamorphic-electronics-3d-acoustics/*

3. Faster ways to flexible electronics: *http://www.sciencemag.org/content/348/6239/twil.full*

4. Self-assembly machines - a vision for the future of manufacturing: *http://www.nanowerk.com/spotlight/spotid=36474.php*

5. Self-assembly of 15,000 semiconductor chips per hour: *http://nextbigfuture.com/2014/07/self-assembly-of-15000-semiconductor.html*

6. Lichtpaneele fertigen sich wie von selbst: *http://www.weltderphysik.de/gebiet/technik/news/2014/selbstorganisation/*

7. Makroelektronik: Schneller produzieren ohne Roboter: *http://www.pro-physik.de/details/opnews/6351951/Makroelektronik_Schneller_produzieren_ohne_Roboter.html*

8. Der Chip der Zukunft - wie eine elektronische Haut: *http://www.mdr.de/wissen/faszination-technik/flexible-computerchips-100.html*

Content

Preface	I
Acknowledgement	III
List of Publications	V
Content	IX
List of Figures	XV
List of Tables	XIX
Summary	XXI
Zusammenfassung	XXIII

<u>Part I</u>

Chapter 1:	**Introduction**	**3-13**
1.1.	**Introduction**	4
1.2.	**Future Electronics**	5
	1.2.1. Stretchable electronics	5
1.3.	**Metamorphic Electronics**	11
Chapter 2:	**Materials, Processing and Design**	**15-38**
2.1.	**Materials**	16
	2.1.1. Materials for stretchable substrates	17
	2.1.2. Materials for stretchable conductors	20
	2.1.3. Materials for devices	23
2.2.	**Processing**	25
	2.2.1. Soft substrate first	25
	2.2.2. Soft substrate last	27

	2.2.3. Transfer printing	28
	2.2.4. Direct printing	30
2.3.	**Design**	32
	2.3.1. Macroscopic stress distribution	34
	2.3.2. Microscopic stress distribution	35
	2.3.3. Stress adaptive metal tracks	36

Part II

Chapter 3:	**Metamorphic Optoelectronics**	**41-55**
3.1.	**Manufacturing of mPCBs**	42
	3.1.1. Fabrication of stretchable metal tracks	42
	3.1.2. Assembly of the components on hard carrier	43
	3.1.3. Rubber encapsulation and detachment	43
3.2.	**Design**	45
	3.2.1. Stretchable metal tracks	45
	3.2.2. Reinforcement bars	50
3.3.	**Metamorphic Optoelectronic Devices**	51
	3.3.1. Inflation of uniform membrane	52
	3.3.2. 3D guided deformation	53
	3.3.3. Inflation of patterned membrane	54
Chapter 4:	**Metamorphic Electronics**	**57-62**
4.1.	**Manufacturing**	58
	4.1.1. Fabrication of μ-transistor chips	58

4.1.2. Fabrication of stretchable metal tracks 60

4.1.3. Assembly of the µ-transistors and detachment 61

4.2. Metamorphic Transistor Arrays 61

Chapter 5: Metamorphic Acoustoelectronics 63-78

5.1. Manufacturing 64

5.1.1. Fabrication of stretchable metal tracks 64

5.1.2. Assembly of the components on hard carrier 65

5.1.3. Rubber encapsulation and detachment 67

5.2. Design 67

5.2.1. Stretchable metal tracks 67

5.2.2. 3D reinforcement frame 69

5.2.3. Circuit and Arrays 71

5.3. Experiments and Results 72

5.3.1. Functionality test of the array on the hard carrier 73

5.3.2. Functionality test of the array on the rubber matrix 73

5.3.3. Functionality test of the array after inflation 73

5.3.4. Sound localizations : planar *vs.* hemispherical array 74

5.4. Metamorphic Acoustoelectronics 77

Chapter 6: Addressable Metamorphic LED Array 79-91

6.1. Manufacturing of Integrated mPCBs 80

6.1.1. Fabrication of stretchable metal tracks 80

6.1.2. Assembly of the devices on hard carrier 82

6.1.3. Rubber encapsulation and detachment 82

6.2. Design of the Integrated mPCB 83

	6.2.1. Metal tracks crossing	83
	6.2.2. VIA	84
6.3.	**Functionality Tests**	85
	6.3.1. Functionality test on hard carrier	86
	6.3.2. Functionality test after encapsulation and transfer	86
6.4.	**Metamorphic LED Display**	89
Chapter 7:	**Metamorphic Touchpad**	**93-101**
7.1.	**Reverse Engineering of a Touchpad**	94
7.2.	**Manufacturing of Stretchable Touchpad**	95
	7.2.1. Fabrication of stretchable touchpad	95
	7.2.2. Rubber encapsulation and detachment	96
7.3.	**Functionality Tests**	97
	7.3.1. Stretchable touchpad in planar orientation	97
	7.3.2. Hemispherical touchpad	99
Chapter 8:	**Other Devices**	**103-115**
8.1.	**Wearable Electronics**	104
	8.1.1. Body as a primary substrate	104
	8.1.2. Body as a secondary substrate	107
8.2.	**Electronics on Fabrics**	110
8.3.	**Large Area Stretchable Electronics**	111
	8.3.1. Large area fabrication	111
	8.3.2. Letter-size stretchable LED arrays	113
Chapter 9:	**Conclusion**	**117-122**
9.1.	**Stretchable to Metamorphic Electronics**	118

9.2. Outcomes of the Thesis 118

9.2.1. Technology 119

9.2.2. Design 120

9.2.3. Functional systems 120

9.2.4. Metamorphic electronics 121

9.3. Future Perspectives 121

References 123

List of Figures

Part I

Chapter 1: Introduction

Fig. 1.1 Number of scientific articles published on stretchable electronics. 6

Fig. 1.2 Metamorphic electronics. 12

Chapter 2: Materials, Processing and Design

Fig. 2.1 Chemical structure of silicones. 18

Fig. 2.2 Thin film wrinkles on EcoFlex surface. 19

Fig. 2.3 Surface activation of EcoFlex. 19

Fig. 2.4 Different methodologies to realize stretchable conductors. 20

Fig. 2.5 Meander shape and buckled metal tracks. 22

Fig. 2.6 “Soft substrate first” process flow. 26

Fig. 2.7 “Soft substrate last” process flow. 27

Fig. 2.8 Different methodologies of transfer printing. 28

Fig. 2.9 Transfer printing. 30

Fig. 2.10 Examples of transfer printing on various substrates. 31

Fig. 2.11 Different meander shape metal track design parameters. 32

Fig. 2.12 CAD simulation of the meander metal tracks. 33

Fig. 2.13 Mechanisms of low and high stress regions. 34

Fig. 2.14 Design approaches of stress adaptive metal tracks by varying widths. 37

Fig. 2.15 Comparison among three metal track designs. 38

Part II

Chapter 3: Metamorphic Optoelectronics

Fig. 3.1 Metamorphic printed circuit board process flow. 44

Fig. 3.2 Comparison of two metal track designs. 46

Fig. 3.3 Failure due to detachment. 48

Fig. 3.4 Multi-cycle stretch-release test. 49

Fig. 3.5 Study of the reinforcement bars. 51

Fig. 3.6 Inflation of uniform rubber membrane. 52

Fig. 3.7 3D guided deformation. 54

Fig. 3.8 Inflation of patterned membrane. 55

Chapter 4: Metamorphic Electronics

Fig. 4.1 Fabrication of μ-transistors. 59

Fig. 4.2 Influence of RTP annealing of the metal contacts. 60

Fig. 4.3 Fabrication of stretchable metal tracks and assembly of μ-transistors. 60

Fig. 4.4 Metamorphic transistor arrays. 62

Chapter 5: Metamorphic Acoustoelectronics

Fig. 5.1 Metamorphic printed circuit boards process flow. 66

Fig. 5.2 Influence of the PI cladding. 68

Fig. 5.3 3D Reinforcement frame study. 70

Fig. 5.4 Circuit diagram and layout of the integrated microphone array. 72

Fig. 5.5 Experimental set up for microphone array testing. 72

Fig. 5.6 Functionality test of the microphone arrays on hard carrier. 73

Fig. 5.7 Functionality test of planar microphone arrays in rubber matrix. 74

Fig. 5.8 Functionality test of microphone arrays after air inflation. 74

Fig. 5.9 Schematic illustration of the principle of the “cone of confusion”. 75

Fig. 5.10 Sound source localizations: planar vs. hemispherical arrays. 76

Fig. 5.11 Metamorphic acoustoelectronics. 77

Chapter 6: Integrated Metamorphic LED Array

Fig. 6.1 Integrated multilayer metamorphic printed circuit board process flow. 81

Fig. 6.2 Multilayer metal crossing in mPCB. 84

Fig. 6.3 VIA in mPCB. 85

Fig. 6.4 Functionality test on hard carrier. 86

Fig. 6.5 VIA study: photographs and stretching results. 87

Fig. 6.6 Peeling off the metal tracks results electrical failure. 88

Fig. 6.7 Integrated metamorphic optoelectronics in EcoFlex. 89

Fig. 6.8 Functionality test of the addressable LED arrays in rubber. 90

Fig. 6.9 Integrated multilayer metamorphic LED arrays. 91

Chapter 7: Approaching 3D Touchpad

Fig. 7.1 Reverse engineering of a commercial touchpad. 94

Fig. 7.2 Schematic principle of a capacitor. 95

Fig. 7.3 Stretchable touchpad design. 95

Fig. 7.4 Fabrication of stretchable touchpad. 97

Fig. 7.5 Functionality test of the touchpad in planar orientation. 98

Fig. 7.6 Functionality test of the touchpad in hemispherical orientation. 99

Chapter 8: Other Devices

Fig. 8.1 Wearable electronics: body as a primary substrate for passive device. 105

Fig. 8.2 Wearable electronics: body as a primary substrate for active device. 106

Fig. 8.3 Wearable electronics: body as a secondary substrate for passive device.108

Fig. 8.4 Wearable electronics: body as a secondary substrate for active device. 109

Fig. 8.5 Active electronics on fabrics. 111

Fig. 8.6 Process flow of the large area stretchable printed circuit board. 112

Fig. 8.7 Letter size LED arrays on hard carrier. 114

Fig. 8.8 Letter size LED arrays on rubber substrate. 115

Chapter 9: Conclusion

List of Tables

Part I

Chapter 1: Introduction

Chapter 2: Materials, Processing and Design

Table 2.1 Young's modulus of various materials. 16

Table 2.2 Potential materials for stretchable carrier substrate. 17

Table 2.3 Conductivity of commonly used metals. 21

Part II

Chapter 3: Metamorphic Optoelectronics

Table 3.1 Study of metal track region. 47

Table 3.2 Study of contact pad region. 50

Chapter 4: Metamorphic Electronics

Chapter 5: Metamorphic Acoustoelectronics

Table 5.1 Study of PI cladding to metal tracks. 68

Table 5.2 Localization comparison between planar and hemispherical array. 76

Chapter 6: Integrated Metamorphic LED Array

Chapter 7: Approaching 3D Touchpad

Chapter 8: Other Devices

Chapter 9: Conclusion

Summary

Recent advancement in the field of electronics has taken a shift to enable the realization of mechanically stretchable electronics which morph to take on new form factors. Mechanical stretchability is necessary to have seamless integration of electronics in our daily life objects and many other purposes where conventional rigid electronic system is insufficient.

This thesis aims to enable a stretchable printed circuit board (sPCB) technology that is compatible with industrial manufacturing. Ideally, the rigid carrier substrate of conventional electronics is intended to be replaced by stretchable rubber substrate with stretchable interconnects. Initially, a method has been developed to realize an industry compatible single layer stretchable PCB. The approach is different from other reported methods in this field, which apply the metallization to the rubber support and mount the components on top and, which suffer from a lower level of alignment and fixation. Instead, in the depicted method a hard carrier is used, which delays the use of the stretchable rubber support to the end of the processing sequence.

The single layer method has been further developed to realize a multilayer integrated sPCB, where different metallization layers are connected through vertical interconnect access (VIA). The method uses hard carrier. Like conventional PCB technology, the hard carrier fabrication is important since it enables: alignment and registration, high temperature processing, conventional robotic chip placement, and "on-hard-carrier" device tests. Moreover, the depicted method enables direct use of commercially available SMDs which is important to realize complex electronic devices.

As final substrate, highly stretchable silicone material (EcoFlex) is used which encapsulates the device layers. To transfer the device layers from hard carrier to soft substrate a single-step, wafer-level, and solvent-free detachment process has been developed which uses the differential interfacial adhesion in between the sacrificial layers.

For highly stretchable interconnects a new meander metal track design is developed which is named as "***stress adaptive***" metal track. The new meander metal track varies in widths to accommodate produced torque in the metal tracks due to the non-uniform stress distribution over the meander loops. The stress adaptive design shows a significant improvement in the stress distributions over the metal tracks in computer simulated stress profile. And, experimental results show a higher level of maximum stretching (320%) and higher number of stretch-release cycles (11000) comparing with a reference design.

A wide range of stretchable systems have been demonstrated including electronics, optoelectronics, acoustoelectronics and sensor arrays. The demonstrators

contain arrays with packaged SMDs, bare dies integrated LEDs, lab-fabricated Si μ-transistors and MEMS microphones using a single metallization layer within a rubber matrix. Furthermore, an integrated multilayer sPCB is demonstrated using chip scale LEDs and transistors to realize an addressable active matrix. These prototypes of integrated multilayer electronics demonstrate method to enable multilayer sPCB technology which could lead to realize any electronic system known today to be stretchable.

Finally, this thesis introduces a new type of electronics which morph to adapt to new topology and form factor. This shape-adaptive electronics is named as metamorphic electronics. Various types of deformation mechanisms have been demonstrated including inflation and/or deflation of uniform or patterned rubber membranes, 3D guided deformations, and vacuum forming in combination with 3D chaperons. The range of topologies includes hemispherical, spherical, concave/convex, pyramid, tower, bumble bee-eye, and more complex 3D shapes.

Zusammenfassung

Die jüngsten Fortschritte auf dem Gebiet der Elektronik wenden sich der Realisierung mechanischer dehnbarer Elektroniken zu. Diese sind in der Lage sich umzuwandeln um neue Formfaktoren anzunehmen. Um eine nahtlose Integration der Elektronik in unsere Alltagsgegenstände und viele weitere Anwendungsfelder zu ermöglichen, bei denen herkömmliche starre elektronische Systeme nicht ausreichen, ist mechanische Dehnbarkeit notwendig.

Diese Arbeit zielt darauf ab, eine dehnbare Leiterplattentechnologie (sPCB) zu demonstrieren, die mit industriellen Herstellungsprozessen kompatibel ist. Idealerweise soll das starre Trägersubstrat der konventionellen Elektronik durch ein dehnbares Gummisubstrat mit dehnbaren Leiterbahnen ersetzt werden. Zunächst wurde eine Methode entwickelt, um eine industrietaugliche, einlagige, dehnbare Leiterplatte zu realisieren. Der dargestellte Ansatz unterscheidet sich von anderen Methoden in diesem Bereich, welche die Metallisierung auf dem Gummisubstrat aufbringen und die Komponenten anschließend darauf montieren. Dadurch leiden diese unter einer geringeren Ausrichtung und Fixierung. Stattdessen wird im dargestellten Ansatz ein harter Träger verwendet, der den Einsatz des dehnbaren Gummimaterials bis ans Ende der Prozesskette verschiebt.

Diese Single-Layer-Methode wurde weiterentwickelt, um mehrschichtige, integrierte sPCB zu realisieren, bei der verschiedene Metallisierungsebenen durch vertikalen Durchkontaktierungen (VIA) miteinander verbunden werden. Auch dieses Verfahren verwendet konventionelle starre Träger für den Herstellungsprozess. Wie in der konventionellen Leiterplattentechnologie ist auch die Herstellung auf starren Trägern wichtig, da sie Folgendes ermöglicht: Ausrichtung und Registrierung, Hochtemperaturprozesse, konventionelle Chip-Bestückung durch Roboter und "On-Hard-Carrier"-Bauteiltests. Darüber hinaus ermöglicht die dargestellte Methode den direkten Einsatz handelsüblicher SMDs, was für die einfache Realisierung komplexer elektronischer Schaltungen wichtig ist.

Als Endsubstrat kommt ein hochelastisches Silikonmaterial (EcoFlex) zum Einsatz, welches die Bauelementebenen einkapselt. Um die Bauelementebenen vom harten Träger auf das weiche Substrat zu übertragen, wird ein einstufiges, waferbasiertes und lösungsmittelfreies Ablöseverfahren eingesetzt, bei dem die differentielle Grenzflächenadhäsion einer Multi-Opferschichten genutzt wird.

Für die hochelastischen Leiterbahnen wurde ein neues Mäander-Metallbahndesign entwickelt, welches als "spannungsadaptiv" bezeichnet wird. Die neue Mäander-Metallbahn variiert in ihrer Breite, um das einwirkende Drehmoment in den Metallbahnen, aufgrund der ungleichmäßigen Spannungsverteilung über die Mäander-Schleifen, aufzunehmen. Das spannungsadaptive Design zeigt eine signifikante Verbesserung der Spannungsverteilungen auf den Metallbahnen und

führt experimentell zu einem höheren Niveau der maximalen Dehnung und der Anzahl der Dehnungszyklen.

Es wurde eine breite Palette von dehnbaren Systemen demonstriert, darunter Elektronik, Optoelektronik, Akustoelektronik und Sensor-Arrays. Die Demonstratoren, auf Basis einer einzigen Metallisierungsschicht in einer Gummimatrix, enthalten Arrays mit gehäusten SMDs, LED-Nacktchips, laborgefertigte Si μ-Transistoren und MEMS-Mikrofone. Weiterhin wird eine integrierte Multilayer-sPCB mit Chip-großen LEDs und Transistoren demonstriert, um eine adressierbare aktive Matrix zu realisieren. Dieser Prototyp demonstriert die Machbarkeit von integrierten Multilayer-sPCB und wird im Prinzip dazu führen, dass jedes heute bekannte elektronische System in ein äquivalentes dehnbares System überführt werden kann.

Schließlich stellt diese Arbeit das bahnbrechende Konzept der metamorphen Elektronik vor, welche sich umwandeln kann um neue Topologien und Formfaktoren anzunehmen. Es werden verschiedene Arten von Deformationsmechanismen demonstriert, darunter das Aufblasen von gleichförmigen oder strukturierten Gummimembranen, 3D-geführte Deformationen und Vakuumformung in Kombination mit 3D-Schablonen. Die Palette der Topologien reicht dabei von halbkugelförmig, kugelförmig, konkav/konvex, pyramidenförmig, turmartig, bis hin zu komplexeren 3D-Formen, darunter Bienenaugen-Strukturen.

PART I

STATE-OF-THE-ART

The first part of this thesis provides an introduction in the field of stretchable electronics and introduces the concept of metamorphic electronics. Current state-of-the-art of stretchable electronics is provided in terms of devices, materials, processing. In the end of the first section a new “stress adaptive” meander shape design is presented for stretchable interconnections with detail design rationale.

CHAPTER 1

Introduction

1.1. Introduction

1.2. Future Electronics

1.2.1. Stretchable electronics

1.3. Metamorphic Electronics

1.1. Introduction

Scientists have invented thousands of revolutionary concepts and devices that have changed the way we live today, and this quest for innovation continues. One of the greatest inventions in the field of electronics was the transistor in 1947 by John Bardeen, William B. Shockley and Walter H. Brattain from Bell Labs for which the inventors were awarded with a Noble Prize in Physics in 1956 [1]. Consequently, four years later 'The Ferranti mark 1', the first commercially available computer was released [2]. The next revolution came when the first silicon (Si) transistors were invented by Gordon Kidd Teal from Texas Instruments in 1954 [1]. Again, after four years in 1958 the first integrated circuit (IC) was invented by Jack St. Clair Kilby [3] from Texas Instruments who was also awarded a Noble Prize in Physics in 2000. Since then the mankind has seen numerous number of new electronic devices *to save, to support,* and *to decorate* lives. These devices have also been changing very rapidly by their dimensions and functionalities. However, they all possess a very common fundamental property: they are STIFF! The next revolution in electronic devices might be its free geometry [4, 5].

Our daily life objects surrounding us have various, and sometimes even very complex types of shapes. For example, a normal PET (polyethylene terephthalate) water bottle, that we use probably for every couple of hours, alone has different and complex shapes from its top to bottom. In addition to this, the material is flexible or deformable. To add another example from nature, human body (only considering outer surface) has very complex geometries. Some organs have plane surfaces; while other regions might have very rough surfaces. Moreover, due to the living characteristics such as walking or swimming, some organs of the body need to be stretchable in addition to being flexible. For instance, skins or muscles near to the knee area have very high stretchability or deformability.

In contrast to these, electronic devices in our households are mostly brittle and rigid, rarely flexible and have pre-defined shapes. The primary reasons behind the bulkiness and the rigidity of current electronic devices are probably the materials and the manufacturing process commonly used [6, 7]. Most of the electronic components used today are fabricated using rigid substrates for example Si, and finally packaged as rigid components and assembled on hard carriers such as PCB (printed circuit board) [8].

The non-flexible and non-stretchable properties of current electronics limit the devices to conform to complex or skin-like surfaces. In other words, the bulky electronics cannot be universal. The future of electronics is not only to be everywhere but also to be anywhere. This new era electronics will be flexible, stretchable, deformable and metamorphic [5].

1.2. Future Electronics

1.2.1. Stretchable Electronics

A well accepted dictionary definition for "stretchable electronics" is not yet available. ***Stretchable electronics is a type of electronics or electronic systems that can be physically stretched upon applying internal or external stress without altering its electrical functions.*** Stretchable electronic systems should be able to sustain more than 1% of strain without changing its electrical properties significantly [9].

1.2.1.1. A Brief History

Stretchable electronics is relatively young in the field of electronics. Yet, the fundamental idea of the stretchable electronics is rather old. For instance, household telephone cables, which exist for more than 100 years, are stretchable. However, a systematic scientific and technical development in the field only started from the beginning of this century. The first scientific demonstrator of the stretchable electronics came from the Princeton University in 2003 [10]. Since then, the field has seen an exponential increase in research activities.

A pioneering contribution to this field came with the introduction of the stretchable conductors by Lacour and Wagner in 2003. They reported a gold-coated polydimethylsiloxane (PDMS) surface with wrinkles that could be stretched [10]. However, the wrinkled/buckled phenomenon of thin films on elastomer was known prior to this and was reported in 1998 by Prof. G. M. Whitesides's group [11]. Later in 2002 Wagner's group used this wrinkled thin metal film as deformable interconnects for conformal integrated circuits [12]. The same group used this phenomenon and pioneered the idea of stretchable electronics [10] and e-skin [13]. Subsequently, Gray *et al.* reported stretchable meander or horseshoe shape conductors in 2004 which are extensively used today [14]. Later, Prof. J. Rogers and co-workers developed buckled metal and/or semiconductor ribbons for stretchable devices in 2006 [15]. They transferred patterned thin metal or semiconductor devices on a pre-stretched rubber substrate, and later releasing the substrate results buckled ribbons. Same group further combined the meander shape metal tracks and buckled technique to get a higher stretchability [16]. Since then the research on stretchable electronics became enormously diverse in terms of materials, processing, designs, and devices. These will be discussed more elaborately in chapter 2.

Figure 1.1 presents the number of journal articles published on stretchable electronics in each year since 2001. The data are obtained from the ***Web of Science*** using the keywords "stretchable electronics" or "stretchable conductor". The last five years this field has grown so enormously, as can be seen from the bars shown in the figure 1.1, which clearly indicates that stretchable electronics has attracted a

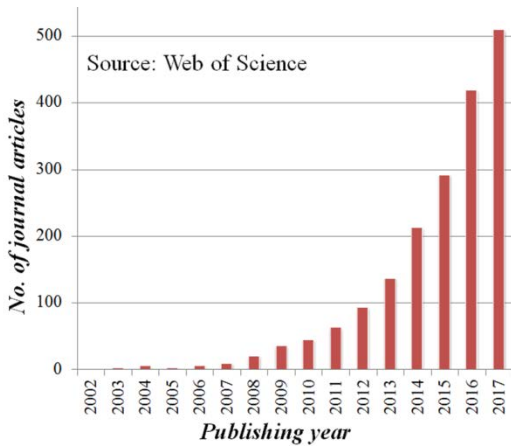

Figure 1.1: Number of scientific articles published on stretchable electronics. *Statistics presenting the number of journal articles published in each year since 2001; showing an exponential increase of research activities on stretchable electronics. Extracted from* ***Web of Science*** *using the key words "stretchable electronics" and/or "stretchable conductor".*

great attention to researchers. Currently, there are several independent groups all over the world actively carrying out their research in stretchable electronics.

1.2.1.2. Stretchable Devices

As discussed in the last section, the field of stretchable electronics has grown immensely for the last few years and consequently, almost every type of fundamental electronic device or component has been demonstrated to realize a stretchable analogue world. The entire demonstrators of stretchable electronic systems can be divided in two categories; the first category uses intrinsically stretchable components and the second category uses standard rigid, non-stretchable SMD components. However, both categories use stretchable interconnects [17].

Stretchable electronics using intrinsically stretchable components

To develop an intrinsically stretchable electronic system all the components and materials used in the system require to be intrinsically stretchable, which means it requires a stretchable substrate, conductor, semiconductor and insulator [17]. Fortunately, polymers can be processed to be stretchable. Additionally, there are a large number of polymers available including conductors, semiconductors and insulators which can be modified as required. In this section the discussion is limited only to the devices; materials and processing are discussed later.

PEDOT:PSS (poly(3,4-ethylenedioxythiophene) polystyrene sulfonate) is one of the widely used intrinsically conductive polymers. The bulk conductivity of pristine PEDOT:PSS films is only ~0.2 S/cm which can be improved to higher than 2100 S/cm [18]. A number of stretchable electronic devices have been reported using this polymer [17]. For example, PEDOT:PSS has been used for highly stretchable

conductive interconnects [19], transparent pressure sensors [20], health monitoring devices [21] and so on [17].

Polymers, which are intrinsically non-conductive, can be modified with conductive materials to obtain or increase its conductivity. This method became very popular among the researchers, since this allows controlling the conductivity precisely which is very important for high-performance electronic devices. To give a few examples, Ag nanowires (AgNWs) have been used to modify PDMS to obtain a high conductivity in order to result intrinsically stretchable conductive polymers. Such composite materials are used to realize stretchable conductors and capacitive strain sensors [22], smart textiles [23] and so on. Similar composite materials using Cu nanowires [24, 25], carbon nanotubes [26, 27], graphene [24, 28], conductive nanoparticles [29, 30] are being used to realize intrinsically stretchable light emitting devices [31], LED displays [32], photodetectors [33], solar cells [34], super-capacitors [35], transistors [36], rechargeable batteries [37], energy harvesters [38], strain sensors [39], temperature sensors [40], pulse sensors [41], pressure sensors [42], hydration sensors [43], human machine interfaces [44] and so on.

However, intrinsically stretchable electronic devices show a few disadvantages. For instance, generally, the demonstrated devices show relatively poor electrical performance and reliability. Moreover, the processing is not truly compatible with the industry. The mechanisms and the devices are developed in the labs. Also special methods are often used to realize the devices. Additionally, the used materials often degrade in open environment[17].

Stretchable electronics using standard rigid SMDs

These types of stretchable electronic devices are different from the intrinsically stretchable devices in various manners. For example, generally, this method uses pristine or partially modified commercially available standard SMD components which are not intrinsically stretchable. Instead, interconnects are engineered to be stretchable. For these reasons, the choice of the materials and the processing is different from the previously discussed methods.

This method became particularly popular among scientists, since direct use of SMD components are possible which gives freedom of choice to select a large variety of devices. This type of device also shows relatively high electrical performance due to the highly developed standards. Moreover, direct use of standard SMDs allows rapid realization of complex electrical system. The demonstrators include but are not limited to stretchable printed circuit boards [45], LED displays [46], acoustic sensors [47], photovoltaics [48], optoelectronics [49], epidermal electronics [50], digital camera [51], stretchable batteries [52, 53], temperature sensors [54], sweat sensors [55], health monitoring devices [56], medical diagnostic [57], metamorphic electronics [58, 59] and so on. In principle, this method of using commercially available SMDs for

stretchable electronics could probably enable any electronic system known today to be stretchable in the future. One of the main limitations of this method is that the components are not intrinsically stretchable and stretchability depends on the stretchable interconnects, which limits the maximum level of stretchability, the integration density of the devices, and non-uniform distribution of the strain over the entire system during stretching.

1.2.1.3. Applications

An entire review of the applications of stretchable electronics is beyond the scope of this thesis since the field has introduced a numerous number of new applications and advanced hundreds of existing devices to new dimensions. For a concise summary, the discussion is focused on several categorized applications.

Unconventional electronics

Stretchable electronics has already enabled new types of applications that would have been difficult to imagine a decade earlier. For instance, Si is well known for its rigidity; even Si can be bendable if it is thin enough and can also become stretchable if it buckles [60]. Based on this thin Si principle, a hemispherical electronic eye camera was developed by J. Rogers's group [61] which is a remarkable invention in this field. Ultrathin Si also enabled high-performance electronics on leather or paper [62]. In addition to these features, Si is also well-known as a physically invariant material, and this makes Si a very popular material for integrated circuits. However, for example, for implantable applications, it is useful to make the material or device disappears after a certain time without harming the body which is known as transient behavior. With certain processing, even, Si could be transient [63]. The research on stretchable electronics also introduced new type of materials for unconventional electronics. For example, conductive silk has been used to realize edible food sensors which could be attached to a curved surface such as apple or orange as a food labeling [64].

Biotechnology and Biomedicine

The applications of the stretchable electronics in the field of biotechnology and biomedicine probably are the most beneficial outcomes among many others [65]. There are several reasons for this. For instance, most of the medical devices are required to be attached to any living organism or organs. But, as we know, the living organs usually do not have flat surfaces, and moreover, they are soft. On the other hand, the electronic devices are made out of rigid materials such as Si, which has a Young's modulus several orders of magnitudes higher than the living tissues. In other words, the conventional electronic medical devices are unable to provide its maximum effectiveness because of the mismatch in the materials and their physical properties. Stretchable electronics overcomes these limitations. For example, neural

engineers use microelectrode arrays (MEAs) as an interface to record neural electrical activities from the nervous system to diagnostic patients who suffer from neurodegenerative conditions such as peripheral nerve injury, amputation, spinal cord injury, degenerative motor neuron disease and so on [66]. The MEAs are also used to enable bidirectional communication through stimulation of neural tissue, which improves lives of millions of people who suffer from congenital defects or disease. Engineers have been using different types of MEAs for these purposes, and most of those devices are rigid comparing with brain tissues. In addition to these, during heart beat or other movements, the brain and the peripheral nerves experience up to 15% strain [67]. Even the flexible MEAs cannot stand this large strain [68]. Stretchable microelectrode array (SMEA) is a better solution for such applications [69-71].

Another example of an invasive application of stretchable electronics is balloon catheters for cardiac electrophysiological mapping [72] which was reported by Rogers's group in 2011. The catheters were integrated with ECG (electrocardiography), tactile sensors, temperature sensors, flow sensors and RF (radio frequency) ablation electrodes. Among many other stretchable electronic devices for biomedicine applications electronic dura meter [73], neurogrid [74], sinusoidal nanobelts [75] are few examples. The stretchable electronics are also widely being used in cell culturing and sensing [76], in cell proliferation and differentiation [77], to investigate cellular [78] and electrophysiological [79] activities, to study and treat vascular diseases [80] and so on.

However, the demonstrators of stretchable electronics in biotechnology and biomedicine are mostly lab-based. The commercial implementation of such devices is far more challenging and requires more extensive studies. Nonetheless, the future stretchable bio-integrated electronics will solve problems that would not be possible using conventional rigid electronics, and would improve and save probably millions of lives.

Conformable wearable devices

One of the most useful features of stretchable electronics is its conformity. This feature enables wearable electronics or epidermal electronics. Numerous numbers of wearable electronic systems have been demonstrated for last few years. These devices can conform to the skin or attached to soft and wavy surfaces, and are able to monitor real time physiological properties of the body. One of the remarkable demonstrators was epidermal electronics in 2011 by J. Rogers's group [50]. "Epidermal electronics" are a kind of electronics that form conformal contacts with the skin surface to achieve robust binding. The group realized a wireless epidermal electronics system that can be mounted directly onto the skin with integrated temperature sensors, strain gauges, ECG sensors, EMG sensors, RF coils, RF diodes and power coils [50]. A number of similar skin-mountable devices with various types of functionalities have been demonstrated later on. For example, wearable sensors

can measure physiological data from the body in real time such as blood pressure [81], oxygen saturation [82], breathing rate [83, 84], heartbeat, human body temperature [85, 86], body movement [87, 88] and so on.

Electronics on fabrics

Fiber-based clothing is one of the most common and probably one of the most ancient products that have been used by all types of human beings all over the world for thousands of years. However, until last decade, this vast industry remained out of attention from electronics world. This is not because there are no applications of electronics in garments, but due to the massively miss-matched materials used for these two fields. The garment industries usually use soft, deformable, breathable, durable, washable fabrics which are not used in conventional electronics. However, with the benefits of flexible and stretchable electronics, the implementation of electronics on fiber-based clothing is no longer as big challenge as of was a few years ago. Essentially, this technology enabled various types of new applications of electronics in fabrics and popularly known as e-textile which is also generalized as wearable electronics [89].

The history of e-textiles can go back to 100 years; however, one of the first modern demonstrators of the e-textile was the animated sweatshirt by Harry Wainwright in 1985 [90]. Nowadays, there have been many more new applications of the e-textile other than only fashion [91]. Especially fiber-based sensors and devices recently became a very important focus, and have been extensively developed [92]. A numerous number of devices have been demonstrated based on e-textile materials and methods which include transistors [93, 94], antennas [95, 96], transducers [97], conductive connectors [98, 99], and even electronic circuitries [100, 101]. These devices have been used for personal protection, sensing [102, 103], medical treatment [104-106], sports [107], energy harvesting [108], energy converter [109], energy storage [110], and so on [111, 112].

Robotics

Stretchable electronics may empower a new era in robotics since it enables seamless interfacing among robots and humans [113]. For example, tactile sensing is being used for robotics in order to determine precise control of the contact to an object [114]. Especially, stretchable electronics have an influence on soft robotics which is a relative new field in robotics [115]. The advances of soft robotics came along with the soft sensors and actuators. Elastomer-based sensors and actuators are particularly interesting for robotic applications since most elastomers are conformable to the skin or curved surfaces [116-118].

Sensors and Actuators

In the field of stretchable electronics, sensors might be the most extensively studied device type. Human skin is the largest electronic organ in the body, and skin has very similar material properties to the commonly used elastomers for stretchable electronics [119]. For instance, skin and elastomers have Young's modulus of 0.1-1 MPa [120] and 0.1-5 MPa respectively. On the other hand, most of the elastomers can be used for pressure and strain sensing with controlled modifications [121]. A number of stretchable sensors have been demonstrated using different resistive or capacitive [122] or piezoresistive or electro-optical [123] properties of the materials [124]. For example, strain sensors, pressure sensors [125, 126], force sensors [127], temperature sensors [128], gas sensors [129], UV sensors [130-132] and so on. These different types of sensors have been used in different purposes including medical applications [72, 133], artificial skin [86, 125] and robotics [113, 116].

Stretchable electronics opened new windows in the actuators research. Especially, the field of soft actuators has been extremely benefited by this. It also enabled new type of applications such as microbots [134], micropumps [135, 136], microcatheters [137], tactile displays [138], moving lens [139] and so on.

Conventional electronics

Other than the devices mentioned previously, stretchable electronics also contributed to the conventional electronics to take a new dimension. This is just a matter of time that today's known rigid electronics will be flexible and stretchable in near future. Researchers have demonstrated numerous numbers of conventional electronic systems to make stretchable. This includes stretchable energy storage [140], energy converter [141], display [26, 142], acoustics [59, 143], transistors [144], capacitors [145], integrated electronics [146] and so on.

1.3. Metamorphic Electronics

Having a pre-defined shape and dimension of current electronic devices will no longer be sufficient for the users in future. Future electronics will be user-friendly; not only by software but also by hardware, which means the user will shape their electronic devices at will. This new type of shapeable electronics is named metamorphic electronics in this thesis.

The word "metamorphic" is derived from "metamorphosis" which is originated from the Greek word "*metamórphōsis"* (*metá* means "after" and *morphḗ* means "form"). Metamorphosis is a very common phenomenon in nature. This is actually a biological process by which an animal physically develops after birth or

hatching by cell growth and differentiation. To give an example a butterfly starts its life from an egg, then to larva to pupa, and finally to an adult. An animal appears very differently and also functions differently through its metamorphosis processes. Metamorphic electronics follows a similar paradigm: these electronics devices can be geometrically deformed by different manners, and also might function differently. ***Metamorphic electronics are the electronics or electronic systems which are stretchable and deformable, and which morph to adapt to a new topology and form factor*** [58].

Metamorphic electronics, in our view, is a new field of electronics. It is in some ways a subgroup of stretchable electronics and deformable electronics. A concept of metamorphic electronics is presented in **Figure 1.2A**, where a patterned rubber membrane is inflated by air. A partial inflation of the membrane produces a hemisphere ($\boldsymbol{a_1}$), and further inflation of the membrane produces a bumble bee-eye shape structure ($\boldsymbol{a_2}$). The same device shows different morphological properties. In addition to this, the final structure also has different local stretchability. This is particularly important. As illustrated by a simple example in **Figure 1.2B** which shows a schematic of a standard PET or glass bottle. Only linearly stretchable electronics is not sufficient to mount electronics on its entire surface. Additionally, the electronic system has to have different local stretchability.

To give another example, the human skin has areas of low and high stretchability. In other words, it is desired to realize stretchable electronics with a tailored local elastic module to enable a more seamless integration with 3D shaped objects or objects which change shape. Such a technology would help to realize "metamorphic electronic systems" which are electronic products that change shape.

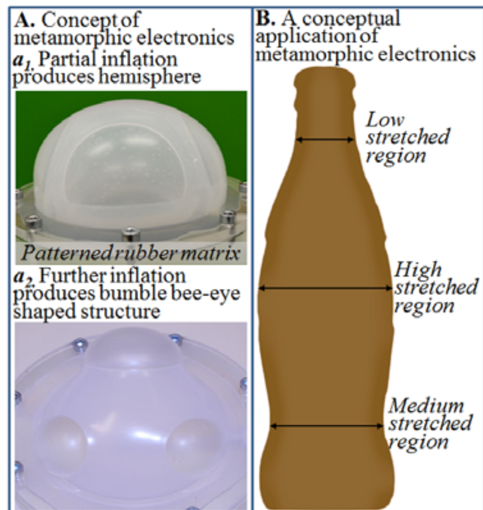

Figure 1.2: Metamorphic electronics. A. *Concept of metamorphic electronics showing inflation of a patterned rubber membrane. Partial inflation of the membrane produces a hemisphere (*$\boldsymbol{a_1}$*), and further inflation of the same patterned membrane produces a bumble bee-eye shape structure (*$\boldsymbol{a_2}$*).* ***B.*** *A conceptual application of metamorphic electronics. To rap a standard PET or glass bottle with electronics, the electronic system has to have different stretchability along its length.*

This thesis primarily aims to develop a method to realize a reliable integrated stretchable printed circuit boards (**sPCB**) technology that is compatible with conventionally printed circuit boards. The technology would facilitate to replace the rigid substrate in the conventionally printed circuit boards (PCB) by a stretchable substrate. If successful, such a technology would enable any electronic product known today to be stretchable.

By considering this as a goal, during this thesis a method to realize integrated metamorphic printed circuit boards (**mPCBs**) has been developed, which are fully compatible with conventional PCB technologies and industrial manufacturing process. Additionally, the method uses standard pristine surface mount devices (SMDs), which broaden the device possibilities.

In this thesis, the pioneering concept of metamorphic electronics is introduced. This new type of electronics advances the primary idea of stretchable electronics to take on new 3D shapes and interesting form factors. As demonstrators, metamorphic electronics, optoelectronics, acoustoelectronics and integrated metamorphic electronic systems have been realized.

Materials, Processing and Design

2.1. Materials

2.1.1. Materials for stretchable substrates

2.1.2. Materials for stretchable conductors

2.1.3. Materials for devices

2.2. Processing

2.2.1. Soft substrate first

2.2.2. Soft substrate last

2.2.3. Transfer printing

2.2.4. Direct printing

2.3. Design

2.3.1. Macroscopic stress distribution

2.3.2. Microscopic stress distribution

2.3.3. Stress adaptive metal tracks

2.1. Materials

Materials always play a major role in the development of any devices, systems, or any technologies. There are numerous materials available with various physical properties. The elastic modulus or Young's modulus (***Y***) is a relevant parameter in the design of stretchable electronic system. It is generally defined as the ratio of stress to the strain within the material's elastic limit [147]:

$$Y = \frac{Stress}{Strain} = \frac{\sigma}{\varepsilon} \qquad (2.1)$$

The stress ($\boldsymbol{\sigma} = \boldsymbol{F/A}$) is the force (***F***) per unit area (***A***) and the strain ($\varepsilon = \boldsymbol{\Delta l/l}$) is the change in length (***Δl***) per unit of original length (***l***). Therefore,

$$Y = \frac{F/A}{\Delta l/l} = \frac{Fl}{A\Delta l} \qquad (2.2)$$

The SI unit to measure Young's modulus is *Pa* or N/m^2. A relatively low value of Young's modulus shows softness, while a high value shows the hardness of a material. **Table-2.1** shows a number of materials with its Young's modulus ranging from liquid to the hardest materials available. To illustrate an idea, let us compare bio-materials (tissue or skin) and conventional electronic materials (PCB or silicon). As can be observed, the hardness of the materials increases by several orders of magnitudes. It is nearly impossible to get the maximum benefit of modern electronic devices in medical or bio applications due to this huge mismatch. On the other

Table-2.1: Young's modulus of various materials.

Material type	Materials	Young's modulus [5, 7-9, 17, 50, 148-150]	
Liquid	Liquid metals	>1	Pa
	Liquid	~1	
	Gels	~10	
Bio	Brain tissue	0.2	kPa
	Muscle	0.5-3	
	Skin	10-200	
	Bone	25×10^6	
Polymers	Dragon Skin	0.2	MPa
	EcoFlex 0010	0.37	
	EcoFlex 0030	0.65	
	PDMS	1-2	
	Rubber	10-100	
Standard electronic materials	ABS plastics	2	GPa
	PVC	3.5	
	Polyimide	5	
	PCB	21-23	
	Gold	70	
	Glass	70	
	Copper	120	
	Silicon	150	
Extremely hard	Graphene	1	PPa
	Diamond	1.22	

hand, the polymers are a better choice for such applications in terms of materials softness.

2.1.1. Materials for Stretchable Substrates

Ready-to-use electronic devices are always mounted or packaged on a carrier substrate. Most of the industries use rigid glass epoxy as PCB (printed circuit board) substrate material [8]. However, the glass epoxy is a rigid and brittle material which is not ideal for stretchable electronics (see table-2.1). There are mainly two approaches to make a substrate stretchable:

1. Elastomeric substrate
2. Origami/kirigami technique

In the second approach, the substrate material does not require to be stretchable. There are several demonstrators of stretchable electronics following these methods [60, 151-153]. Nevertheless, in the first approach- the elastomeric substrate is more popular and widely being used among the researchers in this field [9, 10, 14-16]. This is also the approach followed in this thesis.

Numerous elastomeric materials are available with wide ranges of physical properties [6, 7, 9, 154]. Most of the elastomeric polymers have Young's modulus within 0.1-10 MPa. However, there are many other polymers beyond this range which remain out of this discussion.

Elasticity is a very interesting property of elastomers. There are several elastomeric polymers that can be elongated 1000% of its original length. **Table-2.2** presents a list of a few polymers with its maximum elongation limit, tensile strength (*the resistance of a material to break under tension*) and Young's modulus. All of these materials are strong candidates for stretchable electronics substrate. The selection of the materials depends on the application and processing.

Table-2.2: Potential materials for stretchable carrier substrate [5, 8, 148-150].

Materials	Elongation at break (%)	Tensile strength (MPa)	Young's modulus (MPa)
PDMS	140	6	1-2
Butyl rubber	170	3.51	0.41
Clear Flex 95	175	17	4
Solaris	290	1.24	0.1
Mold Max 30	300	4	0.7
Dragon skin	350	3.54	0.2
VytaFlex 50	400	4	1.4
Polyurethane	760	7.32	7.82
EcoFlex 0030	900	2	0.65
EcoFlex 5	1000	2.4	0.4
PMC121/30	1000	2.7	0.6

Silicone or

polysiloxanes elastomers are widely being used in microfabrication. Silicone elastomers consist of an alternate sequence of silicon and oxygen atoms where each silicon atom bonds to two organic substituents (***Fig. 2.1***). Usually, silicones can sustain high temperatures due to the strong silicon-oxygen bond [155].

Figure 2.1: Silicones. *Basic chemical structure of silicone elastomers.*

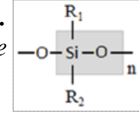

I. PDMS

PDMS (polydimethylsiloxane) is one of the most commonly used silicones [156]. PDMS is inexpensive, easy to process, transparent, permeable to air and biocompatible. In addition to these, the surface properties of the PDMS can be easily modified, for example, cured PDMS surface is hydrophobic, which can be modified to make hydrophilic by O_2 plasma activation or UV treatment of the PDMS surface. The Young's modulus of the PDMS also can be adjusted.

PDMS was the first substrate-material used in stretchable electronics. As mentioned earlier, the pioneering idea of stretchable electronics came with thin metal film coating on PDMS surface which produces wrinkles [10, 12]. Till today PDMS remains one of the most used materials in stretchable electronics where a lower level of stretchability is required.

II. EcoFlex

For high levels of stretchability, EcoFlex is however, now reliable [157]. The physical properties of the EcoFlex will be discussed broadly since EcoFlex 0030 (Smooth-On) is the primary substrate material used in this thesis.

EcoFlex is a platinum catalyzed silicone with low viscosity. Commercial product contains two parts (A & B), which has to be mixed 1A:1B by their volume ratio and cured at room temperature for 10 hours [148].

EcoFlex shares some properties with PDMS. As an example, a thin metal film on EcoFlex also produces wrinkles similar to those of PDMS. **Figure 2.2** shows optical images of wrinkles produced after gold (**Au**) coating on EcoFlex surface. In this case, a 100 µm thick EcoFlex 0030 layer is spin coated on a Si wafer and cured over night at room temperature. A 5 minutes surface activation step is performed using O_2 plasma. Subsequently a 20/200 nm thick Ti/Au film is sputter coated on EcoFlex.

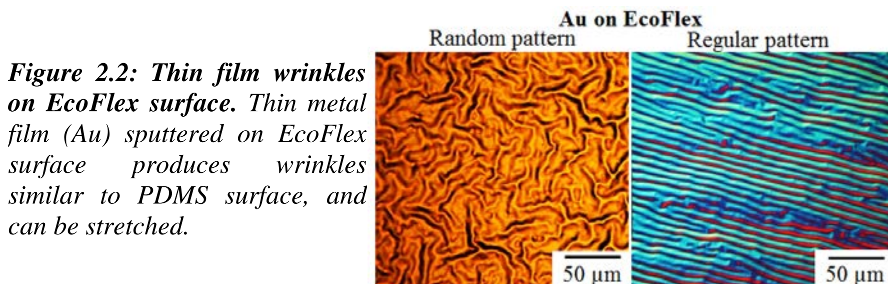

Figure 2.2: Thin film wrinkles on EcoFlex surface. *Thin metal film (Au) sputtered on EcoFlex surface produces wrinkles similar to PDMS surface, and can be stretched.*

The surface properties of EcoFlex, are similar to PDMS, and can also be modified. For example, O_2 plasma remarkably increases the adhesion of metal films. For this test, a Si wafer is spin coated with 100 µm thick EcoFlex layer and cured overnight at room temperature. The sample is then treated with O_2 plasma for 5 minutes, half of the sample is protected from plasma and half is exposed to the plasma. A subsequent 20/200 nm Ti/Au film is sputter coated on the entire surface of the EcoFlex. **Figure 2.3A** shows an optical image of the substrate after Au coating. The area treated with the plasma confirms higher reflectivity and shiny (***right***), while the untreated area appears to be less reflective and rough (***left***).

The sample is then processed through photo-lithography and chemical processes to pattern the Ti/Au. **Figure 2.3B** shows the image of the processed sample. The area treated with plasma survives the processing (***b_1*, *right***), where the untreated area does not (***b_1*, *left***). This is a clear indication of the increased surface adhesion due to the O_2 plasma process. Note that the plasma exposed area shows wrinkles similar to the figure 2.2 and unexposed area does not show such wrinkles (***b_2***).

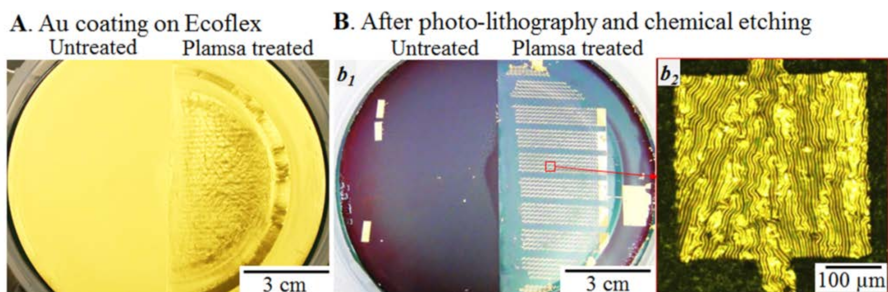

Figure 2.3: Surface activation of EcoFlex. A*. 20/200 nm Ti/Au is deposited on a substrate coated with EcoFlex with O_2 plasma treated (right) and untreated (left).* ***B****.* ***b_1****. The plasma treated region survives subsequent lithography and chemical processes (right), while the region without plasma treatment does not survive such processes (left).* ***b_2****. Shows an image of the wrinkles of Au film on EcoFlex surface produced at the plasma activated area.*

However, the use of EcoFlex in stretchable electronics is comparatively new. One of the first reports of stretchable electronics using EcoFlex was reported in 2009 [158] where the authors demonstrated a stretchable tactile sensor using composite materials of EcoFlex and carbon particles. Since then EcoFlex became a fairly popular material as a stretchable substrate [6, 53, 157, 159, 160].

Among other polymers solaris [161], dragon skin [162], polyurethane (PU) [163, 164], nitrile butadiene rubber [148], acrylic elastomer [37, 165], poly(isobutylene-co-isoprene) (IIR) [166], polyolefin (POE) [167], poly(styrene-block-butadiene-block-styrene) (SBS) [168] are also being used as stretchable substrate for different application purposes [155].

2.1.2. Materials for Stretchable Conductors

Printed circuit boards, no matter how big or small, how simple or complex, always have conductive tracks to connect the mounted components. Thus, conductive tracks play an important role. In the stretchable electronics, conductive tracks play even a more important role because in most cases those are the main parts that directly contribute to the stretchability of the system, since the rigid components are not stretchable.

Since the stretchable conductors are particularly important, this substance has been extensively studied by several research groups all over the world. A number of stretchable conducting materials, technologies, and designs have been reported, which includes inorganic [169], organic [170], liquid [171], or composite [172] materials approaches. **Figure 2.4** groups the general approaches to realize stretchable conductor using different materials and methodologies.

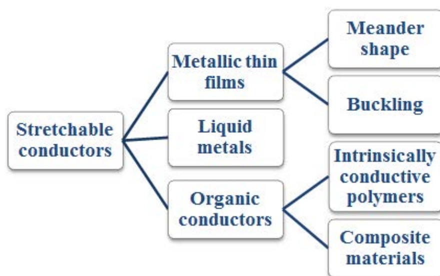

Figure 2.4: Different methodologies to realize stretchable conductors. *The field of stretchable conductors has been one of the main focuses to the researchers in this area. As a result a numerous numbers of methodologies have been demonstrated, and these include inorganic, organic materials or liquid alloys.*

2.1.2.1. Metallic Thin Films

Bulk metals show very high electrical conductivity (**Table-2.3**). Bulk metal films are broadly studied in the field of stretchable electronics. Initially gold (Au) was one of the primary choices of the metals due to its ductility, and also shows high electrical conductivity. The first reported wrinkled gold strips on PDMS surface could be stretched to 22%. However, gold is expensive and eventually, copper (Cu) and/or aluminum (Al) replaced gold. The electrical properties of Cu and Al are also very similar to gold, but relatively inexpensive.

Table-2.3: Conductivity of commonly used metals.

Metals	Conductivity σ (S/m)
Carbon	1×10^8
Copper	5.96×10^7
Gold	4.1×10^7
Aluminum	3.5×10^7
Nickel	1.43×10^7
Platinum	9.43×10^6
Tin	9.17×10^6
Lead	4.55×10^6
Titanium	2.38×10^6

A closed thin film does not show very high stretchability even when it is wrinkled. However, this limitation can be overcome by patterning the metal film. There are mainly two approaches to use bulk metal for higher stretchability other than the wrinkled surface.

i. **Meander shape metal tracks:** Bulk metal itself is not stretchable, but spring shape metals are. Based on this idea, Gray and Chen developed the first 2D spring shape metal interconnects on elastomer surface, which is widely being used in stretchable electronics research [14]. This spring shape metal tracks in 2D surface look similar to U-shape or meander shape or horseshoe shape, and have been named differently among the researchers. A very high level of stretchability of the metal tracks is possible by varying the geometrical structure of the tracks, and a number of designs have been demonstrated by several groups. The design parameters of these metal tracks will be discussed later. **Figure 2.5A** shows the schematic process flow of this method with an SEM image (a_2) of a newly designed meander shape metal track which is developed during this thesis.

ii. **Buckled metal tracks:** A different approach to the stretchable tracks was developed by Rogers's group in 2006 [15, 173, 174]. They transferred metal strips or thin semiconductor ribbons to a pre-stretched elastomer substrate with pre-defined bonding locations to bond the metal or semiconductor ribbons locally to the substrate, and rest of the ribbons remain free to detach. By releasing the pre-stretched elastomer substrate allows the metal or thin semiconductor ribbons to pop-up in the z-direction which is known as buckle formation. This buckle allows the metal tracks to be stretched. The maximum stretchability of the device depends on the pre-stretched substrate. The schematic process flow is shown in **Figure 2.5B** with an SEM image (b_2) of such buckled metal tack in EcoFlex.

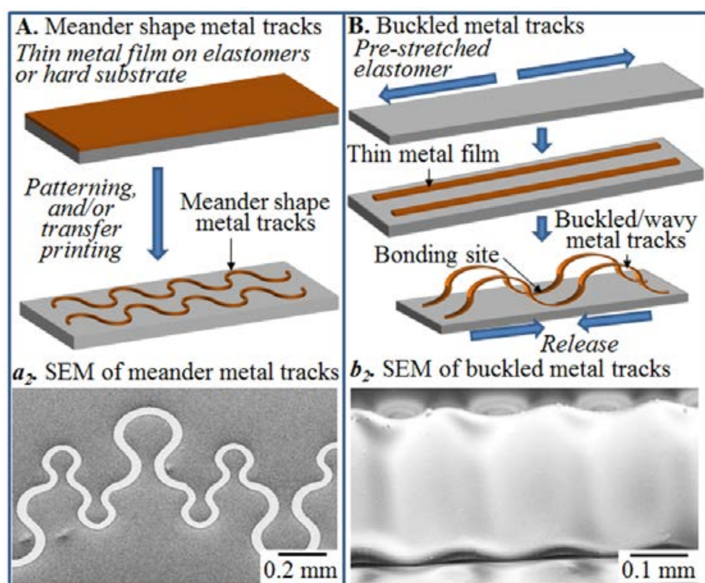

Figure 2.5: Meander shape and buckled metal tracks. A. *Meander shape tracks use geometrically designed 2D spring shape metal strip as stretchable interconnects, and* ***B.*** *buckled method uses transferred metal tracks on a pre-stretched elastomer substrate, releasing the substrate results pop-up of the metal tracks in outer plane direction. Bottom shows SEM images of corresponding metal tracks on EcoFlex substrate.*

In another approach, Rogers's group combined the meander shape metal tracks with the buckling to obtain a higher stretchability [16].

2.1.2.2. Liquid Metals

Several groups have demonstrated liquid metal alloys as an alternative for the stretchable conductors [171, 175]. One of the first demonstrators of using liquid metals came from Whitesides's group in 2007 [176] where they developed a process called "microsolidics". Using this method they could fabricate 3D metallic microstructures in PDMS substrate. However, in the demonstrator, they used relatively high melting point metal alloys which is solid at room temperature. Thus the demonstrators were flexible, bendable or twistable but not stretchable. In the next year the same group used eutectic Gallium-Indium alloy to inject through the microfluidic channels in PDMS. This alloy is liquid at room temperature which makes it stretchable [177]. Later in 2010, the group demonstrated stretchable microfluidic RF antennas using a similar method [178]. Other demonstrators that use liquid metal alloys for stretchable electronics include multiaxial stretchable interconnects [9], deformable fluidic antennas [179], wireless strain sensor [180], artificial skin [168], stretchable micro-

supercapacitors [159], stretchable inductors [181], stretchable loudspeaker [143], biphasic (solid-liquid) thin metal films [182].

2.1.2.3. Organic Conductors

Unlike the inorganic or metallic conductors, organic conductors or polymers are intrinsically flexible and some are stretchable as well. For being intrinsically stretchable the polymer conductors attracted attention to the researchers [170]. As mentioned before, PEDOT:PSS (poly(3,4-ethylenediox-ythiophene):poly(styrene sulfonate)) has been used in stretchable electronics as stretchable conductors. PEDOT:PSS shows reasonable conductivity [19, 20], however, suffers from a relatively low level of stretchability and is environmentally unstable. The stretchability of PEDOT:PSS can be increased by adding additional solvent such as DMSO (dimethyl sulfoxide) [183]. Among other polymers polypyrrole [84, 184], polyaniline [185] also show conductivity and also have been used in stretchable electronics [170].

Polymers also can be mixed with conductive materials to obtain or increase its conductivity as a composite material [172]. This process became popular to the researchers since the process allows controlling the electrical properties precisely which is very important for electronic devices. Ag nanowires [22, 23], Cu nanowires [25], metal nanoparticles [29, 30] are widely being used with polymers to obtain stretchable conductive polymers.

Carbon and carbon-related materials [110, 127, 142, 186] also have attracted great attentions to the researchers. Especially, graphene has become a key focus in the electronics world for its distinctive electrical, optical, and mechanical properties [187-189]. Graphene or patterned in wrinkled form is also being used as stretchable transparent electrodes [24, 28]. Additionally, carbon-based nanowires or nanotubes [26, 27, 190] are also widely being used as an additive for polymer to improve its electrical properties.

2.1.3. Materials for Devices

2.1.3.1. Organic/Composite Materials

To develop an electronic device intrinsically stretchable all the components and its materials require to be intrinsically stretchable, which means such a device requires stretchable conductors, semiconductors and insulators. Fortunately, most of the polymer materials can be processed to be stretchable and there are large numbers of polymers available. Some of the polymers are intrinsically stretchable and conductive and can be modified as required. Additionally, polymers are relatively simple to process, inexpensive and easily scalable. Due to these benefits polymers became popular among the researchers for stretchable electronics. A large number of polymer materials have been developed based on the applications and requirements.

Different groups have developed stretchable semiconductors using different methods, which include molecular materials such as diblock copolymers of polyethylene (PE)-P3HT [191] or triblock copolymers of P3HT-poly(methyl acrylate) (PMA)-P3HT [192]. However, synthesis of molecular material is relatively complex compared with composite polymers approach, which became popular in stretchable materials research and has been developed broadly. One of the first reports of stretchable semiconductors using composite materials method was demonstrated by Shin *et al*. [193], where the group developed a highly stretchable semiconductor using blended P3HT nanofibrils in poly styrene- *block* -poly(ethylene- *co* -butylene)- *block* -polystyrene (SEBS) which was used to fabricate stretchable FETs. Other than these, P3HT NW (nanowire) networks embedded in PDMS [194], composite SWCNTs/PU [36], composite R-GO/PU [40] have been used.

Stretchable insulators are relatively easy to develop since most of the polymers are good insulators and can be directly used as dielectric layers in the devices. For example, PU has been used in the FETs as a gate dielectric material [40, 195]. However, to improve the dielectric property and for a better electrical performance of the polymers different groups have developed composite materials approaches. For example, Liang *et al.* realized FETs using PU-co-poly(ethylene glycol) (PU-co-PEG) as a dielectric material which shows relatively high dielectric constant. Other than these, researchers also used ionic-liquid-based SWCNT gel/PDMS [196], liquid metal/silicone [197] as high-quality dielectric materials.

2.1.3.2. Patterned Bulk Materials

Another method to realize stretchable device is to use conventional materials with certain modifications [146]. For example, the bulk Si can be geometrically patterned similarly to the meander shape stretchable interconnects. If the Si membrane is sufficiently thin, then the meander shape Si membrane will be stretchable [198]. For instance, monocrystalline inorganic semiconductor substrates can be patterned by lithography and chemically etched to produce ultrathin nanostructures such as wires, ribbons, tubes or membranes [199]. A selective doping method of semiconductor nanostructures would produce ultrathin nano-devices which are highly flexible and can be geometrically patterned to be stretchable [15]. It is also possible to use a sacrificial layer to release the patterned ultrathin device layer. For example, SOI (Si on insulator) substrates are being widely used to produce high-quality semiconductor devices by conventional fabrication methods and later etching the underlying oxide layer release the active device layer which is subsequently transferred to a stretchable substrate [60, 200].

The method is not limited to only Si-devices. Crystalline AlInGaP is widely used for red LEDs. This material can be grown on GaAs substrate with a multilayer stack of materials as sacrificial layers which can be used to release the active AlInGaP layer [201]. Similar method is also used for other semiconductor materials

such as GaAs [202, 203], GaN [204], InP [205], diamond [206], CNTs [207], carbon nanomembranes [208] and so on.

2.1.3.3. Standard Rigid SMDs

Another approach to realize stretchable electronics is the direct use of commercial surface mount devices (SMDs). Since the conventional commercial components are not intrinsically stretchable; the stretchability of the entire system depends on the stretchability of the metal tracks in between non-stretchable islands and the available free space. This approach has some benefits since it enables the use of ready evaluated SMDs. This gives a wider range of freedom to choose the devices and functionalities, and provides access to well performing devices. For example, the first demonstrator of stretchable acoustic system uses commercially available standard acoustic devices [47, 59]. A multifunctional wearable device was realized following this method by J. Rogers group [209], where the group used different types of SMDs including capacitors, resistors, inductors, jumpers, ICs, and antennas. Several other groups also used standard SMDs to realize stretchable optoelectronic systems [46, 58], stretchable electronic systems [45, 210], health monitoring devices [209, 211], and so on.

2.2. Processing

The processing of the stretchable electronics does not follow a single route or a common method. It is nearly impossible to categorize the processing in a precise manner. Most of the demonstrated reports use different methods or a combination of several methods to realize stretchable electronic systems. Yet, in this section an effort has been given to categorize the processing methods commonly used.

2.2.1. Soft Substrate First

"Soft substrate first" refers to the processing where soft/rubber substrate is introduced in the beginning of the processing. In an overall perspective, this category uses some processing steps directly on the soft-substrate; the soft substrate may use another rigid carrier substrate or can directly be used as a final substrate. **Figure 2.6** depicts some test structures that have been prepared using this methodology. The following quantitative, experience was gained. Fabrication on soft substrate is challenging and often limited by several parameters. For example, high-temperature processing is not supported due to the soft materials, or precise alignment and registration is always challenging on soft substrate. However, this type of processing has been used frequently to realize stretchable electronics. For example, the first demonstration of stretchable metal electrodes on PDMS was following this method [10, 12], where gold was directly deposited on PDMS coated

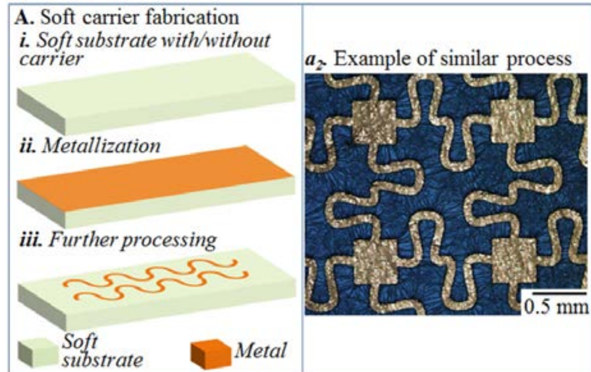

Figure 2.6: "Soft substrate first" process flow. A. *Schematic of the processing steps of the "soft substrate first", and an optical photograph of such process (**a_2**). In this method some of the processing steps are performed on soft substrate which make the method challenging.*

substrate, which formed stretchable wrinkles, and later used to realize capacitive sensors for e-skin [13, 122]. A similar method has been used to realize ultrahigh tensile strain conductors by Zheng *et al.*, where the authors used an O_2 activated pre-stressed elastomer substrate and used to grow Cu in an electro-less plating [212, 213].

Soft substrate such as PDMS is easy to process for soft lithography [214], this feature has widely been used to pattern PDMS and realize various stretchable electronic systems. For example, liquid metals [177] are used by different groups to inject in PDMS channels to form metallic interconnects and radio antennas [178, 179, 215], RFID tags [216] or other electronics [182].

This method is more commonly used in organic or intrinsically stretchable materials processing [17]. For example, Hwang *et al.* used a plasma treated PDMS substrate to spin coat AgNWs and PEDOT:PSS/PU to realize a transparent stretchable strain sensor [35]. A similar approach was used by Ryu *et al.*, where the authors realized elastic strain sensors using dry-spun CNT fibers on EcoFlex substrate [160]. The dry spray method is also used to realized electroluminescent devices using composite materials of AgNWs, ZnS:Cu micro particles, and PDMS [217]. In a different approach Boland *et al.* used natural rubber band to soak graphene flakes, which were dispersed in N-methyl-pyrrolidone by liquid exfoliation techniques. The author used the rubber bands for dynamic sensing [218].

One of the remarkable demonstrators following "Soft substrate first" was reported by Xu *et al.* [209], where the group used a PDMS coated substrate to realize multifunctional sensors, circuits, and radios for the skin. The fabrication involves multilayers of materials such as plasma activated PDMS, two layers of PI, Cu metallization layer and SiO_2, several photolithography and chemical processing, and microfluidic assembly of the components. The group used water-soluble tape to transfer the electrodes from a fabricated substrate to final device substrate and used shadow mask to pattern the assembling pad sites. A similar method was also used to

realize an epidermal electronics for near-field communication [56] or for electrophysiological measurements [219].

2.2.2. Soft Substrate Last

"Soft substrate last" method is a conceptual approach that is a contribution of this thesis. The method is relatively more compatible with standard semiconductor processing, which uses soft or rubber substrate at the end of the processing sequence. The processing starts with a standard hard carrier that allows high temperature processing, precise alignment, and registrations. The method also allows using standard SMD components without any modification and permits different assembling methods including robotic assembly or advanced self-assembly. In principle, the entire fabrications, assembly and device performance test are carried out on a hard carrier, and the soft rubber matrix is introduced at the end of the processing sequence to 'peel off' or 'transfer' the device on stretchable substrate.

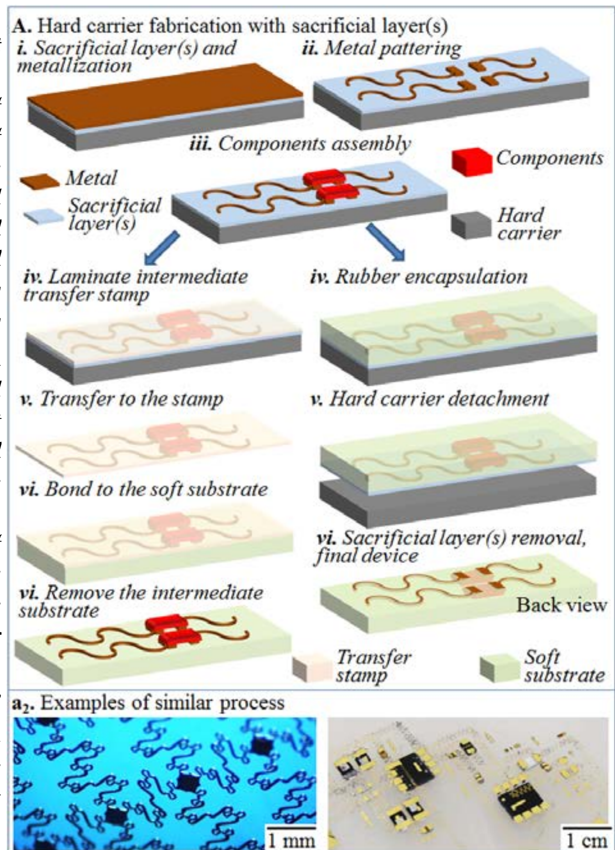

Figure 2.7: "Soft substrate last" process flow. A. *Schematic of the processing steps of the "soft substrate last", and optical images of prepared samples produced using similar methods (**a**$_2$). The method uses standard fabrication processes on hard carrier and soft substrate is introduced in the end of the processing sequence. Single or multilayer of sacrificial materials are used to release the active device layer from carrier substrate. The examples (**a**$_2$) show two complete devices in stretchable substrate fabricated following this method.*

Figure 2.7 presents the similar process flows that have been used during this thesis (***Fig 2.7 A***) and examples of the realized electronics systems (***Fig 2.7 B***).

2.2.3. Transfer Printing

Transfer printing probably is one of the most useful and promising methods to realize unconventional electronic systems. The mechanisms and possibilities of the transfer printing methods are widely reviewed by Carlson *et al.* [220], where the authors discussed different approaches of transfer printing of materials assembly. In this review, the authors classified three different categories of transfer printing is summarized in **Figure 2.8**. In principle, the first method uses a stamp coated or bonded with the components or inks and subsequently transferred to the receiving substrate (***Fig 2.8A***). For example, Zaumseil *et al.* used a PDMS stamp coated with gold which they transferred to GaAs substrate [221]. Since the method uses adhesive and cohesive forces of the materials to transfer ink from one substrate to another substrate, it is important to control these forces for different materials and stamp combinations. Several methods have been reported to control the adhesion forces as required. For example, Childs *et al.* used UVO (ultraviolet-ozone) treatment of the

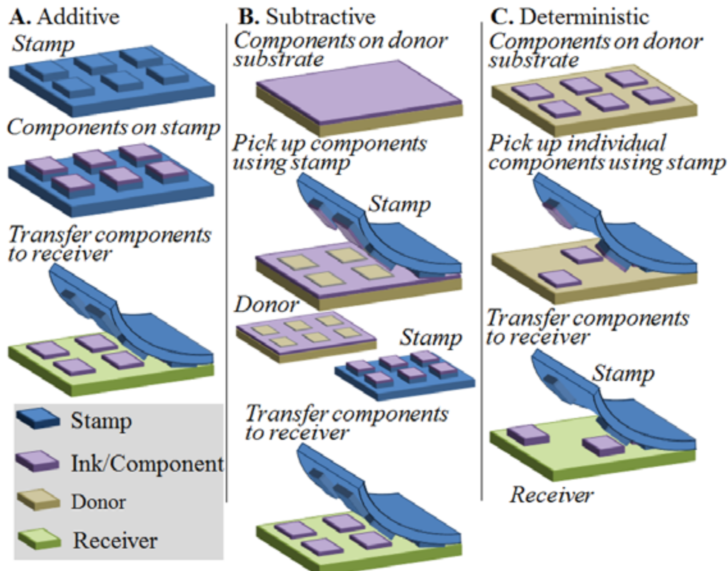

Figure 2.8: Different methodologies of transfer printing. A*. Additive printing uses a stamp coated/bonded with components;* ***B.*** *subtractive printing uses a stamp to pick up the components from a donor substrate and transfer to the receiver substrate, and* ***C.*** *deterministic printing transfers selective components from donor to receiver. Adapted from [220].*

PDMS stamp to modify its surface properties [222, 223]. In the second method, the stamp is used to retrieve the components or ink from a donor substrate and subsequently transferred to the receiver (***Fig 2.8B***). For instance, Kim *et al.* used UV (ultraviolet) curable PUA (polyurethane acrylate) mold as a stamp and NPB coated Si wafer as a donor. The NPB (4,4 -bis[N-1- napthyl-N-phenyl-amino]biphenyl) layer acted as the ink and was transferred using the stamp to form nanoholes or nanolines on the donor substrate [224]. A similar method was used by Wang *et al.* to pattern organic semiconductor materials [225]. The authors used epoxy as a stamp and Si/ITO (Indium tin oxide) as a donor substrate which were coated by ink such as copper phthalocyanine (CuPc), metal-free phthalocyanine (H2- Pc),N,N′-di(naphthalen-1-yl)-N,N′-diphenylbenzidine (NPB), and tris(8-quinolinolato)aluminum (AlQ_3) by thermal evaporation.

The third method is more dynamic (***Fig 2.8C***). In this method, specific components are deterministically transferred from donor substrate to receiver substrate using an intermediate stamp. Since the components or group of components are selected independently to be transferred, it gives freedom of choosing different components or materials. Lee *et al.* used this method to transfer print thin film transistors on flexible substrate over a large area [226]. The authors used SOI wafer to realize µs-Si devices and transfer those to a receiver substrate using a PDMS stamp. They demonstrated two mechanisms of deterministic transfer printing of the devices, one of which uses a physical bonding of the device to the stamp and the other uses chemical bonding by soft lithography technique. A similar approach was used by Baca *et al.*, where the authors used PDMS stamp to transfer Si ribbons from a donor substrate [199].

Similar transfer printing methods have been studied during this thesis aiming to transfer pre-assembled components to a stretchable substrate. For instance, fluidic self-assembly (FSA) [227] shows high efficiency for assembling µ-components with a very high yield [228]. The method is also compatible with a wide range of materials and substrates; however, the process can be complicated for some specific applications. For example, in this assembly method the assembling pads are coated with low melting solder by dip coating in a molten solder bath [229]. The method is not selective unless the substrate is masked with a resist. But, using a resist as a masking material make the assembly process complicated since the resist is adhesive to the components and get stuck to the resist during assembly process. Additionally, fluidic self-assembly directly on rubber substrate is challenging. To solve these issues, one approach is developed here which is to assemble the components on a standard flexible substrate such as polyimide film and transfer the components to the final stretchable substrate. **Figure 2.9** shows an example of this method that has been tested during this thesis.

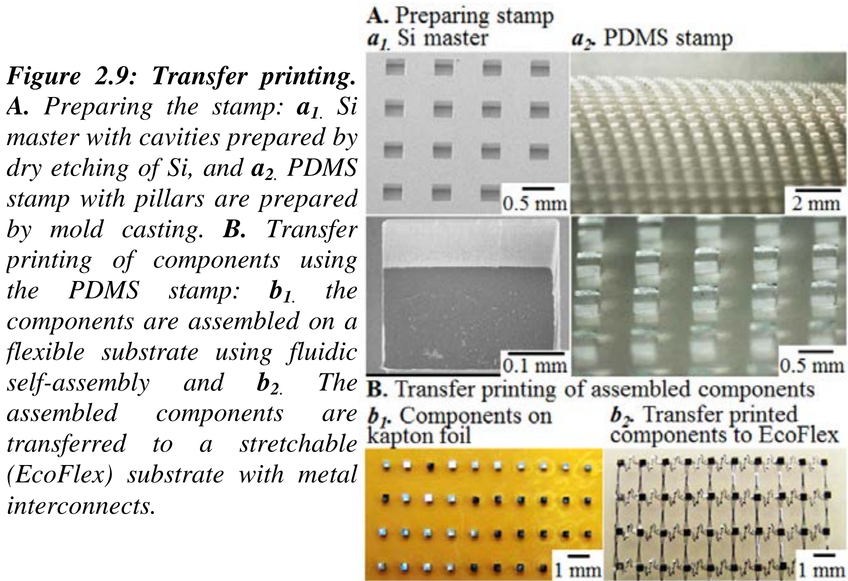

Figure 2.9: Transfer printing. ***A.*** *Preparing the stamp:* ***a_1.*** *Si master with cavities prepared by dry etching of Si, and* ***a_2.*** *PDMS stamp with pillars are prepared by mold casting.* ***B.*** *Transfer printing of components using the PDMS stamp:* ***b_1.*** *the components are assembled on a flexible substrate using fluidic self-assembly and* ***b_2.*** *The assembled components are transferred to a stretchable (EcoFlex) substrate with metal interconnects.*

Figure 2.9A shows images of a prepared stamp. First, a Si substrate is patterned by dry etching (***a_1***) and coated with a thin layer of Trichloro(octadecyl)silane (Sigma-Aldrich) to reduce the surface adhesion inside a vacuum desiccator. PDMS mold is poured and cured on top of the patterned Si substrate and detached from the Si substrate as a transfer stamp (***a_2***). **Figure 2.9B** shows the donor substrate with assembled µ-components by fluidic self-assembly [227] on a kapton film (***b_1***) and the final rubber substrate after transferring the µ-components using the stamp (***b_2***). The yield of transferring µ-components is nearly 100%.

Transfer printing is compatible with a wide range of materials, and can be adapted to various subsequent methods as needed. **Figure 2.10** shows a few examples of transfer printed metal structure on different substrate that have been established and studied during this thesis. In the depicted examples, the metal structures are initially fabricated on Si carriers with sacrificial layers and transferred to various types of materials which include flexible substrates (***i***-***vi***), stretchable substrates (***vii***, ***viii***) and human skin (***ix***).

2.2.4. Direct Printing

Direct printing or writing method is also widely being used in stretchable electronics research. This includes inkjet printing, 3D printing, screen printing, and so on. These methods are relatively easy, cheap, and scalable to large area which makes direct printing a popular method [230, 231].

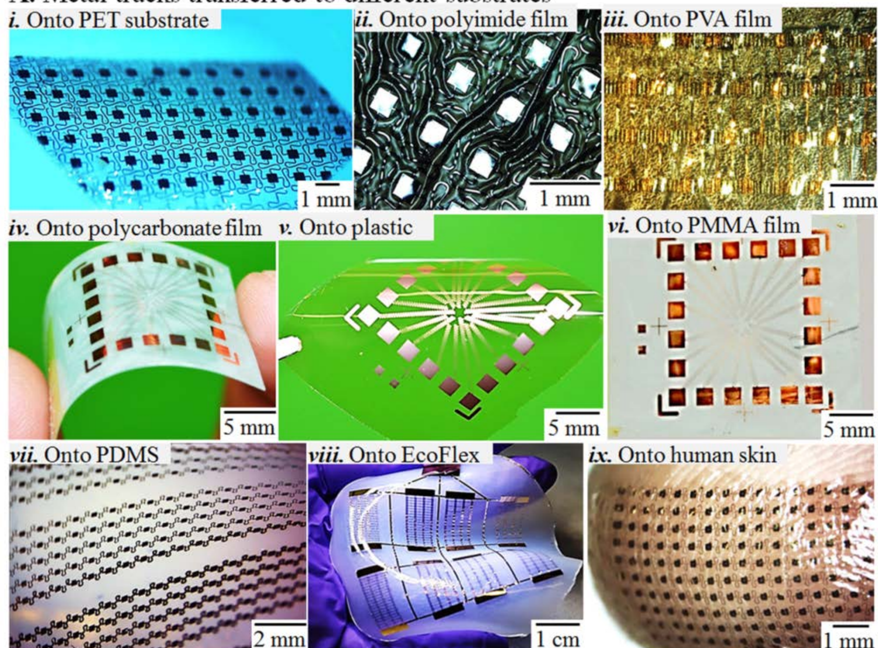

Figure 2.10: Examples of transfer printing on various substrates. *Thin metal structures are initially fabricated on Si carrier substrate with additional sacrificial layers, and has been transferred to various types of materials including flexible substrate (**i-vi**), stretchable substrate (**vii**, **viii**), and human skin (**ix**).*

Inkjet printing has become a great interest to the researchers in microfabrication due to its adaptability and low-cost manufacturing process [232]. Like a conventional inkjet printer, the method uses a liquid ink which is passed through a nozzle by capillary force to a printing substrate and the ink dries onto the substrate by evaporation [233]. The minimum feature resolution of the method is limited by several parameters such as the viscosity of the ink, nozzle diameter, substrate, distance between the nozzle and the substrate material, and so on. However, a resolution of 5 µm is possible using polymer inks for certain substrate [234].

3D printing has gained a great attention recently due to its wide range of materials choice and applicability. It has also been widely used in stretchable electronics research and became particularly popular due to the low-cost and easy manufacturing [235, 236]. For large area and cost-effective fabrication screen printing is relatively easy, and has also been used to realize stretchable electronic devices [237, 238].

2.3. Design

The first demonstrator of highly stretchable interconnects using geometrical design was reported by Gray and Chen in 2004, the study was inspired by 3D helical spring. They studied U-shape Au wires with different amplitudes, widths and thicknesses [14]. The maximum strain achieved by the group was 54 ± 2% which was very close to the theoretical strain value of 57%. Since then different groups studied numerous meander shape metal interconnects with various parameters.

Stretchable interconnects have been extensively studied by several research groups. Especially the Vanfleteren group from Ghent University explored this area in depth by computer-aided modeling and practical experiments. One of the first reports on this area by the group was in 2007 [239], where the group optimized the design previously reported by Gray *et al.* [14]. The studied designs were slightly different from the original design by Gray, the Vanfleteren group used horseshoe shape meander structures instead of U-shape structure. Addition to this, a finite element analysis (FEA) estimated that a multitrack interconnects would suffer less stress than a single track which was also verified experimentally. In a further study, the group systematically studied three metal tracks: elliptical shape, U-shape, and horseshoe shape with same amplitude (700 µm), wavelength (500 µm), width (90 µm), and thickness (15 µm) of the metals. The FEA shows that the horseshoe shaped metal tracks suffers about 39% less strain than the elliptical shape metal tracks [240]. They also observed that the strain can be reduced by reducing the width of the metal tracks [241].

Figure 2.11 schematically shows the main parameters those are used to design meander shape metal tracks. These parameters are defined during the design:

Meander radius- ***R***

Meander angle- ***θ***

Meander width- ***W***

Wavelength- ***λ***

Amplitude- ***A***

And, this parameter is defined during the fabrication:

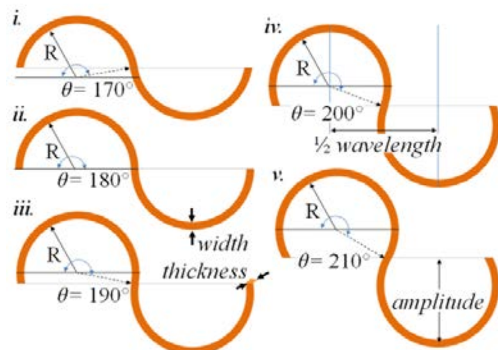

Figure 2.11: Different meander shape metal track design parameters. *The design parameters of the meander shape metal tracks those are important to study the stress profile during stretching test.*

Meander thickness- ***T***

All these parameters influence the stretchability and stress distribution of the metal tracks during the stretching tests. For example, with an ***R*** value of 450 µm design (***v***) in ***Fig 2.11*** shows a reduced stress value of 46% compared with design (***ii***) in ***Fig 2.11*** [239].

During this thesis, a number of meander shape metal tracks have been studied both using FEA and experimentally to find an optimized meander design. The initial study uses the conventional U-shape and horseshoe shape meander Cu tracks as shown in **Figure 2.12**. Both metal tracks use 50 µm wide and 10 µm thick Cu tracks, emerged in 1 mm thick Silicone rubber matrix. The other design parameters are varied as shown in the figures.

For FEA of the stress profile of the metal tracks, COMSOL multiphysics is used. The 3D model is designed similar to the real system, where metal tracks are submerged into a 1 mm thick silicone rubber matrix. The rubber is fixed from the left side and being stretched from the right side.

Figure 2.12A and **2.12B** show the computer simulated 3D model for U-shape and horseshoe shape metal tracks respectively when elongated 150% to its original

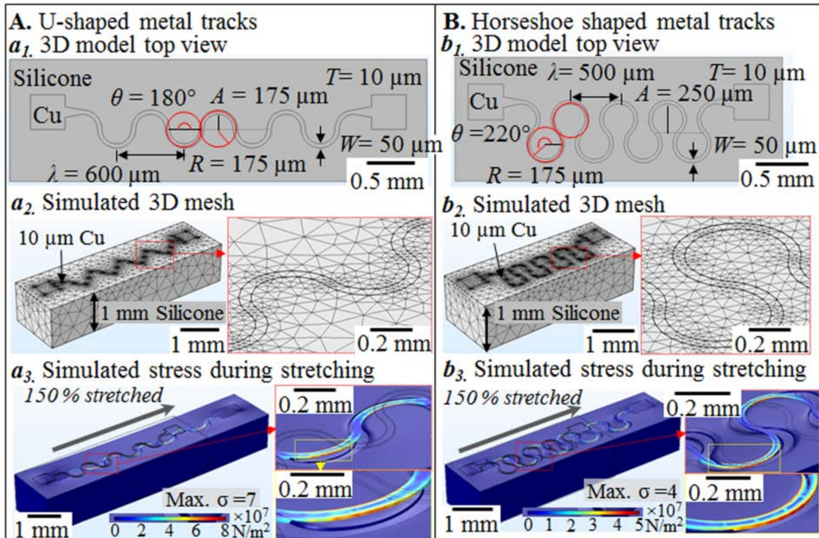

Figure 2.12: CAD simulation of the meander metal tracks. A. *U-shape metal track, top view of the model with metal track emerged in 1 mm thick EcoFlex (*$\boldsymbol{a_1}$*), simulated 3D mesh of the model (*$\boldsymbol{a_2}$*), and 3D stress profile of the system during 150% stretching (*$\boldsymbol{a_3}$*). Similarly, in* ***B.*** *horseshoe shape metal track, top view (*$\boldsymbol{b_1}$*), simulated 3D mesh (*$\boldsymbol{b_2}$*) and 3D stress profile (*$\boldsymbol{b_3}$*).*

length. Simulations predict maximum stress for the U-shape metal track is 7×10^7 N/m^2 and for the horseshoe shape metal track is 4.5×10^7 N/m^2. This means horseshoe shape metal track suffers less from the applied stress during stretching operation.

The FEA for both metal tracks show that during the stretching the rubber matrix feels nearly no stress, while the metal tracks suffer from high stress. This is expected since the rubber, in principle, can accommodate higher level of strain, and responses to the applied stress. However, the bulk Cu is intrinsically unable to responds to this high level of strain. As a result, the meander shape metal track responds to the applied stress by straightening its length.

The observation of the stress profile of the metal tracks shows two primary characteristics: *first,* (***Fig. 2.12 a_3*** & ***b_3*, insert, top**) the high stresses regions are the upper and lower turning points of the meander loops, while the connection regions of the metal tracks show very low stress. *Second,* (***Fig. 2.12 a_3*** & ***b_3*, insert, bottom**) the metal tracks show high level of stress at the inner and outer surfaces of the loop regions.

To understand the physical mechanisms of these characteristics let us consider a simpler model where only a horseshoe shape metal track is computed without rubber substrate keeping the width and the thickness of the metal track same. The stress profile of the metal track during 150% elongation is presented in **Figure 2.13**.

2.3.1. Macroscopic Stress Distribution

For the macroscopic stress distributions over the metal track, let us draw a line (***Fig. 2.13A***) through the center points of the meander track which are actually the connecting points of each loop. This red dot line is the neutral axis in the xy-plane of the metal track. During the stretching operation this neutral axis follows the strain of the rubber matrix as long as it remains attached to the substrate, thus it feels relatively low stress. However, a different scenario is observed in the outside regions of this neutral axis which cannot follow the strain of the substrate. Since the metal track is not intrinsically stretchable, the geometrically patterned track tries to straighten itself in respond to the applied strain which results in torsion ($\boldsymbol{\eta}$) of the

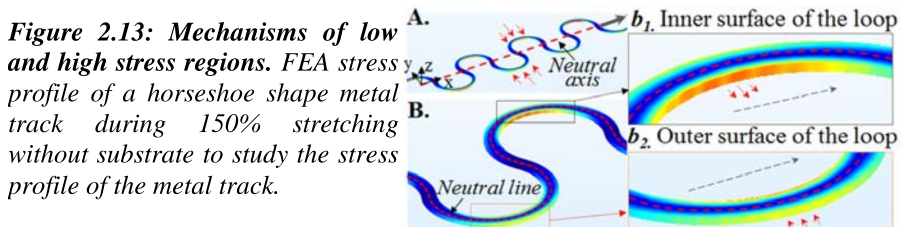

Figure 2.13: Mechanisms of low and high stress regions. *FEA stress profile of a horseshoe shape metal track during 150% stretching without substrate to study the stress profile of the metal track.*

metal tracks. The red dot arrows in ***Fig. 2.13A*** show that the outside loops from the neutral axis feels torsion towards the neutral axis due to the applied strain. A consequence of this mechanism is that the metal tracks from these high torsion regions detach from the rubber substrate faster than the neutral plane. This leads to macroscopic twists in the metal tracks. Physically, the resultant torsion (η) is proportional to the change in the amplitudes (ΔA) of the metal tracks due to the stretching.

i.e. $\eta \propto \Delta A$ (2.3)

Where, ΔA = ***Original amplitude of the metal track – amplitude after stretching***

Note that the value of ΔA depends on the total stretching of the metal tracks.

2.3.2. Microscopic Stress Distribution

The second characteristic is that the metal tracks show high level of stress at the inner and outer sides of the loop regions, is shown in ***Fig. 2.13B***. Here, another red dot line is drawn along the middle of the meander metal track. The inserts show the inner (b_1) and outer sides (b_2) of the loops. Similar to the macroscopic stress distribution, the red dot line represents a neutral line within the metal track. The stress along this neutral line of the metal track is minimum during stretching operation (*gray arrow*), and gradually increases towards the sides and is maximum at the side surface. The inner and outer sides feel different forces due to the applied stress (*red arrows* in b_1 and b_2).

As mentioned earlier, during the stretching the loop regions try to move to the neutral axis (***Fig. 2.13A***) of the metal track. To do so, the inner side at the loop regions of the metal track feels tensile strength, while the outer side feels compressive strength. These two different forces result in a microscopic torque (τ).Physically, the microscopic torque, τ at the loop region is:

$\tau \propto \varepsilon W/T$ (2.4)

Where, ε is the strain in the metal track, W is the width and T is the thickness of the metal track. This means that for a fixed strain, the resultant torque in the loop region depends on the physical dimensions of the track. According to the equation, metal track with an equal width and thickness would be ideal for multidimensional stretching which is sometimes challenging. Also note that the different stress values of the metal track in this region are due to the fundamental material properties. The tensile strength (inner side) value is higher than the compressive strength (outer side) [242].

From the above discussions, it is clear that one of the main limitations of designing the meander shape metal track is the stress distribution. Since the idea of

meander shape metal track is to use the geometrical configuration to enable stretchability so few of the design parameters are fundamentally constrained. However, significant improvement is possible by designing and engineering a smart metal track that can accommodate a higher level of strain and is able to distribute the stress over a larger area to minimize the torque and twist in the metal track.

During this research, a novel idea is developed to minimize the torque and twist in the high-stress regions by letting the torque propagate to relatively low-stress regions. A reasonable solution to this problem can be to adjust the width of the metal track along its length to accommodate stress, twist and torque locally. The mechanism would be that the high-stress regions, which are the upper and lower turning points in the conventional meander structure, would produce the torque. However, those points will not respond to the produced torque; rather the torque should propagate to other locations due to the variation of the widths in the tracks. Based on this principle two designs are initially studied which are referred as "stress adaptive metal tracks".

2.3.3. Stress Adaptive Metal Tracks

Design 1

In this design (***Fig. 2.14A***), the high-stress loops in the conventional meander track are replaced by narrow ($W = 40$ µm) meander loops, and these narrow meander loops are connected by wider ($W = 50$ µm) meander structures. **Figure 2.14A** shows the FEA of this design (***Fig. 2.14A*** a_1) and the stress profile of the metal tracks while elongated to 150% (***Fig. 2.14A*** a_2). The insert shows the magnified view of the high-stress regions in the tracks. The design shows a maximum stress of 4×10^7 N/m^2 in the loop region. However, experimentally it is observed that the produced torque in the loop cannot propagate to the surrounding metal track. This is because the connecting metal tracks are wider than the loop regions which results from a higher rigidity.

Design 2

In the second approach (***Fig. 2.14B***), the design has been changed by connecting two wide ($W = 50$ µm) inverse meander loops by a narrow ($W = 40$ µm) meander structure. The narrow meander tracks are placed centering on the neutral plane as previously shown in figure 2.13A. **Figure 2.14B** shows the FEA of this design and the simulated mesh (***Fig. 2.14B*** b_1). The simulated stress profile of the metal tracks is shown (***Fig. 2.14B*** b_2) while elongated to 150% with the magnified view of the high stress regions in the track (***insert***). The design shows a maximum stress of 3×10^7 N/m^2 in the loop region. This is a significant improvement in maximum stress distribution.

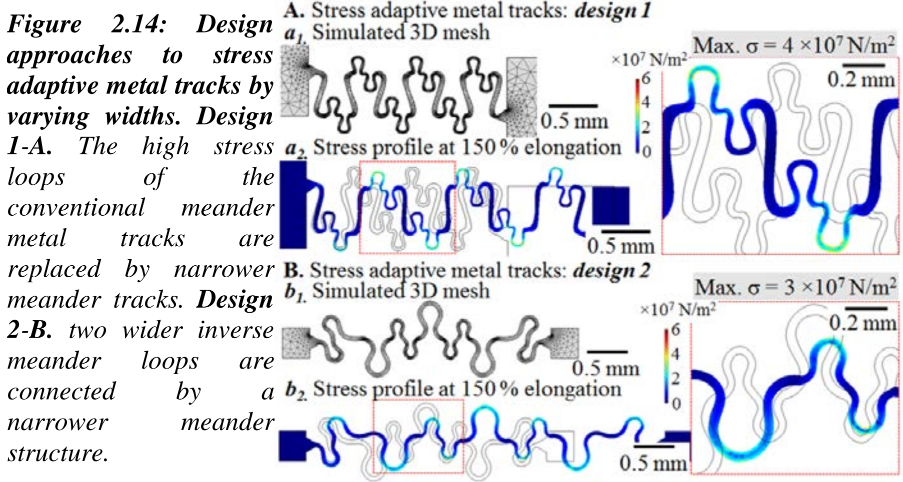

Figure 2.14: Design approaches to stress adaptive metal tracks by varying widths. Design 1-A. *The high stress loops of the conventional meander metal tracks are replaced by narrower meander tracks.* ***Design 2-B.*** *two wider inverse meander loops are connected by a narrower meander structure.*

Furthermore, the experimental observation of the second design shows a clear improvement in the stress distribution mechanism during stretching test. As discussed previously, the aim of the variation in the widths is to transfer the twist from the high stress region to lower stress regions. **Figure 2.15** shows images of the three different designs in original state (***left column***), after stretching test (***middle column***), and failure location (***right column***). The first two (***Fig 2.15 A*** & ***B***) represents conventional meander shape metal track designs and the last metal track (***Fig 2.15 C***) is the improved stress adaptive design.

The middle column shows an interesting mechanism of the different designs during and after stretching. For example, yellow circles in ***Fig 2.15 A*** & ***B*** present the torsion regions which occur due to the macroscopic stress distribution over the metal tracks. FEA of the metal tracks suggests that these regions suffer from a lower level of stress during the stretching test (discussed in *section 2.3.1*). On the other hand, red circles in ***Fig 2.15 A*** & ***B*** indicate the torque, produced due to the different compressive stress and tensile stress in the high-stress regions which is a result of microscopic stress distribution at the loops (discussed in *section 2.3.2*). Experimentally, it is observed that these are the primary locations where failure occurs in the conventional designs (right column).

Considering these facts, design in ***Fig 2.15 C*** shows an enormous improvement, but not yet entirely, in the stress distribution and its effect over the metal tracks to minimize the torque in the high-stress regions. In this design, as aimed, the torque produced in the high-stress regions propagates to the low-stress region which is narrower and placed near to the neutral axes. As a result, the narrow metal track produces a twist over its own loop. Since this loop is close to the neutral axes than

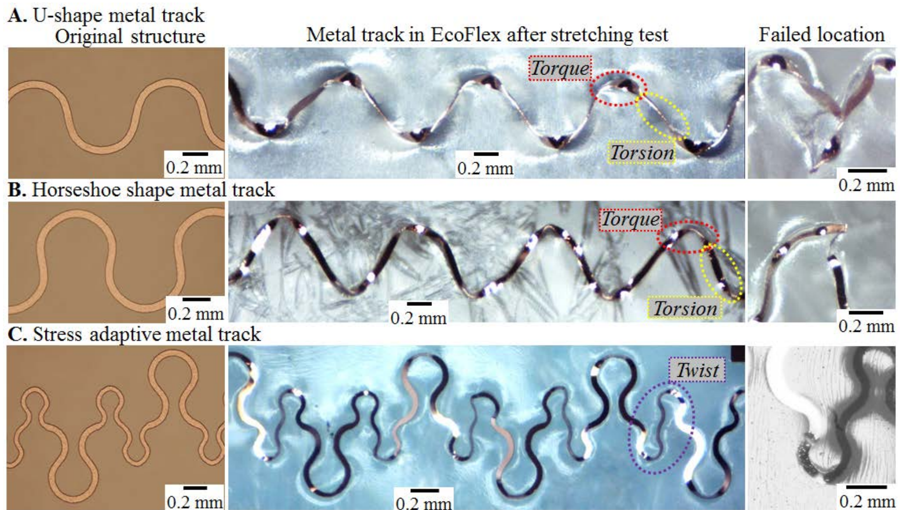

Figure 2.15: Comparison among three metal track designs. A. *and* ***B.*** *represent conventional U- and horseshoe shape metal tracks respectively, and* ***C.*** *is the improved stress-adaptive metal track design. The first column is the original structure, second column is the metal track in EcoFlex after stretching test, and third column is the failure location of the metal track.*

the wider loops, it fails less. However, the stress adaptive metal track still fails occasionally at the junction of the narrow and wide loops.

This new stress adaptive meander metal track design has been used to demonstrate various electronic systems in this thesis for stretchable metal interconnects. Further quantitative study of the stress adaptive metal track will be presented later with active devices.

In summary, the first part of this thesis provides an introduction of the stretchable electronics and discusses the applications, importance and possibilities of this emerging technology. The novel idea of metamorphic electronics is also introduced which advances the stretchable electronics in a new dimension.

A detail discussion and current state-of-the-art have been provided on stretchable electronics in terms of devices, materials, processing, and designs. Along with the discussions a few results have been presented as proof of concepts. In the end of the first part, a new stress adaptive meander metal track design has been presented with a detailed design rationale.

PART II

EXPERIMENTS AND RESULTS

Light emitting diodes (LEDs) are one of the simplest elements to demonstrate functional electronic and optoelectronic systems. LEDs usually have only two electrical contact pads. Moreover, the entire functionality of the system can be studied just by our bare eyes if the LEDs emit within visible wavelengths. Due to these simplicities bare dies single wavelength LEDs are choose to demonstrate the first metamorphic optoelectronic systems in **chapter 3** of this thesis. Three-terminal surface mount μ-transistors are presented in **chapter 4** as a more complex metamorphic electronics demonstrator. In **chapter 5**, **6** and in **chapter 7** more complex integrated metamorphic electronic systems are presented. **Chapter 8** represents the accumulation of a few additional devices, and in **chapter 9** conclusions.

CHAPTER 3

Metamorphic Optoelectronics

3.1. Manufacturing of mPCBs

3.1.1. Fabrication of stretchable metal tracks

3.1.2. Assembly of the components on hard carrier

3.1.3. Rubber encapsulation and detachment

3.2. Design

3.2.1. Stretchable metal tracks

3.2.2. Reinforcement bars

3.3. Metamorphic Optoelectronic Devices

3.3.1. Inflation of uniform membrane

3.3.2. 3D guided deformation

3.3.3. Inflation of patterned membrane

In this chapter, a method to manufacture single-layer stretchable printed circuit boards is described for metamorphic optoelectronic applications. Unlike most reports, this approach delays the use of the stretchable rubber support until the end of the processing sequence. Specifically, the entire circuit containing interconnects and unpackaged chips or chip-scale packaged surface mount devices are fabricated on a hard carrier.

3.1. Manufacturing of mPCBs

Figure 3.1 provides an overview of the main process steps to realize metamorphic printed circuit boards (**mPCBs**) next to photographs of corresponding test structures. The depicted approach is different from other methods, which apply the metallization to the rubber support and mount the components on top and, suffers from a lower level of alignment and fixation. Instead, a hard carrier is used, mounted components and metal tracks are fixed and surrounded with EcoFlex, and subsequently peeled off to complete the device. The hard carrier is important since it enables: (*i*) alignment and registration, (*ii*) high temperature processing, (*iii*) conventional robotic chip placement or (*iv*) advanced chip placement of microscopic dies using fluidic self-assembly [227], and (*v*) “on-hard-carrier” device tests.

3.1.1. Fabrication of Stretchable Metal Tracks

Figure 3.1A describes the first part of the processing sequence of fabrication of stretchable metal tracks on hard carrier. A 500 µm thick Si wafer (MicroChemicals, Ulm, Germany) is cleaned in H_2SO_4 + H_2O_2 for 15 minutes and rinsed with DI water. A thick layer of poly(methyl-methacrylate) (**PMMA**) (AR-P 6510, Allresist, Strausberg, Germany) is spin coated at 1500 rpm and baked on a hot plate for 3 minutes at 180 °C. Subsequently, an 8 µm thick polyimide (**PI** 2611, HD Microsystem, Neu-Isenburg, Germany) is spin coated at 1500 rpm and prebaked at 180 °C for 10 minutes on a hotplate and later fully cured in a convection oven at 200 °C for 5 hours under N_2.

The PMMA and the PI layer acts as a release and a peeling layer respectively. The peeling layer acts as a mechanical support during the detachment process (***B***) and is only removed after the fabrication of the stretchable circuit is completed (***C***). The function of the PI pealing layer is to provide a mechanically flexible but not stretchable peeling foil, which has a low adhesion to the PMMA (*blue*) coated carrier (*gray*) and a strong and adjustable adhesion to the metal, circuit elements, and rubber matrix on top. The required adhesion to the rubber matrix and metallization layer is achieved by plasma activation of the polyimide surface (30 SCCM Ar, 100 W RF power for 2 minutes).

As a metallization layer, a 20 nm/200 nm thick sputter coated layer of Ti/Cu has been used. The wafer is then patterned for electroplating with photolithography using negative resist AZ 15NXT (MicroChemicals) and a subsequent standard descumming process (5 minutes, 100 W RF power, 50 SCCM O_2) is performed to remove any residues from the patterned metal. Then a thick layer of Cu (10 µm) is electroplated on top of Cu seed layer using Cu 100 electrolyte (nb technologies, Bonn, Germany). A low current density (~15 mA/cm^2) is applied to grow a smooth Cu layer at room temperature. Thick metal tracks (>5 µm) are found to be more robust than previously used thin (<1 µm) metallization layers [46]. Later, the resist is stripped using standard remover (NI555 at 80 °C) and a subsequent chemical etching process is carried out to etch the 200 nm Cu seed layer using standard Cu etchant (HNO_3) and 20 nm Ti in 1% HF.

A set of lithographic steps involving registration is required to define the locations of the solder bump based interconnects (***a_2***); a patterned 10 µm thick photoresist layer (AZ 15 NXT) is used with openings to the contact pads to apply the depicted solder bumps (*bright gray*) using a dip coating process in a liquid solder bath (Indalloy #117, MP. 47 °C, Indium Corp., NY) [228]. The fabrication process is completed after removing the second layer of photoresist.

3.1.2. Assembly of the Components on Hard Carrier

The process is compatible with various types of chip attachment and assembly methods including solder bump based interconnects, flip-chip die attach, robotic pick-and-place or engineered self-assembly using molten solder. In the demonstrated case, a semi-automated pick-and-place machine is used to assemble the components under a microscope in combination with solder bumps to achieve alignment [229]. In the depicted demonstrator two terminals chip-scale (L=1 mm, W=0.6 mm, H=0.2 mm) surface mount LEDs (459 nm, Creative LED GMBH, Schaan, Liechtenstein) are used. Specifically, the LEDs are placed onto the solder bumps which are located on the receiving substrate. Reflow of the solder causes the chips to attach and self-align as a result of the reduction of the surface free energy of the solder.

The approach enables "on-hard-carrier" functionality tests (***Fig. 3.1A, a_3***). The illustrated result shows an array containing 80 LEDs under test. The "on-hard-carrier" functionality test can be compared with the function after release and during operation of the stretchable circuit which is important to establish and overcome failure modes.

3.1.3. Rubber Encapsulation and Detachment

Figure 3.1B describes the rubber encapsulation and detachment process. A castable 3 mm thick and thermo-curable (room temperature, 15 hours) layer of EcoFlex (EcoFlex 00-30, Smooth-On, Spaichingen, Germany) has been used as a stretchable encapsulation layer (***B_1***). A 5 minutes long O_2 plasma activation step of

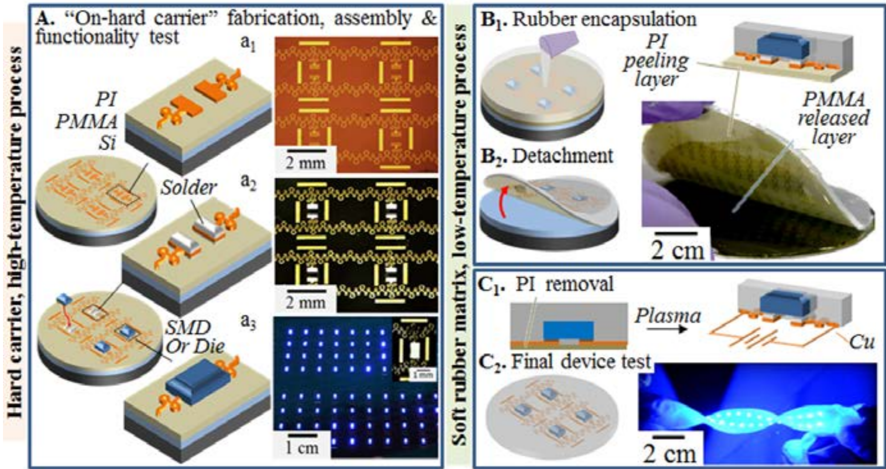

***Figure 3.1: Metamorphic printed circuit board process flow** delaying the introduction of the rubber substrate towards the end of the processing sequence and increase level of fixation of the parts and metallization layer when compared to reversed "on-rubber" mounted structures. **A.** "On-hard carrier" fabrication, assembly, and functionality test. (**a_1**) PI peeling (greenish gray) layer, metallization (orange), (**a_2**) solder bumps (bright gray), (**a_3**) die attach, and on hard carrier functionality tests follow standard PCB fabrication, alignment, mounting, and device testing procedures. **B.** Rubber matrix application and detachment; the PI peeling layer (green) is used as a common non-stretchable film like support during the peeling process. The PMMA remains on the hard carrier. **C.** Removal of the non-stretchable PI peeling layer leaving all faces surrounded by EcoFlex with the exception of the metallization layer which can be contacted from the bottom.*

the assembled circuit elements is used to increase the bond strength to the EcoFlex. The plasma activation step reduced the onset of cavitation and delamination during stretching.

A solvent-free detachment process (***B_2***) has been developed to detach the components and stretchable circuit from the hard carrier and to increase the range of devices and components that can be used. For example, the plastic package of the LED gets damaged in Acetone which is commonly used to remove PMMA. Instead of using a solvent the detachment process uses the differential interfacial adhesion of the stacked layers to define an interface that can be cleaved. Specifically, the PI (*greenish gray*) layer has a low adhesion to the PMMA (*blue*) coated carrier. Moreover, the rubber matrix is strongly bonded to the PI (*greenish gray*) layer using the previously mentioned plasma activation step which leads to the formation of covalent bonds at this interface. As mentioned, the detachment process works particularly well using the introduced PI (*greenish gray*) film which forms a uniform

non-stretchable and supporting peeling layer beneath the circuit. The non-stretchable nature and low level of adhesion to the PMMA coated carrier is important to eliminate the introduction of defects during the detachment process. In other words, the sandwich structure is reinforced by the PI film. It is not stretched during the detachment process and no defects are introduced during this step. A video has been recorded to illustrate the detachment process in which the video shows the detachment of an LED array while being operated [243]. The LEDs continue to light up during the detachment process.

After detachment the Cu tracks are still covered with the PI peeling foil which needs to be removed to complete the structure (***Fig. 3.1C$_1$***). Electron cyclotron resonance (ECR) plasma etching (40 SCCM O_2, 10 SCCM CF_4, 100 WRF, 30 minutes at 0.0025 mbar, SQ160 Roth and Rau AG) has been used to accomplish this step.

The final stretchable device has a surface mount like geometry, which means one of the faces of the copper tracks is accessible for electrical contacts leaving the other three faces protected with EcoFlex. This arrangement is different from others produced in earlier reports. In the depicted case, the metal tracks and components are not "floating" on top of the rubber support. Instead, at least three faces are surrounded by EcoFlex to increase the level of fixation. Moreover, the active devices remain completely embedded in EcoFlex (surrounded and under-filled), which provides protection during plasma etching, processing and final operation. The increased level of fixation and underfill with EcoFlex in the device region improves the maximum level of elongation before the metal tracks detach from the rubber support. It is also possible to fully encapsulate the circuit using a second EcoFlex layer.

3.2. Design

Different design aspects have been studied in this research to develop a new meander shape metal track as discussed previously in ***section 2.3*** and the receptor pads for the components to provide stress relieve in critical locations. The following discussions will focus on measures to provide stress relieve in the metal track region and in the contact pad region.

3.2.1. Stretchable Metal Tracks

The presented approach (***Fig. 3.2A***) uses a variation of the well established "horseshoe shape conductors" which were originally reported by Gray and Chen [14]. Different from the original design (***A***, ***left***), new meander shape metal ribbons vary in widths and radius of curvatures (***A***, ***right***). Moreover, reinforcement bars are introduced to offer stress relief in the contact pad region connecting the devices

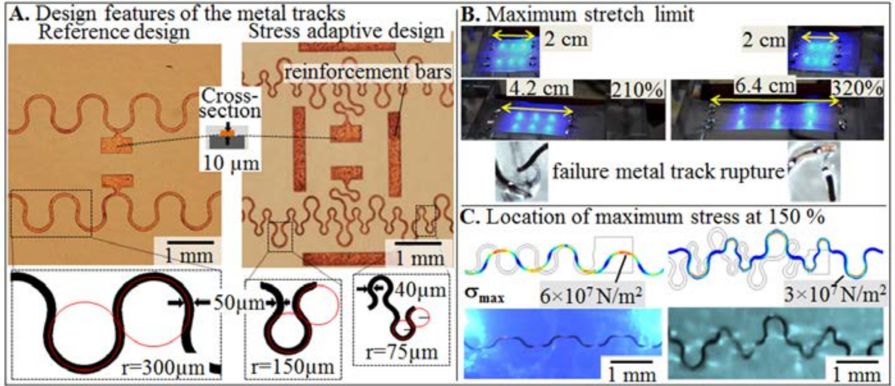

***Figure 3.2: Comparison of two metal track designs,** stretch limit, location of maximum stress: reference **(left)** and stress adaptive design **(right)**. **A.** Photo of a reference design without strain relieve (**left**) and the stress adaptive design altering the width and adding reinforcement bars in critical locations (**right**). **B.** Last video frame of functioning LED array stretched to 210% (**left**) and 320% (**right**) before failure occurred; metal tracks rupture beyond this limit (**insert**). **C.** Computed stress profile at 150% x-axis stretch; the peak stress value is reduced by a factor of 2 in the stress adaptive design; the computation and photographs depict the onset of out-of-plane flexing and torsion.*

where defects occurred. The two depicted designs use the same wire length (68 mm to span an un-stretched 20 mm distance).

As mentioned, different from the original design (***left***) new meander shape metal ribbons vary the widths and radius of curvature (***right***) which named as the “stress adaptive” metal tracks (SAMT) in chapter 2. The rational for this design change is as follows: The weakest points in the reference structure are the upper and lower turning points of the meander which are inline with the direction of elongation. These locations are exposed to high levels of torque and stress (previously discussed in ***section 2.3***). Torque propagates to these points due to the build up of higher and lower levels of stress at the outer and inner edges of the relatively wide and uniform meander. It eventually leads to premature rupture of the metal track in this region. A combination of two measures is used to improve this section (***right***).

Table 3.1 provides a summary of various metrics comparing the reference with the stress adaptive design. A computer controlled stretching platform is used in the long term cycling tests. The metrics are based on the following experiments:

Table-3.1: Study of metal track region.			
Single-stretch experiments	Reference design	Stress adaptive design	Improvement factor
(*i*) "**Single-stretch limit to cause a *metal track rupture*** "			
Maximum elongation limit	215%	320%	1.5x
(*ii*)"**Single-stretch limit to observe *onset of metal track detachment***"			
Maximum elongation limit	160-180%	205-245%	1.3x

Multi-cycle experiments	Reference design	Stress adaptive design	Improvement factor
(*iii*) **"Cycle count at 200% elongation to cause *full metal track detachment*"**			
Counts	30	>500	>16x
(*iv*) "**Cycle count at 150% elongation to cause *metal track rupture***"			
First conductor to fail	252	3411	13x
Last conductor to fail	1312	6280	5x
Average conductor to fail	1120	5840	5x

(i) "Single-stretch limit to cause metal track rupture" is an experiment depicted in **Figure 3.2B**, where the structure is stretched until the metal track ruptures. The stress adaptive design sustained 315% (±12%, from 8 measurements) (elongated by a factor of 3.15) before permanent electrical failure occurs (***B, right***). This is close to the theoretical limit of 340% considering the ratio between the 68 mm long meander shape metal track connecting the 20 mm spaced (un-stretched) contact pads. The established reference structure with uniform width (50 µm) sustained 215% (±16%, from 8 measurements) during the same test (***B, left***). In both cases rupture occurs in the upper and lower turning points of the meander. These points are inline with the stretch direction (discussed earlier). A finite element computation (COMSOL Multiphysics) of the stress profile next to a photograph of the test structures stretched to 150% confirms that the upper and lower turnings are the locations of maximum stress. A reduction of the peak stress value by a factor of 2 is calculated for the stress adaptive design (***Fig. 3.2C, right***) which explains why it can be stretched to a higher level.

(ii) "Single-stretch limit to observe the onset of metal track detachment" represents an experiment to study the onset of metal track detachment. Careful observation of both test structures reveals that the metal tracks begin to detach from the EcoFlex matrix when being stretched to high levels. A total of 16 samples (8 each, for reference and stress adaptive design) have been characterized to record the onset of detachment under a microscope. The onset occurred between 160-180% and

205-245% in the reference structure (***left***) and stress adaptive design (***right***), respectively. In both structures detachment starts at the locations where the twist in the metal structure is largest. The location is again the upper and lower turning points of the meander which are inline with the direction of elongation. The computation (***Fig. 3.2C***) provides insight into the reason; again, the detachment and delamination is a result of buildup of higher and lower levels of stress at the outer and inner edges of the meander, which leads to a flexing and torsion and eventual detachment of the ribbon like metal tracks. Detachment of the metal track can thus be understood as a mechanism to provide stress relief; the structure is no longer coupled to the rubber substrate and a distribution of stress is possible reducing the hot spots. However, for real applications detached metal tracks need to be prevented for several reasons. First, partially detached metal tracks are insufficiently stable for the stretchable PCBs to be touched by hand. Second, the detached region commonly gets larger with the number of stretch and release cycles. The metal tracks begin to flex and bend into unpredictable directions. Such adverse conditions lead to random arrangements and electrical shorts between tracks (***Fig. 3.3***). Considering long term use, the level of deformation should thus be limited to values where no detachment occurs.

Figure 3.3: Failure due to detachment. *Photograph of a failed structure after a total of 5 stretch and release cycles at 220%. Metal tracks detached from the rubber substrate and cause shorts.*

(iii) "Cycle count at 150% to cause complete metal track rupture" is based on an experiment where a larger data set is acquired to determine the average and range between the first and last failure. The test sample containing 16 meanders; each meander is spanning a non-stretched distance of 20 mm; one half uses the stress adaptive design (***Fig. 3.4 left****, yellow box*, designated with the letter ***N***), and the other half uses the reference design (***Fig. 3.4 right****, green box*, designated with the letter ***R***). A modest 150% stretch and release cycle is applied in this test. A single frame and magnified section of a larger dataset is shown in **Figure 3.4A**, where the left figure shows the metal tracks at its original state (un-stretched) and the right figure shows the metal tracks when stretched to 150%. **Figure 3.4B** shows frames from the recorded video during the multi-cycle stretching test. Each frame is taken after each failure. The "first conductor to fail" fails after 252 and 3411 cycles in the reference (***iii***) and in the stress adaptive design (***vii***) respectively. In relative terms, the first failure is delayed by a factor of 13.5. The "last conductor to fail" fails after 1312 and 6280 cycles in the reference (***vi***) and in the stress adaptive design (***x***) respectively.

On average, the occurrence of rupture considering the 20 mm long tracks is delayed from 1120 to 5840 cycles using the stress adaptive design. This represents a 5 fold improvement.

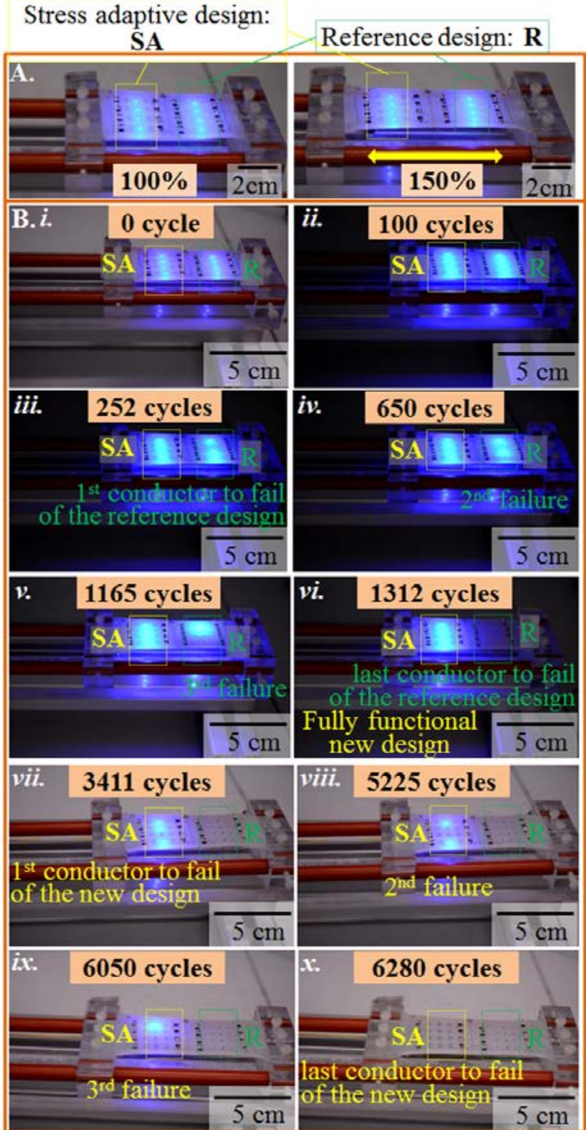

Figure 3.4: Multi-cycle stretch-release test. *Images from the long term cycling tests comparing the reference design (**green dotted region**) with the stress adaptive design (**yellow dotted region**). **A.** Pristine test structures in the relaxed (**left**) and 150% stretched (**right**) condition at the outset of the test. **B.** Recorded images of the onset of failure as a function of cycle counts using a 150% stretch and release cycle. The left column of the test sample presents the stress adaptive design (the locations are designated with the letter **SA**) and the right column presents the reference design (the locations are designated with the letter **R**). The "1st conductor to fail" of the reference design occurs after 252 cycles (**iii**). After 1312 cycles all the reference designs fail, while the stress adaptive design remains fully functional (**iv**). The "1st conductor to fail" of the stress adaptive design occurs after 3411 cycles (**vii**). It took 6280 cycles to cause a complete failure of the stress adaptive design (**x**).*

3.2.2. Reinforcement Bars

Figure 3.5 describes the reinforcement bars to protect the contact pad and intermediate surrounding from high levels of stress; corresponding metrics are summarized in ***Table-3.2.*** The rational of reinforcement bars is to locally change the material properties of the sPCB to have reinforced islands where the chips are assembled. Ideally as the PCB is stretched globally the islands are not stretched. Consequently, the (*i*) shear force acting on the assembled components, (*ii*) lateral pull on the contact pads and (*iii*) force acting on the metal track connection can be reduced. Out of the three, the metal track connections to the pads fail first in the experiments. The ideal design (different from what is shown) would be a sufficiently thick non-stretchable frame, for example, using a second patterned metallization layer underneath the assembled chips. However, even using a single metallization layer, reinforcement bars can be defined and located in the vicinity of the components to offer some protection. For example, experimentally, it is found that the reference design (***Fig. 3.5***, ***left***) without reinforcement bars is sensitive to fail if elongated in the y-direction. Specifically, the intermediate metal track connection to the pad (***red circle***) fails due to rupture at elongations exceeding 200% and this value is improved to 325% using the reinforcement bars (***Fig. 3.5B***, ***right***).

Table-3.2: Study of contact pad region.			
Single-stretch experiments	Reference design	Stress adaptive design	Improvement factor
(*i*) Bare contact pad displacement without and with reinforce.			
x-direction	-8%	-4%	2x
y-direction	+ 50%	+ 20%	2.5x

(iv) "Bare contact pad displacement without and with reinforcement bars" represents an experiment to study the level of strain reduction in the pad region and intermediate surrounding as a result of the reinforcement bars. The results are shown in **Figure 3.5** presenting computation data (COMSOL Multiphysics) next to photographs of the stretched structures. The data compares the displacement of the contact pads with (***right***) and without (***left***) reinforcement bars as the structure is stretched to 150% of the original length along the x-axis (***A***) and y-axis (***B***), respectively. **Note**: The structures are studied without assembled chips to isolate the effect of the reinforcement bars. As the rubber matrix is stretched the distance between the pads changes; the smaller the change the better; the distance is proportional to the force acting on the metal track connection and joints once the chips are assembled. The level of protection due to the reinforcing bars can be seen comparing the left with the right side.

First, the elongation along the x-axis (***Fig. 3.5A***) when compared to the y-axis (***Fig. 3.5B***) is far less critical considering the depicted pad layout. Only a small reduction (-8%, ***left***) in the pad distance, which is barely visible (-4%, ***right***) in the reinforced design, can be detected as the structure is elongated along the x-axis (***Fig.***

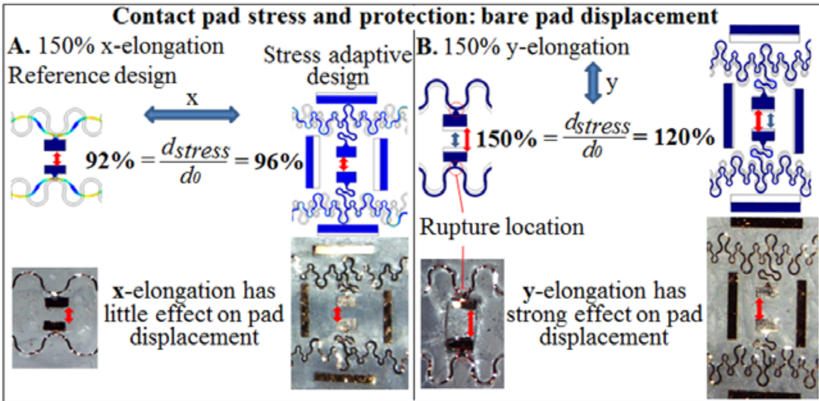

***Figure 3.5: Study of the reinforcement bars.** Comparison of two metal track designs, level of strain relieve in the contact pad region: reference **(left)** and stress adaptive design **(right).** Computed and measured contact pad displacement with and without reinforcement bars at a 150% stretch along the x (**A**) and y-axis (**B**), respectively. y-axis elongation (**B**) is far more critical, where the pad distance and strain follows the external strain and no strain protection is recorded in the reference design (**left**). In comparison, the reinforced structure (**right**) leads to a 2.5 fold strain reduction.*

3.5A). This means, considering the strain on the pads and connecting wire, both are fairly robust when being stretched in the x-direction.

However, this is no longer the case for the y-direction (***Fig. 3.5B***). For example, in the reference structure (***left***), the relative change in the pad distance is equal to the relative external elongation; no protection of the pads and connecting wire can be observed. This leads to premature interconnect failure in the pad region once a chip fixes the pad distance due to high levels of stress. As a result, reinforcing bars are required to maintain a sufficient level of robustness to allow stretching the structures in the y-direction. For example, in the stress adaptive design (***right***) a 2.5 fold reduction of the relative external elongation is achieved in the pad region, which enabled the realization of the inflatable metamorphic electronic demonstrators discussed below where a biaxial stress resiliency is required.

3.3. Metamorphic Optoelectronic Devices

A key mechanism to form metamorphic electronics is controlled deformation of stretchable devices. It is possible to obtain electronic systems in very complex geometrical shapes by introducing different forms of deformations. A few deformation mechanisms and resultant products are shown here as proofs of concept.

3.3.1. Inflation of Uniform Membrane

Figure 3.6 shows the experimental results of inflatable metamorphic lighting structures. In the depicted case a uniform 3 mm thick layer of EcoFlex is used (***Fig. 3.6A***) to prepare several different topologies. All test structures uses an 8 cm in diameter circular polymer ring to form a pressure seal and electrical connections with an opposing surface. The test structure (***Fig. 3.6A***) contains 24 LEDs and morphs from a planar (***i***) to a partial hemisphere (***ii***) to a full hemisphere (***iii***) shape. The air inflation of the planar membrane to a hemisphere is recorded while the device under operation, the video shows that all the LEDs function properly and are not affected due to the inflation process [244].

Figure 3.6B shows results of inflation of two uniform 3 mm thick layer of

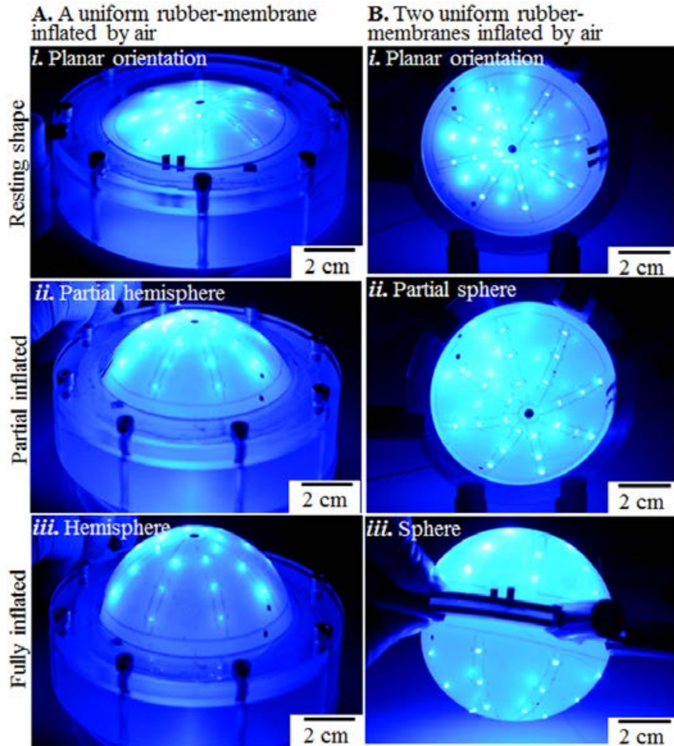

Figure 3.6: Inflation of uniform rubber membrane. *Air inflation of a uniform rubber membrane (**A**) and two uniform rubber membranes (**B**) produce hemisphere and full sphere respectively. A different level of inflation results different shapes from planar (**i**), to a partial hemi-/sphere (**ii**), to a full hemi-/sphere (**iii**). The rubber membranes are sealed in circular rings and air is pumped from side through an air valve.*

EcoFlex membranes which produces a full sphere. The structure (***Fig. 3.6B***) morphs from a planar (***i***) to a partial sphere (***ii***) to a full sphere (***iii***) [245].

During inflation the rubber matrix and the electronics in it faces bi-axial stretching which is different from one directional linear stretching. For such cases the system requires to sustain equal level of stretching both in x- and y- axis. Assuming the radius of the planar oriented sample in resting shape (***Fig. 3.6A i***) has a radius of ***r*** which gives an area of

$$A = \pi \times r^2$$

For a fully inflated hemisphere (***Fig. 3.6A iii***) with same radius, the area is

$$A = 2\pi \times r^2$$

This means that the inflation of a planar surface to a hemisphere requires 200% biaxial elongation to its original length. As discussed before, the depicted device can be stretched up to 320%, which is far above of the stretching required to form a hemisphere or sphere.

3.3.2. 3D Guided Deformation

Further control to the morphological changes of the metamorphic electronics is possible by using additional 3D guided shapes. For example, inflation of a rubber membrane within a 3D cage will results various geometrical shapes. This shape could be more interesting and more complex by inflation of two membranes within a spherical cage with different types of openings in two sides.

To demonstrate this concept a relatively simple cage is used as shown in **Figure 3.7A**, where a uniform rubber membrane is inflated within a cage. The membrane deforms from planar shape (***i***), to a partial hemisphere (***ii***), and to a more complex topology (***iii***). The cage is printed using a 3D printer; this gives a large freedom to the design and to the shapes. In **Figure 3.7B** a slightly different approach is shown, where a glass funnel is used as a vacuum forming guide. Air is sucked from the top of the funnel as a result the rubber membrane deforms from planar (***i***), to a hemisphere (***ii***), and then to a 3D cone-like shape (***iii***). All test structures use an 8 cm in diameter circular polymer ring to form a pressure seal and electrical connections with an opposing surface.

The cage (***A***) and the funnel (***B***) act as chaperons to gain additional control to the deformation. The final shape of the deformed electronics depends on the chaperons, which enable a large number of degrees of freedom to the morphological shapes and to the geometries that could be achieved by these techniques.

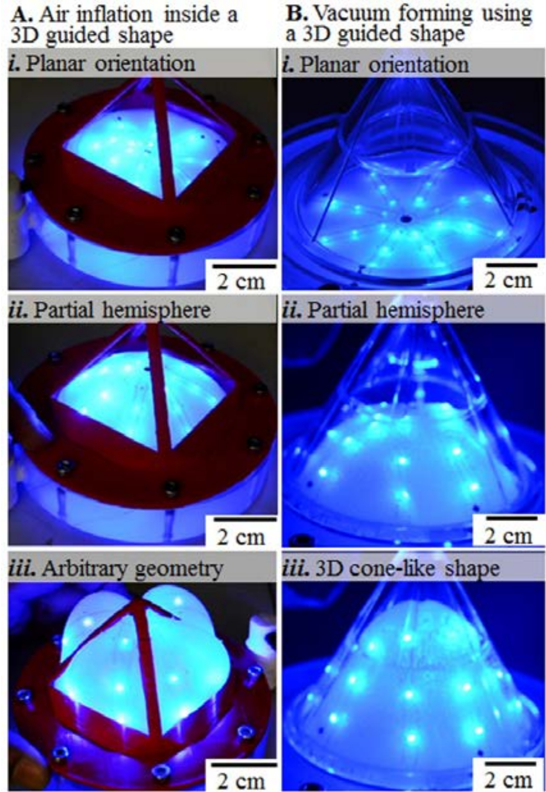

Figure 3.7: 3D guided deformation. A. *A uniform rubber membrane is inflated within a cage to get additional control to the morphological changes of the structure. The membrane deforms from planar shape (**i**), to a partial hemisphere (**ii**), to a more complex geometry (**iii**). **B.** A rubber membrane is deformed within a glass funnel using vacuum forming technique to form planar (**i**), to a partial hemisphere (**ii**), to a 3D cone-like shape (**iii**). The cage (**A**) and the funnel (**B**) act as chaperons to control the deformation.*

3.3.3. Inflation of Patterned Membrane

A simple method to control the morphological changes of the metamorphic electronics is patterning the rubber membrane. This approach allows to obtain topologies which are challenging to fabricate following previously mentioned methods. **Figure 3.8** shows images of two demonstrators of the inflation of patterned membrane. In the first case (***Fig. 3.8A***) the membrane is patterned very densely in circular rings (***r***= 1 to 4 cm) to obtain a wavy surface and in the second case (***Fig. 3.8B***) the membrane is patterned to form a bumble bee-eye shape structure. In both cases the membrane has a thickness of 3 mm (un-patterned) and 1.5 mm (patterned).

The depicted methodologies (***Fig. 3.7*** & ***Fig. 3.8***) are different from conventional balloon designs where the resting shape resembles the target structure, which is a concept that has been used in the field of stretchable electronics. Resting shapes demonstrated here show little similarities with the final structure. For example, the concept depicted in **Figure 3.8B** uses a rubber membrane where the thickness is adjusted locally to produce a desired 3D topology. Localized extrusions

Figure 3.8: ***Inflation of patterned membrane. A.*** *A membrane is patterned very densely in circular rings (**r**= 1 to 4 cm) to obtain a non-linear wavy surface and **B.** a membrane is patterned to form a bumble bee-eye shape structure.*

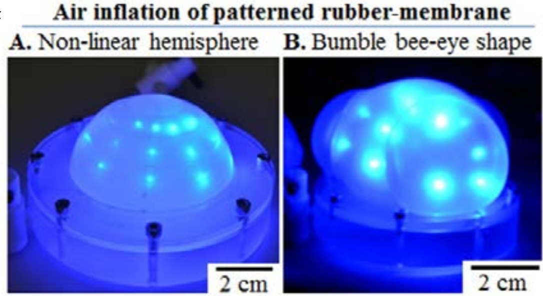

occur where the membrane thickness is reduced. From a theoretical design point of view the Laplace pressure equation

$$P = 2\gamma / R$$

can be used to predict the local radius of curvature ***R***. The equation provides a relationship between the pressure ***P***, the rubber tension γ, and the localized radius of curvature ***R***. Without applied pressure the membrane stays flat which represents an infinitely large radius of curvature. As the pressure increases the membrane bulges which reduces the radius of curvature ***R.*** At the same time the tension begins to increase following

$$\gamma = E \times \Delta l / l_o \times h$$

with Young's Modulus ***E***, strain $\Delta l / l_o$, and membrane thickness ***h***. The illustrated structures agree well with the anticipated spherical shapes and radii of curvatures over the range of pressures (15 – 40 mbar above atmospheric pressure) have been tested, which suggests that the layer of Ecoflex dominates the elastic properties on a macroscopic level.

The demonstrated method and technology presented in this chapter is limited to a single metallization layer which limits the complexity of the electronic systems. Also, only two-pad surface mount LED dies has been used as device, which requires only a limited number of interconnects to demonstrate the functionality of the system. However, this presents a method to realize mPCB and demonstrates the very first idea of metamorphic electronics.

Further improvement of the technology and demonstrators of more complex devices are required.

CHAPTER 4

Metamorphic Electronics

4.1. Manufacturing

4.1.1. Fabrication of μ-transistor chips

4.1.2. Fabrication of stretchable metal tracks

4.1.3. Assembly of the μ-transistors and detachment

4.2. Metamorphic Transistor Arrays

The transistor is the main building block of the modern electronics. One of the main reasons for today's high performance and highly dense electronics is that the development of transistors both in performance and by dimensions. So, successful implementation of any new electronics technology largely depends on how well transistors are adapted to the technology and vice versa. Similarly, the successful realization of metamorphic electronics also requires a metamorphic transistors array which is demonstrated in this chapter.

4.1. Manufacturing

The manufacturing of metamorphic transistor arrays is divided in three sections. Fabrication of the metal-oxide-semiconductor-field-effect µ-transistors (MOSFET), fabrication of the stretchable metal tracks, and realization of a metamorphic transistor arrays are presented in the first, second, and in the last section respectively.

4.1.1. Fabrication of µ-Transistor Chips

The detail fabrication process flow of Si MOSFET is schematically shown in **Figure 4.1A**.

Doping: The transistors are fabricated using spin-on-dopant (SOD). 500 µm thick p-type Si wafer (MicroChemicals, Ulm, Germany) with a resistivity of 10-20 ohm-cm is cleaned in $H_2SO_4 + H_2O_2$ for 15 minutes and subsequently rinsed with DI water. For masking, a 500 nm SiO_2 layer is grown using a wet oxidation process at 1050 °C (Tempress). The oxide is patterned by photolithography using AZ 1518 photoresist and etching in HF before the resist is removed (***Fig. 4.1A i***). A subsequent piranha ($H_2SO_4 + H_2O_2$) cleaning process is performed. Next n-type SOD (Filmtronics, P509) is spin coated at 1500 rpm for 60 seconds and baked at 250 °C for 30 minutes (***Fig. 4.1A ii***). The annealing process is performed at 1050 °C under N_2 flow (400 SCCM) for one hour. Later SOD residues and SiO_2 mask are etched in HF for 8 minutes to remove everything from the surface (***Fig. 4.1A iii***). Alignment marks for the source and drain are covered manually with the photoresist before the etching process is performed, and the resist mask is removed after the etching. Later a cleaning process is performed.

Gate Oxide: On the clean surface high quality 100 nm dry oxide is grown for the gate oxide at 1000 °C (***Fig. 4.1A iv***) and is patterned using photolithography and later etched in HF. The resist is removed with remover AZ100 and the wafer is washed in DI water and dried under N_2 (***Fig. 4.1A v***).

Metallization: The metallization layer is fabricated by photolithography and lift-off using AZ NXT15 negative resist. A subsequent descumming process is performed to remove any residues. E-beam evaporation is used to coat the surface with 100 nm Al + 50 nm Pt + 200 nm Au. Lift-off is done in Dimethylsulfoxide (DMSO) for overnight. A rapid thermal process (RTP) is performed at 400 °C for one minute (***Fig. 4.1A vi***). Both devices with RTP and without RTP are tested to study the influence of the process. The RTP process leads to a clear improvement in the device characteristic (***Fig. 4.2***) due to improved film-to-film and film-to-substrate interfaces.

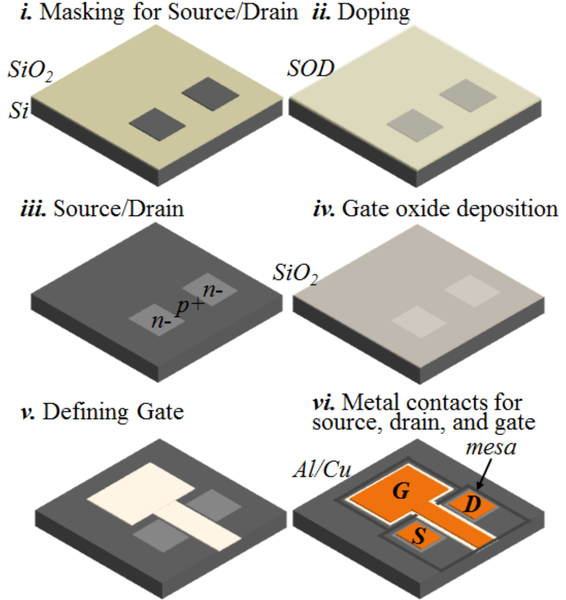

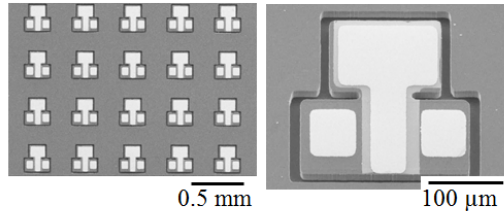

Figure 4.1: Fabrication of µ-transistors. *Fabrication of transistors (**A**) start with masking the Si substrate by 500 nm wet SiO_2 (**i**) and doped for source and drain using spin-on-dopant (SOD) (**ii**). 100 nm thick dry SiO_2 is used as gate oxide (**iii**), and for metal contact layers of Al/Pt/Au (100/50/200 nm) is used (**vi**). (**B**) SEM images of the fabricated transistors.*

Mesa etch: A final lithography is necessary to form trenches in order to isolate the active devices from the surrounding bulk substrate to eliminate cross-talk. 20 µm deep trenches are applied through dry etching (***Fig. 4.1A vi***). A comparison between devices with and without trenches shows no significant influence on the transistor behavior.

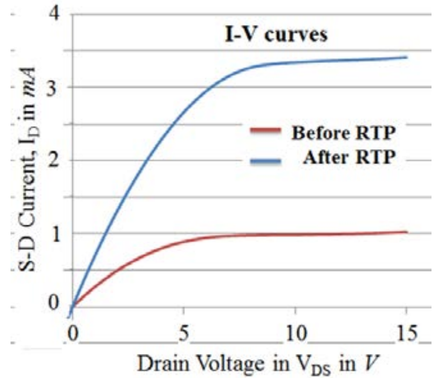

Figure 4.2: Influence of RTP annealing of the metal contacts. *Output characteristics of transistor before (**red**) and after (**blue**) annealing of the metal contact pads using rapid thermal process (RTP). The annealing has a clear influence to the electrical properties of the transistor.*

4.1.2. Fabrication of Stretchable Metal Tracks

The fabrication process of the stretchable metal tracks is similar to the process previously discussed in section **3.1.1**. A schematic process flow is shown in **Figure 4.3**. An 8 µm thick PI layer is spin coated on top of a PMMA coated substrate. A 20 nm/200 nm of Ti/Cu is sputter deposited on top of the O_2 plasma activated PI layer. The wafer is then patterned by photolithography using a negative resist and a thick layer of Cu (10 µm) is electroplated. Later the resist is stripped and a subsequent chemical etching process is carried out to etch the 200 nm Cu seed layer (***Fig. 4.3A i***). A corresponding optical photograph of the stretchable metal tracks on a hard carrier is shown in **Figure 4.3 A *i, right***.

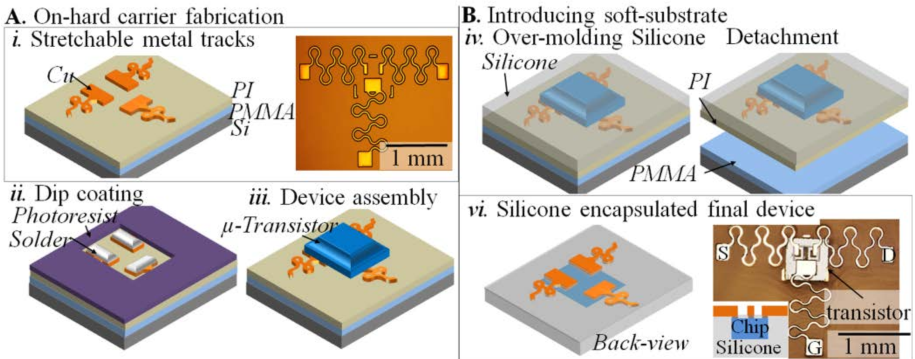

Figure 4.3: Fabrication of stretchable metal tracks and assembly of µ-transistors. A. *"On-hard carrier" fabrication of patterned stretchable metal tracks on sacrificial layers and a corresponding photograph (**i**), solder bumps (**ii**), and transistor assembly (**iii**).* ***B.*** *Introducing soft substrate by over molding rubber matrix (**iv**), detachment (**v**), and final device after removing the PI peeling layer leaving all faces surrounded by EcoFlex and exposed from the back for electrical contact and a corresponding photograph of the final device (**vi**).*

A second lithography process is performed to mask the metal strip for the soldering process. The wafer is dipped into the solder bath to coat the receptors (***Fig. 4.3A ii***). The fabrication process is completed after removing the second layer of photoresist.

4.1.3. Assembly of the µ-Transistors and Detachment

The SMD components are assembled on the wafer following the standard pick-and-place technique (***Fig. 4.3A iii***). On-wafer device test is performed to check the interconnections and compare device performance before and after transfer. After assembling the components, EcoFlex mold is poured on top of the wafer and cured overnight at room temperature (***Fig. 4.3A iv***). The EcoFlex layer is peeled using the PI layer (***Fig. 4.3A v***). As a final step, the sacrificial PI pealing layer is etched in plasma (40 SCCM O_2 + 10 SCCM CF_4, 100 WRF, 0.00250 mbar) for 30 minutes (***Fig. 4.3A vi***). **Figure 4.3A *vi right*** shows an image of the transistor with stretchable metal tracks encapsulated in EcoFlex and the inset shows a corresponding cross-section of the device.

4.2. Metamorphic Transistor Arrays

The test structure here contains an array of ~100 transistors. Unlike in the case of the LEDs, the electrical function of all individual transistors is difficult to test.

Figure 4.4A shows an image of the inflated transistor array to morph to a 3D hemisphere (***left***) and a magnified view of a single transistor from the inflated hemisphere (***right***). **Figure 4.4B** presents the transfer (***left***) and output (***right***) characteristics of the transistors from measurements. The measured characteristics under three different conditions are shown: (i) a pristine transistor on the original substrate (***red curve***) and a transistor embedded in Ecoflex in (ii) un-stretched (***green***) and (iii) stretched condition (***purple***). The pristine transistor (***red***) shows a slightly higher current and a smaller threshold voltage than in the case of stretching (***purple***). The threshold voltage (V_t) increases from 1.29V to 1.41V. This small increase is a result of the plasma etching step used to remove the PI peeling layer. However, the transistor characteristic is stable once the device is assembled and encapsulated in EcoFlex (***green***) and no changes can be observed as the matrix is bi-axially stretched (***purple***) to **200%**.

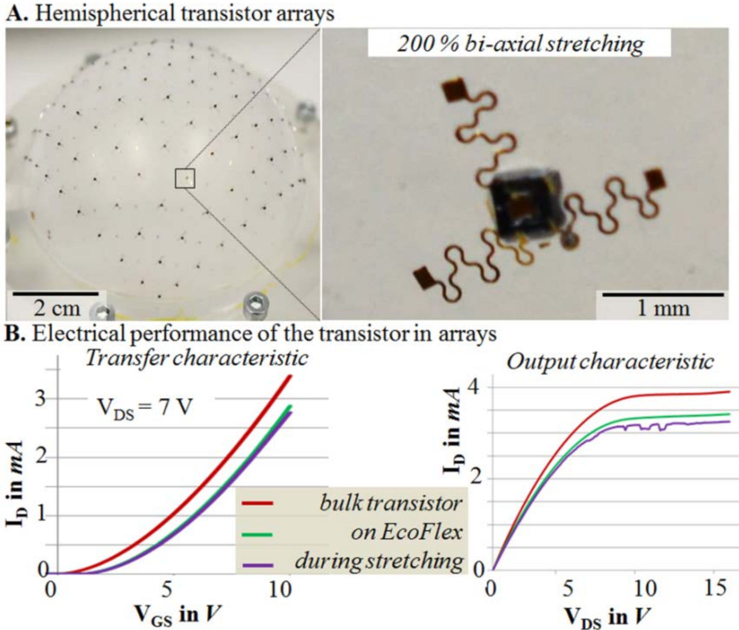

***Figure 4.4: Metamorphic transistor arrays. A.** Air inflated hemispherical transistor arrays (**left**) and a single transistor showing 200% biaxial stretching after inflation (**right**). **B.** Transfer (**left**) and output (**right**) characteristics of a transistor in three different conditions: pristine transistor (**red**), after rubber encapsulation and transfer (**green**), and in rubber matrix after inflation (**purple**). The transistor characteristics remain nearly same once the device is encapsulated in EcoFlex (**green**) and when bi-axially stretched (**purple**) to **200%**.*

At present, each transistor is located in an electrically isolated location and it is not possible to test the function of all the transistors within the array. The required routing of 300 connections is presently not possible. A multiplexed circuit and triple layer routing would be required to access the 100 elements and 300 contact pads which is a goal for future studies.

CHAPTER 5

Metamorphic Acoustoelectronics

5.1. Manufacturing

5.1.1. Fabrication of stretchable metal tracks

5.1.2. Assembly of the components on hard carrier

5.1.3. Rubber encapsulation and detachment

5.2. Design

5.2.1. Stretchable metal tracks

5.2.2. 3D reinforcement frame

5.2.3. Circuit and Arrays

5.3. Experiments and Results

5.3.1. Functionality test of the array on the hard carrier

5.3.2. Functionality test of the array on the rubber matrix

5.3.3. Functionality test of the array after inflation

5.3.4. Sound localization: planar *vs.* hemispherical array

5.4. Metamorphic Acoustoelectronics

Microphones are being widely used, starting from our daily life to scientific research. However, stretchable microphone array has not been reported before. The stretchable characteristic enhances the functionality of acoustic sensor arrays. In this specific case, the physical dimension of the array, i.e. the inter-distance between the microphones and the 3D topological orientation can be adjusted. For example, researchers have been trying to manufacture large arrays of microphones in spherical shapes for beam forming and/or sound source localization [246], dimensional room acoustic [247], music recording [248], speech enhancement [249], and beam-forming [250] applications.

In this chapter, metamorphic acoustoelectronic systems are presented using conventional MEMS (micro-electro-mechanical system) microphones in various 3D shapes.

5.1. Manufacturing

The manufacturing process is mainly divided into three steps. The first step is on-hard-carrier fabrications that support high-temperature processing. The second step is assembling SMDs, and the last step is introducing the rubber matrix. No high-temperature processing is necessary after introducing the rubber substrate.

5.1.1. Fabrication of Stretchable Metal Tracks

Figure 5.1 provides an overview of the main process steps to realize metamorphic microphone arrays next to photographs of corresponding test structures. The depicted approach is similar to the processes described in section ***3.1.1***.

Figure 5.1A illustrates the individual stack of layers and describes the first part of the processing sequence, involving the application of a **(*i*) peeling layer, (*ii*) stretchable metal track layer, (*iii*) reinforcing metal track cladding, (*iv*) solder layer, (*v*) device layer, and (*vi*) reinforcing frame.** The first part of the sequence is completed using (***vii***) **on-hard-carrier-functionality tests** (***right***).

(i) Peeling layer: A spin coated 8 µm thick layer of polyimide **PI** on top of a **PMMA** coated Si wafer is used. The function of the peeling layer is to provide a mechanically flexible but not stretchable peeling foil, which has a low level of adhesion to the PMMA (*blue* in ***Fig. 5.1***) coated carrier (*gray* in ***Fig. 5.1***) and a strong and adjustable level of adhesion to the metal, circuit elements, and rubber matrix on top. The required strong adhesion to the rubber matrix and metallization layer is achieved by plasma activation of the polyimide surface (30 SCCM, O_2, 100 W RF power for 2 minutes).

(ii) Stretchable metal track layer: For the metallization layer a 20 nm/200 nm thick sputter coated seed layer of Ti/Cu is used, which is patterned by photolithography. A 10 µm thick layer of electroplated Cu is used to increase the mechanical robustness of the metal tracks (*reddish* in ***Fig. 5.1***).

(iii) Reinforcing metal track cladding: This newly introduced layer is different from the methods discussed in earlier chapters. This 10 µm thick PI layer is spin coated on top of the metal tracks and patterned by photolithography. This layer fulfils several functions. The patterned PI layer covers the top and sidewalls of the 10 µm tall and 50 µm wide metal tracks and acts as an intermediate cladding layer between the metal and the rubber matrix. Lithographic alignment and registration with sub 5 µm accuracy over a 10 cm wide substrate are required to maintain a constant overlap of the cladding layer and coverage of the sidewalls of the metal tracks. The insert provides a close-up tilted SEM image of the PI encapsulated metal track. This protecting PI cladding increases the mechanical stability of the metal tracks when being stretched; metrics will be discussed later.

(iv) Solder layer: The patterned PI layer offers an additional function. The patterned layer serves as a mask in the solder bump application process. Specifically, the PI mask has 600 µm × 350 µm wide openings to the contact pads. The openings enable the application of the depicted solder bumps using a parallel dip coating process in a liquid solder bath [26].

5.1.2. Assembly of the Components on Hard Carrier

(v) Device layer: In the demonstrated case, a semi-automated pick-and-place process is used to assemble the components. The depicted demonstrator contains a total number of 5 analog MEMS microphones (3.76 × 2.95 × 1.2 mm, Knowles SPU0414HR5H-SB). The peripheral SMD resistors (1.6 × 0.8 × 0.45 mm) and capacitors (1.6 × 0.8 × 0.8 mm, and 2 × 1.2 × 1 mm) adjust the cut off frequency and gain of the microphone.

(vi) 3D reinforcing frame: The function of the 3D reinforcing frame is to increase the robustness of the structure. Specifically, to shield the transition region and electrical connections to the rigid objects from high levels of stress. The reinforcement frames (*violet* in ***Fig. 5.1***) are printed using a 3D printer (Ultimaker 2+). The frames are 8 mm wide, 10 mm long, and 1 mm high. The printable Polyester (FlexiFil, Form Futura) is relatively stiff; it has Young's modulus of 95 MPa; as a comparison EcoFlex has a Young's modulus of 0.7 MPa.

(vii) On-hard carrier functionality tests: The depicted approach enables "on-hard carrier" functionality tests. For example, in the depicted hard carrier functionality tests, the circuit draws 0.5 *mA* and the microphones function as anticipated. The amplitude response of the five channels in the frequency range from 500 Hz to 5 kHz compares well from one channel to the next. The amplitude deviation is within a 15% margin.

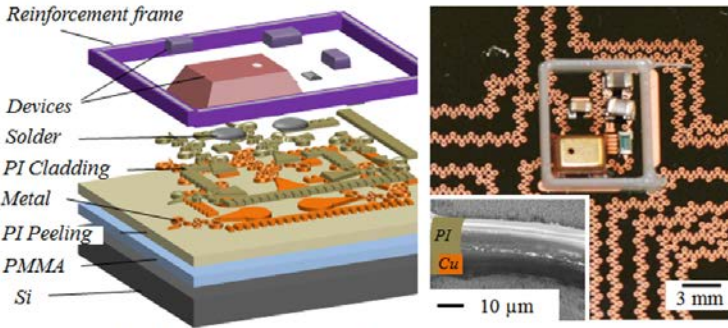

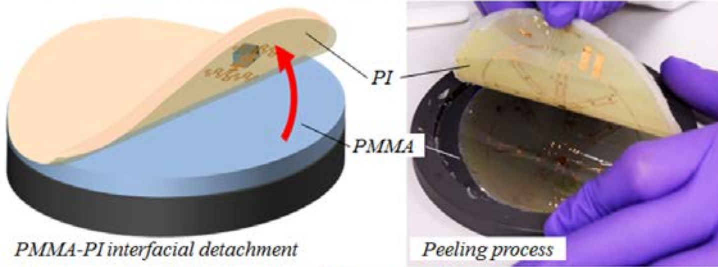

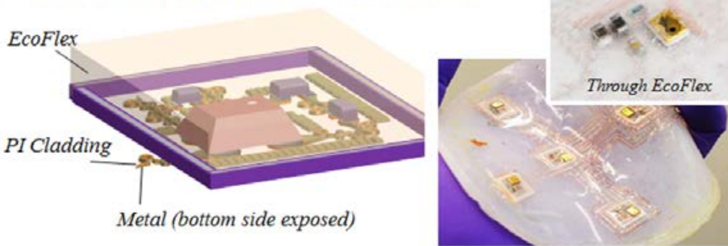

***Figure 5.1: Metamorphic printed circuit boards process flow**, schematics and corresponding photographs yielding a metamorphic microphone array. **A.** "On-hard carrier" fabrication, assembly, and functionality test. The fabrication (**left**) involves the application, patterning and alignment of several layers, specifically: a PMMA release layer (blue), a PI peeling layer (greenish gray), a metallization layer (orange), a PI cladding layer (patterned greenish gray), a solder bump layer (gray), a device layer (reddish) and a reinforcement layer (violet). On hard carrier functionality tests follow to confirm the anticipated function (**right**). **B.** Over-mold rubber matrix encapsulation showing PMMA-PI interfacial detachment, separating the PI peeling layer (greenish gray) from the PMMA coated carrier. **C.** Structure after PI layer removal (plasma etch) exposing the bottom contacts.*

5.1.3. Rubber Encapsulation and Detachment

Figure 5.1B describes the rubber encapsulation and detachment process. The detachment process is similar to the process discussed in section ***3.1.3***. A wafer-scale, solvent-free detachment process is used to detach the components and the stretchable circuit from the hard carrier. The microphone and many SMD components get damaged in most liquids and solvents. Instead of using a solvent, the detachment process uses the differential interfacial adhesion of the stacked layers to define an interface that can be cleaved.

Figure 5.1C describes the final step to yield the test structure. After detachment, the Cu metal tracks continue to be covered with the PI peeling foil which needs to be removed. Electron cyclotron resonance (ECR) plasma etching (40 SCCM O_2, 10 SCCM CF_4, 100 W RF power, 30 minutes at 0.0025 mbar, SQ160 Roth and Rau AG) is used to accomplish this step.

5.2. Design

5.2.1. Stretchable Metal Tracks

Geometrical design of the metal tracks used in this experiment is identical to those discussed in section ***3.2.1*** except that in this case the metal tracks are supported by an additional 10 µm thick PI cladding. The PI cladding surrounds the metal tracks and acts as an intermediate interface between the metal tracks and the rubber matrix. Note that in this case, the metal tracks are not in direct contact with the rubber matrix.

Since comparative studies between a reference design and the stress adaptive design have already been discussed in section ***3.2.1***, in this section the discussion is limited only to the effect of PI cladding on the same metal tracks design.

Figure 5.2 compares the stress adaptive meander design (discussed in section ***3.2.1***) without PI cladding (***Fig. 5.2A***), and with PI cladding (***Fig. 5.2B***) to further stabilize the structure. The results are summarized in **Table 5.1**.

Maximum elongation limit: The PI cladding of the metal tracks has little to no influence on the single stretch limit to cause metal tracks rupture.

Metal track detachment in single-stretch limit: The detachment of the metal tracks from the rubber matrix is problematic. It is difficult to notice since the tracks continue to function electrically. However, ultimately it leads to random arrangements, crossovers and shorts between neighboring tracks (see ***Fig. 3.3***). The metal tracks with PI cladding improves the onset of detachment from 240% to 290%

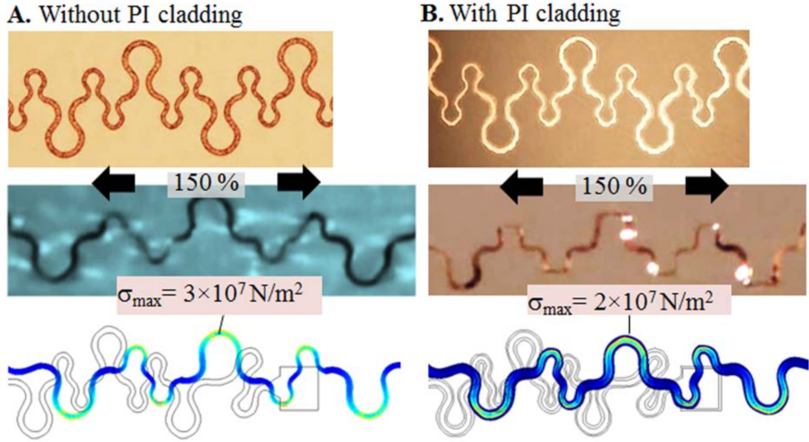

Figure 5.2: Influence of the PI cladding. *(**A**) Stress adaptive design without PI cladding, and (**B**) with PI cladding; photographs of the metal tracks on hard carrier (**first row**), photographs of elongated metal tracks to 150% of the original length (**second row**) with corresponding computer simulated stress profile (**third row**).*

which represents an improvement factor of 1.2x (***Table 5.1***). This can be understood in the following way. The PI cladding surrounds the bottom and sidewalls of the metal track, which leads to an additional level of adhesion due to the combination of an increased surface area and bond strength between the PI cladding and the rubber matrix.

Table 5.1: **Study of PI cladding to metal tracks.**			
	Without PI cladding	With PI cladding	Improvement factor
Single-stretch experiments			
Single-stretch limit to cause a metal track rupture			
Elongation Limit	310%	320%	1x
Single-stretch limit to observe onset of metal track detachment			
Elongation Limit	240%	290%	1.2x
Multi-cycle experiments			
Average cycles count at 150% elongation to cause metal track rupture			
Conductor to fail	5840	11050	1.9x
Cycles count at 150% elongation to cause full metal track detach			
Conductor to detach	600	2750	4.5x

Multi-cycle stretch and release: The second metal tracks (***Fig. 5.2B***) perform very well in a multi-cycle stretch and release experiments. The bottom half of table 5.1 presents the results. Each dataset is based on the characterization of eight parallel meanders spanning a non-stretched distance of 20 mm. A modest elongation to 150% of the original length is applied in this test. On average, the occurrence of rupture is delayed from 5840 to 11050 cycles which represents a 1.9 fold total increased. A potential explanation is that the cladding provides an increase level of lateral stabilization.

Metal track detachment in multi-cycles: The multi-cycle stretch and release experiments are also used to study the level of detachment as a function of cycles. On average, the event of detachment is delayed from 600 to 2750 cycles which represents a 4.5 fold total increase. The underlying mechanism of delaying the detachment is again, the introduced PI cladding that surrounds the metal track. This intermediate PI cladding provides an additional level of adhesion to the rubber surroundings due to a combination of an increase surface area and bond strength between the PI cladding and the rubber matrix. The PI cladding contributes the most to the improvement of the metal track detachment failure type; however, the metal track detachment continues to be the first failure type to occur in practical applications.

5.2.2. 3D Reinforcement Frame

The SMD components and the microphones used in this study are relatively large and rigid objects. The advantage is that they are commercially available which provides a general access and possibility of adaptation to other device types. However, the use in the context of stretchable or metamorphic electronics is challenging. Localized forces in close vicinity and at the interface between the rigid and soft material lead to a premature failure of this region. Commonly observed failure types are interfacial delamination and creation of cavitations between the rubber matrix and the hard and non-stretchable objects as the structure is stretched. The soft matrix separates from the hard objects and the metal tracks in these regions experience an extra load, a higher level of stress, and pulling forces. Eventually, this leads to the rupture of the connecting metal tracks in close vicinity to the hard objects. The computations fail short to predict this behavior. In an attempt to delay the onset of this chain of events, a reinforcing frame is added to the structure which surrounds the rigid components.

Figure 5.3 compares photographs, intercomponent distances, calculated strain, and corresponding stress profiles before and after the introduction of the reinforcement frames. Changes in the intercomponent distance are measured to calculate the local strain. For example, in the un-stretched case (***Fig. 5.3A***), the relaxed distance between the capacitor (***brown part***) and the microphone can be measured; it is 1.85 mm. When inflated to the hemisphere, this distance increases to 4 mm without reinforcement frames (***Fig. 5.3B***) and 2.1 mm with reinforcement

frames (***Fig. 5.3C***). This location experiences a y-axis strain value of $\Delta l_y/l_y = 2.15\,mm/\,1.85\,mm = 1.16$ (***center***) and $\Delta l_y/l_y = 0.25\,mm/\,1.85\,mm = 0.14$ (***right***), respectively. The ratio yields an 8.3 fold improvement. Similar results are

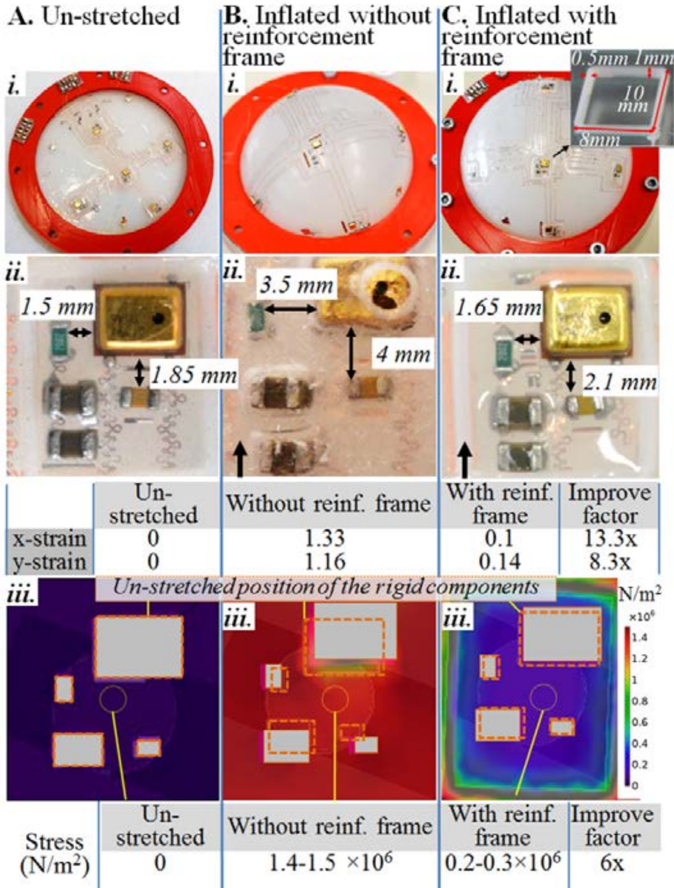

Figure 5.3: 3D Reinforcement frame study*; photographs, computation, strain, and stress values.* ***A.*** *Un-stretched shape,* ***B.*** *inflated shape without reinforcement frame, and* ***C.*** *inflated shape with reinforcement frame. Inflation increases the inter-component distance (****black arrows****), the relative change yields the tabulated* ***x-*** *and* ***y****-axis strain values; the inflated reinforced design (****right****) has lower strain values. The (COMSOL) finite element study (****bottom****) shows the same general behavior; the dotted line and gray region represent the component location before and after deformation, respectively. The tabulated stress values (****bottom****) are recorded in the yellow circle. A 6 fold smaller value is recorded in the reinforced design*

found considering the x-axis. In the un-stretched case (***A***), the relaxed distance between the resistor (***green part***) and the microphone is 1.5 mm. After inflation, this distance increases to 3.5 mm (without reinforcement frame, ***Fig. 5.3B***) and 1.65 mm (with reinforcement frame, ***Fig. 5.3C***) and the strain value ratio becomes 13.3 in this case. The strain value ratio provides a first-order estimate of the level of strain and stress protection which is gained using the introduced reinforcement frames.

Figure 5.3 (***iii***) shows images of the computed stress evolution of the morphing structure without and with reinforcement frame. These images provide further insights into the process. The dotted frames locate the positions of the components in un-stretched condition and the gray areas represent the position after deformation into a hemispherical shape. The computed relative change in the inter-component distance agrees well with the measured values. To provide some number of the stress and a relative comparison the values have been extracted from the center of the image and obtained 0 Ncm^{-2} (***Fig. 5.3A iii***), 145 Ncm^{-2} (***Fig. 5.3B iii***) and 25 Ncm^{-2} (***Fig. 5.3C iii***) respectively. In short, a 6-fold reduction, considering the mechanical stress can be attributed to the introduction of the reinforcement frames. As a qualitative statement, the reinforcement frames helps to fabricate metamorphic structures, which could be deformed multiple times without breaking the metal track connections in close vicinity to the SMDs. As an example, the reinforced structure is inflated and deflated 50 times and the device continues to function; longer-term cycling test has not yet been performed. Several designs without reinforcement failed after 5-15 cycles.

5.2.3. Circuit and Arrays

Figure 5.4 illustrates the circuit diagram for each set of microphone (***A***) and the layout of the microphone array within a 100 *mm* in diameter substrate (***B***) with the corresponding photographs. The circuit is planned according to the recommended design from the microphone manufacturing company [251]. The parameters of the resistors ($R=20\ kOhms$) and the capacitors ($C_1= 47\ nF$ and $C_2=0.1\ \mu F$) are chosen to have a gain of 6 *dB*. A fixed 3 *V* battery is used as a power source in order to avoid any noise from a DC power supply. C_3 $(=10\ \mu F)$ is used externally to remove the DC offset from the signal.

The inter-distances of the microphones (***B***) are important in order to understand and calculate the amplitude and phase differences. The distances are measured between microphone's middle points. Assuming that the velocity of the sound in the air at room temperature is 345 *m/s*, then, for instance, an acoustic wave propagating from the top to the bottom (-y direction) in the same plane will have an internal time difference (ITD) between microphone 1 (m_1) and microphone 3 (m_3) of 159 μs. While for the same signal, microphone 2 (m_2) and microphone 4 (m_4) will have no or a very little ITD. Similarly, an acoustic wave propagating from the left to right (+x direction) in the same plane will have an ITD between microphone 4 (m_4) and

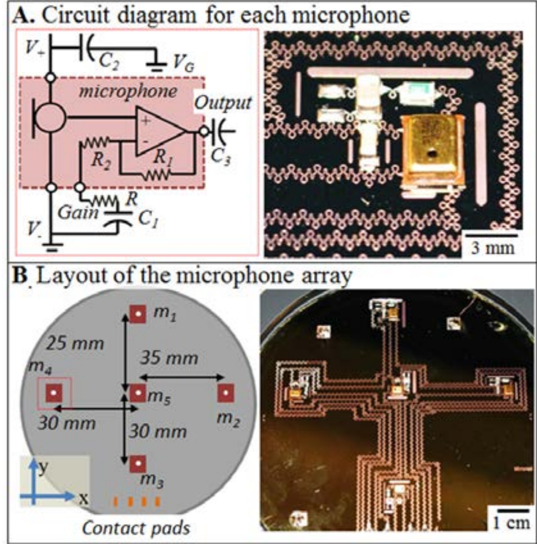

***Figure 5.4: Circuit diagram and layout of the integrated microphone array.** A. Circuit diagram (**left**) and a corresponding photograph (**right**) for an integrated microphone system. **B.** Schematic layout of the array of five microphones within a 100 mm carrier substrate showing interdistances of the microphones (**left**) and a corresponding photograph of the array on hard carrier (**right**) with all the relevant SMD components mounted.*

microphone 2 (m_2) of 188 μs. While for the same signal, microphone 1 (m_1) and microphone 3 (m_3) will have almost no ITD.

5.3. Experiments and Results

Figure 5.5 depicts the schematic and experimental setup for the microphone functionality test. The microphones are characterized in a semi-anechoic room. A coaxial loud-speaker is used as the acoustic source and the sounds are recorded using all the microphones simultaneously. The speaker is placed 1 m away from the microphones. Two different frequencies are tested (1 *kHz*, and 5 *kHz*). Only the results from 1 *kHz* measurements are reported here. The microphones signals are recorded using a computer with an audio interface at a sampling rate of 192k at 24 bits. The recorded audio

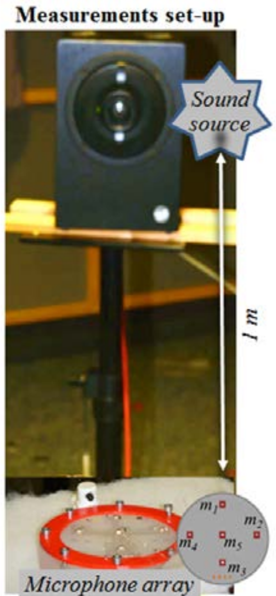

***Figure 5.5: Experimental set up for microphone array testing.** Photograph and schematic of the experimental set up for the microphones testing showing a loudspeaker for acoustic source and metamorphic microphone arrays for acoustic recording. The distance between the sound source and the microphones is 1 m.*

files are analyzed and plotted using a MATLAB computer program. The experimental set-up and the parameters for the microphone testing are kept unchanged for each test.

5.3.1. Functionality Test of the Array on the Hard Carrier

The hard carrier functionality test measurement is performed to verify if all the microphones function properly and respond to the frequency. For example, in the depicted hard carrier functionality tests, the circuit draws 0.5 *mA* and the microphones perform as anticipated. The amplitude response of the five channels in the frequency range from 500 Hz to 5 kHz compared well from one channel to the next. The amplitude deviation is within a 15% margin.

Figure 5.6 presents an image of an array of microphones on hard carrier under test (***Fig. 5.6A***) and the results (***Fig. 5.6B***). The graphs present the sinusoidal waveform that was recorded using the array using 1 *kHz* acoustic test signal.

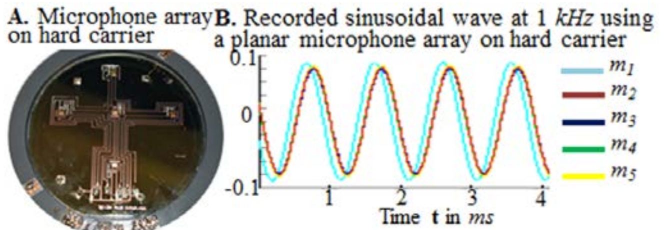

Figure 5.6: Functionality test of the microphone arrays on hard carrier. A. *An image of an array on hard carrier under test and* ***B.*** *result from the microphone array measurement on hard carrier at 1 kHz. The different colors represents different microphone signal.*

5.3.2. Functionality Test of the Array on the Rubber Matrix

Figure 5.7 shows an image of the planar microphone array in rubber matrix under test (***a_1*, *left***) and the recorded 1 *kHz* acoustic signal using the planar array (***a_1*, *right***). The instantaneous amplitude differences (***a_2***) and the internal time difference (ITD) derived from the phase differences (***a_3***) are plotted to estimate the sound source localization (discussed later).

5.3.3. Functionality Test of the Arrays after Inflation

The microphone array in rubber matrix can be inflated to form a hemisphere. This method would easily solve many challenges in the field of acoustic research.

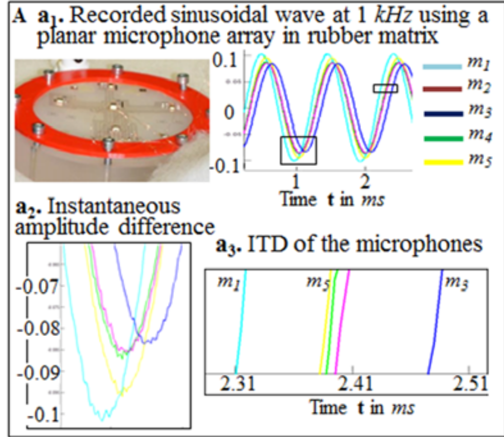

Figure 5.7: Functionality test of planar microphone arrays in rubber matrix. A. *An image of a planar microphone array in rubber matrix under test (**left**) and recorded test signals (**right**) at 1 kHz. The instantaneous amplitude differences (a_2) and the internal time difference (ITD) derived from phase differences (a_3) are shown. These values will be used later.*

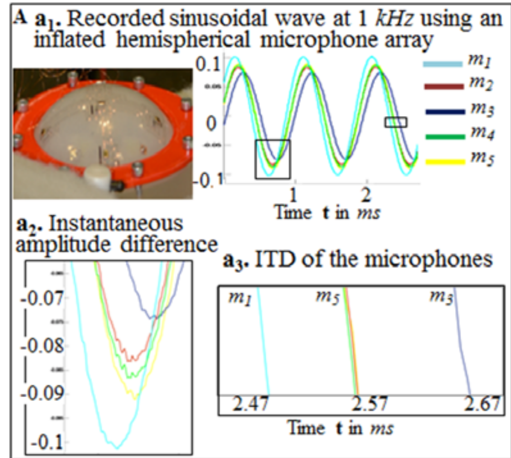

Figure 5.8: Functionality test of microphone arrays after air inflation. A. *An image of an inflated microphone array in rubber matrix under test (**left**) and recorded test signals (**right**) at 1 kHz. The instantaneous amplitude differences (a_2) and the internal time difference (ITD) derived from phase differences (a_3) are presented. These values will be used later.*

Figure 5.8 shows an image of an inflated hemispherical microphone array test (***a_1*, *left***) and the recorded 1 *kHz* acoustic signal (***a_1*, *right***). The instantaneous amplitude differences (***a_2***) and the internal time difference (ITD) derived from the phase differences (***a_3***) are plotted to estimate the sound source localization (discussed later).

5.3.4. Sound Localizations: Planar Array *vs.* Hemispherical Array

In this section, the planar microphone array is compared with the hemispherical microphone array configuration to localize a sound source. To estimate the location a large body of algorithms is available. Typically, they deal with variations of the signal amplitude and phase across the array. The signal amplitude commonly depends on the orientation of the microphone. For example, a directional

microphone pointing at a noise source will provide a stronger signal and the amplitude distribution across the array is therefore often considered. However, in the depicted case omnidirectional MEMS microphones are used and only a small (± 10%) amplitude variation is recorded across the array.

The values from **Figure 5.7** (planar orientation) and **Figure 5.8** (hemispherical orientation) are used to estimate the location of a sound source. At first, the direction of the sound is estimated using the amplitude differences. For example, m_1 (cyan in ***Fig. 5.7*** $\boldsymbol{a_2}$) has the highest amplitude and m_3 (blue in ***Fig. 5.7*** $\boldsymbol{a_2}$) has the lowest amplitude. This means that m_1 points in the direction of the sound source.

For further localization, the cone of confusion algorithm is used (***Fig. 5.9***) [252]. It is based on the internal time difference t_{in} of the received signal between microphone pairs i and n. In short, the time difference for each pair is used to compute the "cone of confusion angle ϑ_{in}"; as illustrated in **Figure 5.9** (the cone axis lies along the connecting line between the microphone pair) using $\vartheta_{in} = \cos^{-1}(c \cdot t_{in}/\, d_{in})$, where c is the speed of sound, and d_{in} is the distance between the respective microphone pair. Each microphone pair yields a separate cone from where the signal could be from and the intersection of all possible cone pairs yields the best possible location estimate.

The cone of confusion algorithm assumes that that the distance of the sound source, l is: $l >> d_{in}$ and that the acoustic waves travelling to the microphones are parallel. ***Figure 5.9 B*** illustrates the geometrical configuration of the problem to find out θ [252].

The result of the sound localization for the planar array is presented in **Figure 5.10A**. In this case, two intersecting cone volumes are estimated as possible locations, one above and one below the X-Y plane. They are presented by the shaded gray regions, each having a volume of 12600 cm^3. The red circle shows the actual

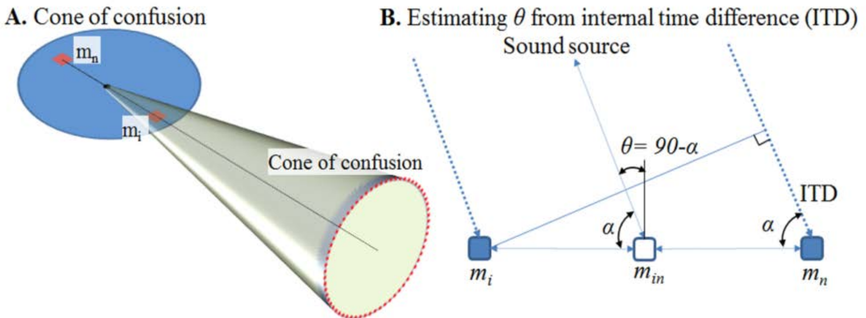

Figure 5.9: Schematic illustration of the principle of the "cone of confusion" *produced by two microphones (**A**) and calculation of θ from ITD (**B**).*

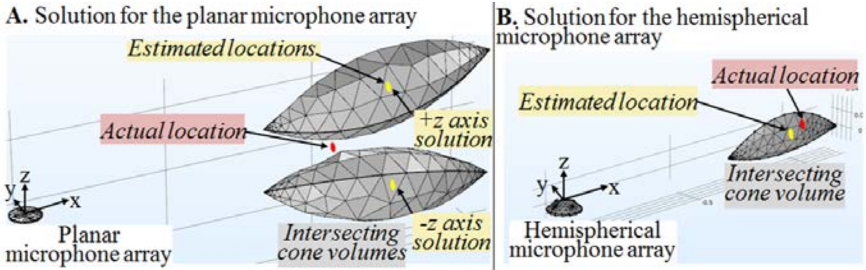

Figure 5.10: Sound source localizations: planar vs. hemispherical arrays. *Sensed location as the microphone array morphs from a (**A**) planar to a (**B**) hemispherical shape. The red spot presents the actual sound source location in the experiment. The gray regions represent the sensed location using the "cone of confusion" algorithm; the algorithm translates the time difference into a volume. The yellow dot represents the sensed location using a center of gravity concept (main body).*

position, and the yellow dots represent the estimated location (the center of the gravity of the intersecting cone volume) using the ITD. The distance between the actual location and the estimated locations is 24 cm each. Note that none of these solutions enclose the real position of the source.

The result of the sound localization for the hemispherical array is presented in **Figure 5.10B**. Unlike the planar array, the hemispherical array provides only one solution which encloses the real position of the source. In this case, the intersecting cone volume is 1100 cm^3. The deviation between the actual location and the estimated locations is 8 cm.

Table-5.2 summarises the results of the two arrays and compares the sound source location estimations (***Fig. 5.10 A & B***). The intersecting cone volume is decreased by a factor of 12 for the hemispherical array compared to the planar array. The distance between the estimated location and the actual sound source is 24 cm using the planar configuration and improves to 8 cm as the topology morphed to the hemispherical shape.

Table-5.2: Localization comparison between planar array and hemispherical array.

	Planar array	Hemispherical array	Improvement factor
Intersecting cone volume	2 * 12600 cm^3	1100 cm^3	12x
Distance between estimated and actual location	24 cm	8 cm	3x

These experiments show that a change in morphology influences the device functionality. With a planar microphone array, it is not possible to locate the correct position of a sound source if the source is placed in the same plane. The three-dimensional arrangement overcomes this limitation.

5.4. Metamorphic Acoustoelectronics

A number of deformation mechanisms have been discussed in ***section 3.3*** to form very complex shapes. Those processes remain valid also for acoustoeletronic

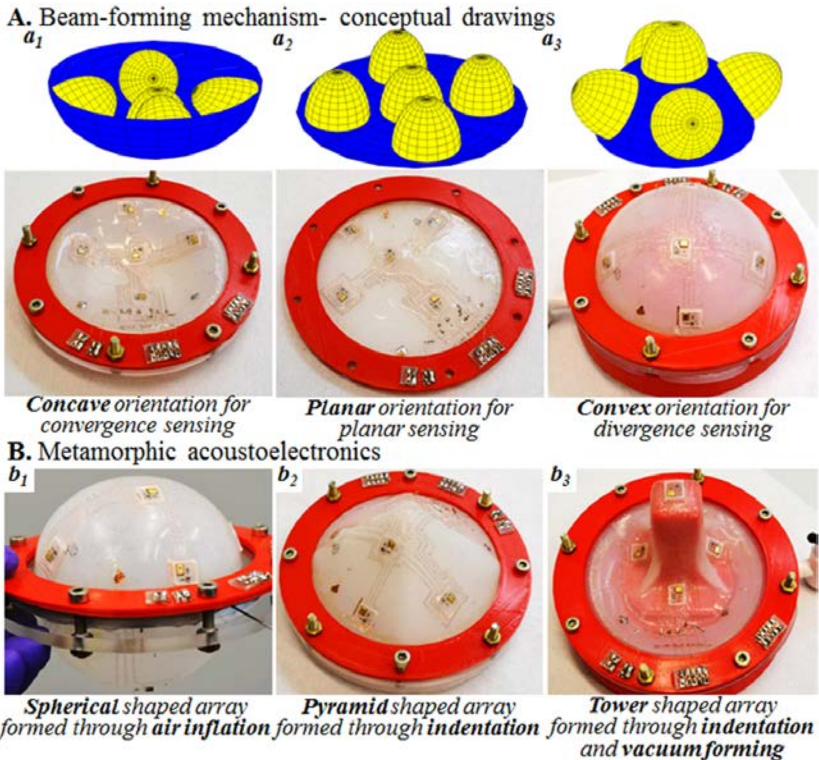

Figure 5.11: Metamorphic acoustoelectronics. A. *Conceptual drawings and corresponding photographs illustrating (**a_1**) concave, (**a_2**) planar, and (**a_3**) convex topologies.* ***B.*** *Deformation concepts using: (**b_1**) air inflation to morph into a sphere, (**b_2**) indentation to morph into a pyramid, and (**b_3**) indentation and vacuum forming to morph into a tower.*

systems presented in this chapter. As a few demonstrators, some of the processes are applied here to realize metamorphic acoustoelectronic systems (***Fig. 5.11***).

The basic idea of metamorphic acoustoelectronics is to use morphological changes to adjust the receive characteristic, for example, from a concave (***Fig. 5.11a$_1$***) to a planar (***Fig. 5.11a$_2$***) to a convex (***Fig. 5.11a$_3$***) shape. **Figure 5.11A** schematically presents the conceptual drawings of the beam forming mechanism while the microphone array deforms from planar array to convex or concave shape. Conceptually, this deformation of an array would enable acoustic focusing. Experimentally, this is possible through deflation and inflation with air or liquids. A few examples are given. In the first case, the stretchable structure acts as a simple air inflatable membrane, here a ring type clamp is used to form a pressure seal (***Fig. 5.11A***).

However, other geometries are shown as well, including a full sphere inflating the cavity between two rings clamped membranes (***Fig. 5.11b$_1$***), a pyramid formed through indentation using a pyramidal guide (***Fig. 5.11b$_2$***), and a tower shape formed through a combination of indentation and vacuum forming using a 3D shape guide (***Fig. 5.11b$_3$***). These morphological changes have no effect on the individual function of the microphones within the array. The frequency response continues to agree well with the response of the hard carrier. However, from a system point of view, the morphological changes can be used to adjust the receive characteristic.

In principle, flexible and stretchable sensor arrays could be fabricated. The arrays could be wrapped around a 3D shaped body for material or medical diagnosis including 3D imaging. Material related diagnostics including fatigue, crack, distance or thickness measurements could be improved. In medical science, acoustic sensors arrays are widely used in applications such as echocardiogram, gastroenterology, anesthesiology, gynecology, neonatology, cardiology, urology, and neurology. There should be many more applications of metamorphic acoustoelectronic systems.

CHAPTER 6

Addressable Metamorphic LED Array

6.1. Manufacturing of Integrated mPCBs

6.1.1. Fabrication of stretchable metal tracks

6.1.2. Assembly of the components on hard carrier

6.1.3. Rubber encapsulation and detachment

6.2. Design of Integrated mPCB

6.2.1. Metal tracks crossing

6.2.2. VIA

6.3. Functionality Tests

6.3.1. Functionality test on hard carrier

6.3.2. Functionality test after encapsulation and transfer

6.4. Metamorphic LED Display

An industry-compatible method to realize integrated mPCBs remains challenging. For example, to realize a complex electronic system the circuit board requires to be multilayered which means the metal tracks need to be in different layers. Additionally the metal tracks in different layers should be interconnected through VIAs (vertical interconnect access). A few approaches have been reported to realize VIA using liquid alloy [253] and solid phase materials [254]. However, an industry-compatible processing of reliable VIAs remains a primary challenge in the field of stretchable electronics [157].

This chapter addresses these issues and discusses challenges to realize an industry-compatible method to fabricate integrated stretchable electronic systems. The depicted method is compatible with industrial processes and uses commercially available pristine surface mount devices (SMDs). Specifically, a multilayer integrated metamorphic printed circuit board technology (**mPCBs**) is reported, which replaces the rigid insulator of a conventional printed circuit board (PCB) with a highly stretchable silicone rubber (EcoFlex).

6.1. Manufacturing of Integrated mPCBs

6.1.1. Fabrication of Stretchable Metal Tracks on a Hard Carrier

Figure 6.1A illustrates the first steps of the processing sequence. These include application of (***i***) **a release (PMMA) & a peeling (PI) layer,** (***ii***) **first metal track layer (Cu),** (***iii***) **isolation layer (photopatternable PI),** (***iv***) **VIA (Cu),** (***v***) **second metal track layer (Cu), and** (***vi***) **device layer (SMDs).** The first part of the processing sequence ends with (***vii***) **on-hard-carrier-functionality tests**.

(i) Release & peeling layer: This step is similar to the process described in ***section 5.1.1.*** In the depicted approach spin coated poly(methyl-methacrylate) (**PMMA**) is used as a release layer (*green* in ***Fig.6.1***) and spin coated 8 µm thick layer of polyimide (**PI** 2611) is used as a peeling layer (*blue* in ***Fig. 6.1***).

(ii) First metal track layer: For the metallization layer a 50 nm/200 nm thick sputter coated layer of Al/Cu is used which is patterned by photolithography (***Fig. 6.1A, i***). The beneath Al layer is later used as a mask to etch the peeling PI layer after the device is released from hard carrier. A 10 µm thick layer of electroplated Cu is used to increase the mechanical robustness of the metal tracks (reddish layer) [46].

(iii) Isolation layer: A second 20 µm thick photopatternable PI (PP PI) layer (HD 4100, HD MicroSystems, Neu-Isenburg, Germany) is spin coated on top of the metal tracks and patterned for VIA opening by photolithography (***Fig. 6.1A, ii***). This layer fulfils several functions. The patterned PP PI layer covers the entire surface of the substrate; top and sidewalls of the 10 µm tall and 50 µm wide metal tracks. This layer isolates the first metallization layer from the second metallization layer.

(iv) VIA: The patterned PP PI layer offers an additional function. This layer serves as a mask in the VIA plating process. Photolithographically patterned PP PI layer has predefined openings for VIAs on top of the first metallization layer (***Fig. 6.1A, ii***). Specifically, the PP PI mask has 300 µm × 500 µm wide openings to the contact pads. A descumming process is performed before electroplating the VIAs in order to remove any residues from the PP PI layer at the openings. For descumming O_2 plasma (30 SCCM, O_2, 100 W RF power for 5 minutes) is used in a reactive ion etcher. The descumming process improves the subsequent processes and also

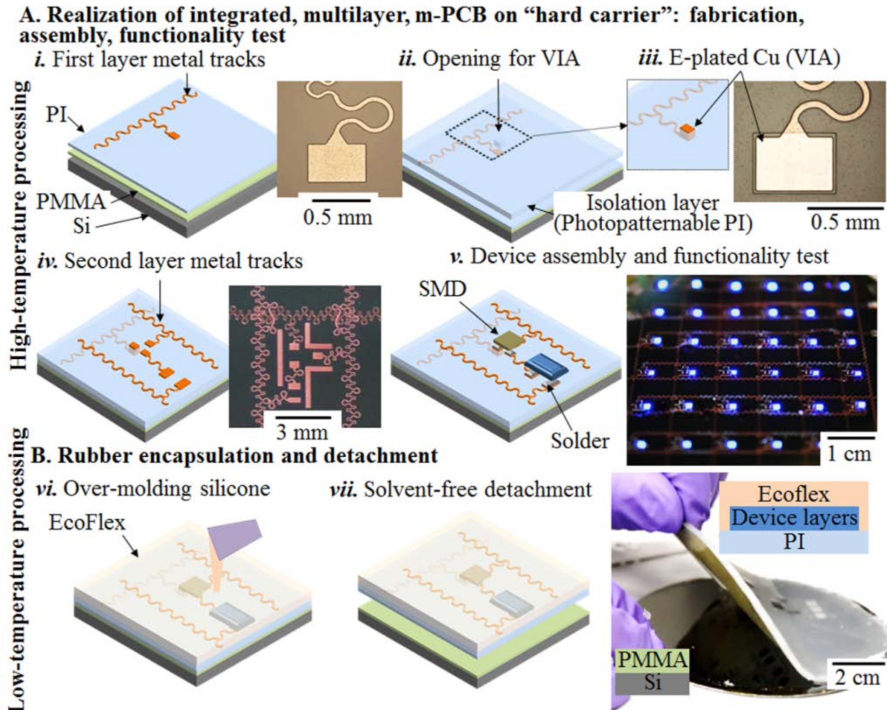

Figure 6.1. Integrated multilayer metamorphic printed circuit board process flow. A. *"On-hard carrier" fabrication, assembly, and functionality test. The fabrication involves the application, patterning, and alignment of several layers, specifically: a PMMA release layer (green), a PI peeling layer (blue), first metallization layer (orange) (**i**), a photopatternable PI layer (transparent blue layer) (**ii**), electroplated Cu for VIA (**iii**), second metallization layer (**iv**), and a device layer (**v**). On hard carrier functionality tests follow to confirm the anticipated function (**right**).* ***B.*** *Rubber matrix encapsulation (v**i**) and PMMA-PI interfacial detachment (v**ii**), separating the PI peeling layer (blue) from the PMMA (green) coated Si carrier (gray). The right image shows a photograph of the peeling process.*

increases the electrical performance of the device. The VIAs are realized by electroplating of Cu in the openings using the bottom Cu electrodes as a seed layer in the electroplated solution (***Fig. 6.1A, iii***).

(v) Second metal track layer: For the second metallization layer a 20 nm/200 nm thick sputter coated seed layer of Ti/Cu is used on top of the plasma activated PP PI layer. This is patterned by photolithography (***Fig. 6.1A, iv***) to electroplate another 10 µm thick layer of Cu to increase the mechanical robustness of the metal tracks (reddish layer). Later the unwanted Cu is chemically removed.

A set of lithographic steps involving registration is required to define the locations of the solder bump-based interconnects; a patterned 10-µm-thick photoresist layer (AZ 15 NXT, Allresist, Strausberg, Germany) is used with openings to the contact pads to apply the depicted solder bumps using a parallel dip-coating process in a liquid solder bath [228].

6.1.2. Assembly of the Devices on the Hard Carrier

(vi) Device assembly*:* In the demonstrated case, a semi-automated pick-and-place technique is used like before. The depicted demonstrator contains a number of lab-fabricated field effect µ-transistor (µ-FET) ($0.5 \times 0.5 \times 0.5$ mm) and an equal number of commercially-available light emitting diodes (LED) ($1 \times 0.6 \times 0.2$ mm, 459 nm).

(vii) On hard carrier functionality tests: The depicted approach enables “on-hard-carrier” functionality tests. This is different from other methods which build on a soft elastomeric rubber substrate [50, 53]. This is beneficial since it allows for the identification of failure modes of the circuit and devices before and after the detachment, bend, or stretch the structure. For example, in the depicted hard carrier functionality tests (***Fig. 7.1A v, right***) all the LEDs function properly and response to the addressing system.

6.1.3. Rubber Encapsulation and Detachment

Figure 6.1B describes the rubber encapsulation and detachment process. Like earlier methods, a castable 3 mm thick and thermo-curable (room temperature, 15 hours) layer of EcoFlex is used as a stretchable encapsulation layer. To increase the bond strength between the assembled circuit elements, PI, and the EcoFlex a preceding 5 minutes long O_2 plasma activation step is used. The plasma activation step reduces the onset of cavitation and delamination during stretching. Note that the EcoFlex is not directly in contact with the first metal tracks. The first metal tracks are covered and surrounded with the isolating PP PI layer. However, the top electrodes and the devices are in direct contact with EcoFlex. The EcoFlex forms a strong bond to the oxygen plasma activated PP PI layer and components. It also leads to at least a partial under-fill of the assembled components which increases the level of fixation.

A wafer-scale, solvent-free detachment process is used like before to detach the components and the stretchable circuit from the hard carrier. After detachment, the PI peeling foil is removed using ECR plasma etching (40 SCCM O_2, 10 SCCM CF_4, 100 W RF power, 60 minutes at 0.0025 mbar). This process also removes the isolated PP PI layer from everywhere except beneath the metal tracks. The resulting structure has a surface mount like geometry i.e. one of the faces of the copper tracks is accessible for electrical contacts leaving the other three faces protected with PI/EcoFlex.

6.2. Design of the Integrated mPCB

In the standard PCB technology different layers of metal tracks are separated by isolation layers, and the metallization layers are connected through VIAs. A similar approach is used in this research where two different layers of metal electrodes are separated by a 20 µm thick layer of PP PI which acts as an isolation layer.

6.2.1. Metal Tracks Crossing

Figure 6.2 shows the schematic (***A***), images of top view (***B***) and side view (***C***) of a crossing region of two metal layers. As mentioned previously, the first metallization layer is buried beneath a uniform 20 µm thick layer of PP PI. This thick PP PI layer assures a complete isolation between two layers of metal tracks. Since the PP PI is uniformly spin-coated over the entire surface, it follows the surface profile of the substrate, and covers the top and sidewalls of the buried metal tracks. This leads to an inhomogeneous surface in the places where the first metal tracks are buried. This surface topography continues to the second metallization layer which produces a crossing. The optical microscope image in **Figure 6.2B**, (***i***) and SEM image (***ii***) shows a top view of the crossing region of two metal tracks, where the bottom metal tracks is darker than the top metal tracks due to the PP PI isolation layer. **Figure 6.2C** shows false-colored SEM images of side views of a crossing region. The inhomogeneous surface topography can be seen clearly in (***i***). The false-colored SEM images in (***C***) shows a crossing region, where two metallization layers are separated by a PP PI layer (***blue*** in ***ii***). The bottom metal track (dark reddish) is covered by the PP PI layer (blue) and is less sharp. The undercut (shadow region) of the top electrode is due to the chemical process used to remove the seed layer.

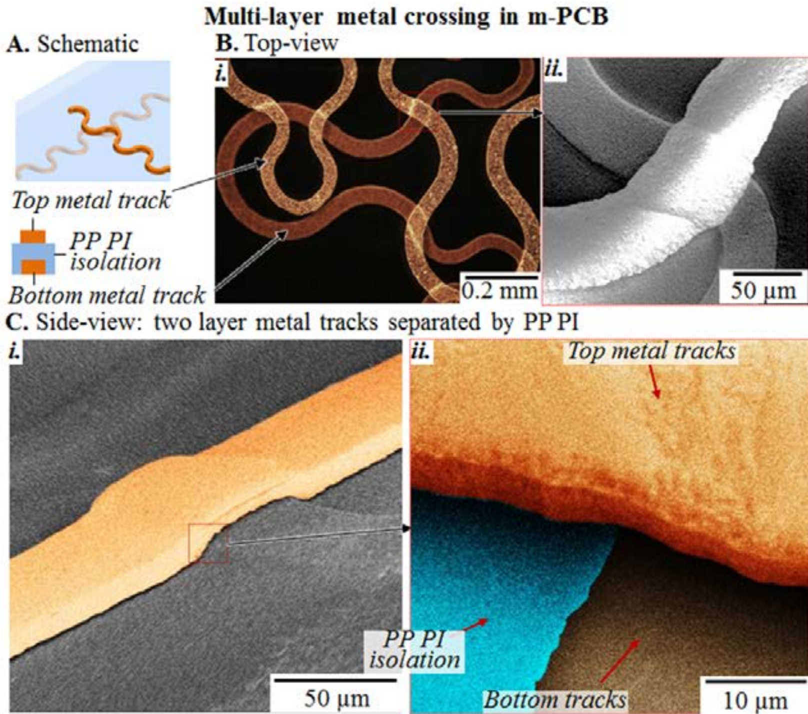

Figure 6.2: Multilayer metal crossing in mPCB. *Schematic view of two metal layers crossing in mPCB (**A**) and images of top view of a crossing (**B**). The optical image (**i**) and the SEM image (**ii**) show the surface topography at the crossing region. (**C**) Shows a false colored SEM images of the crossing region (**i**). Two metal tracks separated by PI layer (blue) (**ii**).*

6.2.2. VIA

Figure 6.3 shows schematics ($\boldsymbol{a_1}$) and images ($\boldsymbol{a_2}$-$\boldsymbol{a_4}$) of VIAs. The VIAs are used to make electrical connection between the bottom metal tracks and the top metal tracks. In the depicted case, the VIAs are grown by electroplating of Cu using the bottom metal tracks as a seed layer. This ensures excellent electrical connection between the bottom electrodes and the VIA. The VIAs are placed beneath one of the contact pads ($\boldsymbol{a_2}$) of a rigid component in order to gain additional mechanical support during stretching test. The height of the VIA is defined by the thickness of the isolation layer and can be adjusted from 10 µm to 50 µm. The false-colored SEM image ($\boldsymbol{a_3}$) shows tilted view of the different material layers in the VIA region. The beneath bright blue layer is the PI peeling layer, the dark blue layer in the top is the isolation PP PI layer. The Cu-reddish are the different layers of metal. The bottom metal track (bluish red) is covered by the isolation PP PI layer, VIA (yellowish), and

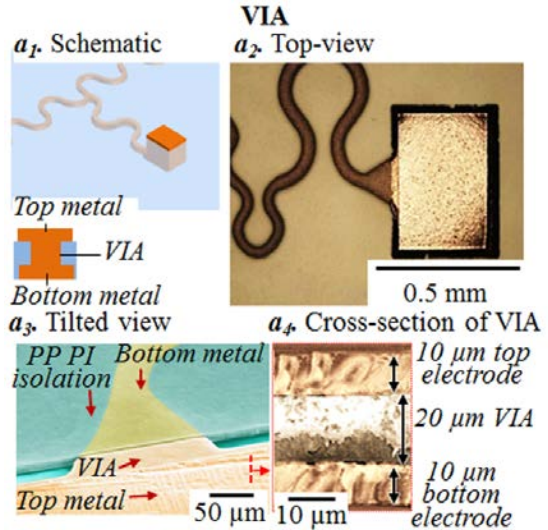

Figure 6.3: VIA in mPCB. *Schematic of the VIA: side view (**a_1**, top) and cross-section (**a_1**, bottom), and a corresponding image of a VIA (**a_2**). (**a_3**) A false-colored SEM image showing different layers of the materials in the VIA region (from bottom to top): bright blue –PI peeling layer, bluish red- first metal track (covered by PI), yellowish-VIA, dark blue-isolated PI layer, reddish-top metal track. The cross-section SEM image (**a_4**) shows the individual stack of the metals at the VIA region, 10 µm thick bottom and top electrodes are connected by a 20 µm thick VIA grown by e-plating.*

top metal tracks (bright-yellowish). The cross-sectional view in (***a_4***) shows the three metallization layers in the VIA region.

6.3. Functionality Tests

The addressable LED arrays presented here are designed using only two metallization layers and using a single transistor for each LED as shown in **Figure 6.4A**. The bottom electrodes (*blue lines,* V_g) are to address the gates in a column, while the top electrodes (*red lines*) are used for sources and drains. Each source line (V_+) can address each row, and all drain lines are grounded together (V_-). Connecting the individual contact pads of the each V_g line, each V_+ line, and V_- to an Arduino (ARDUINO MEGA 2560) board allows us to address each LED individually using a computer. **Figure 6.4B** shows an image of the Si-based µ-transistor used in this test which is fabricated using a conventional CMOS process previously discussed in **Chapter 4**.

6.3.1. Functionality Test on the Hard Carrier

Figure 6.4C shows images of the integrated LED arrays on a hard carrier (***left***) and a region with a transistor and a LED (***right***). The depicted approach allows the functionality test of the device on hard carrier. This is critical since it allows determining correct functionality of the system and comparing the performance after

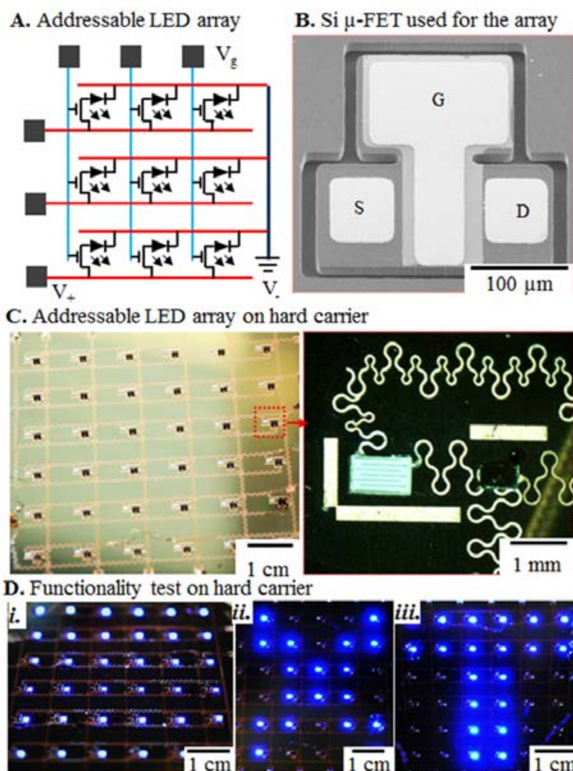

Figure 6.4: Functionality test on hard carrier. A. *Schematic layout of the matrix showing addressing system.* ***B.*** *SEM image of a Si based µ-FET used in the matrix.* ***C.*** *Images of the final device on hard carrier showing a complete array of 6 × 6 pixels (**left**) and a single pixel (**right**).* ***D.*** *Device test on hard carrier, showing a fully working matrix (**i**) and anticipated addressing matrix; an '**X**' (**ii**) and a '**T**' (**iii**) are shown.*

the circuit is released to soft substrate. This also helps to study and overcome failure faces. **Figure 6.4D** shows the function of the active matrix. All the LEDs function properly (***i***) and respond to the addressing system as anticipated; in this case an '**X**' (***ii***) and a '**T**' (***iii***) are demonstrated.

6.3.2. Functionality Test after Encapsulation and Transfer

As mentioned before, the peeling process works particularly well due to the peeling PI layer, and no defect is introduced in this step. The functionality of the device in rubber matrix after peeling and before peeling was compared. The device functions equally on a hard carrier and in a rubber matrix.

The VIAs play a major role to the system, and remain one of the novel elements in the field of stretchable electronics. Thus the VIAs are studied extensively in this research by varying its dimensions and locations. For the first test, VIAs with different dimensions are fabricated while keeping the height of the VIA the same to study the optimized dimensions (length × width) for a maximum elongation level. In the second test the VIA is placed in two different places: (***i***) beneath one of the contact pads of a SMD and (***ii***) at an isolated place in between two metal tracks. In the measurement, the intention is to find the maximum level of elongation until

different VIAs are failing. Note that the VIA dimensions do not play a major role on hard carrier functionality test, since the system non-flexible and not deformable.

Figure 6.5 shows the images of VIAs with different dimensions and locations. The experimental results are added in the tables with the corresponding figure. **Figure 6.5A** corresponds to the tests where the VIAs are placed beneath the contact pads and **Figure 6.5B** corresponds to the tests where VIAs are placed in between two metal tracks at an isolated location. Six different dimensions of VIA have been studied ranging from 25 × 35 µm to 350 × 500 µm. The average values are obtained from 6 different samples each having 6 VIAs. An automated stretching platform is used for the stretching test which is controlled by a computer.

The study reveals that the smallest VIA with dimensions of 25 × 35 µm does not function properly. This is probably due to the limitation of the technology and materials used in this research. However, the remaining VIAs function properly. The maximum level of elongation of the device shows a linear dependency to the VIA dimensions, i.e. the larger the cross-sectional area of the VIA, the more stretchable the system is. This is because the larger VIA has more mechanical stability in the rubber matrix during a single stretch test. For example, in the case of the VIA placed beneath the contact pad, the VIA with dimensions of 50 × 70 µm can be elongated up to 135% to its original length, while the VIA with dimensions of 350 × 500 µm can be elongated to 260% to its original length (***Fig. 6.5A table***). As a comparison, a single layer metal track with same design can be elongated to 320% to its original length [58]. Clearly, VIA limits the maximum stretchability of the device. This result is more critical in the case of the VIA placed in between the metal tracks (***Fig. 6.5B***) at an isolated location. For instance, the maximum elongation level in this case

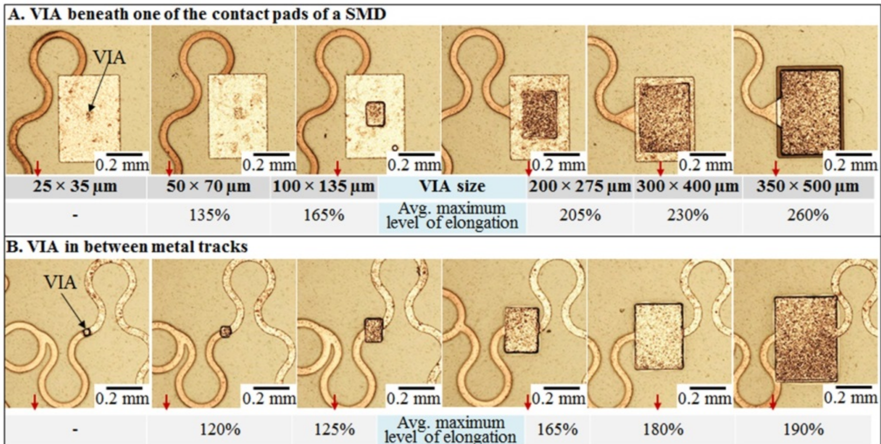

Figure 6.5: VIA study: photographs and stretching results. *Images of VIAs in different dimensions placed beneath a contact pad of a SMD (**A**) and in between two metal tracks (**B**), and corresponding results (**tables**). The average values of maximum level of elongations are taken from six test samples with 6 VIAs each.*

remains only 190% (***Fig. 6.5B table***).

It is worth to mention that in the depicted final device the components are embedded in the rubber matrix. The second metallization tracks are submerged into the rubber matrix and are surrounded by the rubber from three sides. However, the first metallization tracks remain attached to the rubber only by the isolated PP PI layer. This is a drawback of the system, since the exposed metal tracks are easily peeled off from the rubber matrix. Experimentally, it is observed that after a few cycles the metal tracks start to peel off from the rubber substrate and start to deform randomly which eventually results open circuit (***Fig. 6.6***). Manual test reveals that even the device remains non-functional due to open circuits, the VIA remains electrically connected, which means for multi-cycle tests the limiting factor is the short circuit between the metal tracks. To improve this in an additional test a thin layer of (approximately 20 µm) EcoFlex is spin coated from the back side of the substrate to embed the device and minimize the peeling off of the metal tracks. This results in a lower amount of maximum elongation level, but improves the cycling number dramatically. For example, the VIA with dimensions of 350 × 500 µm placed beneath the contact pad survives more than 20 times more cycles while embedded than the un-embedded case. However, for the later demonstrators in this study, systems without embedding are used.

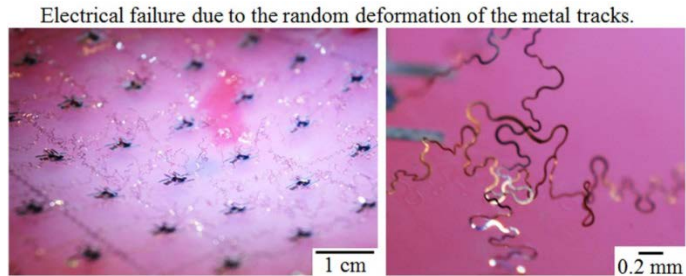

Figure 6.6: Peeling off the metal tracks results electrical failure. *The metal tracks start to peel off from the rubber substrate and deform randomly which eventually leads to electrical failure.*

Figure 6.7A shows images of the active matrix encapsulated in EcoFlex. Photograph of a full addressable LED array (***a_1***), a single pixel (***a_2***), and crossing of two metallization layers (***a_3***) are shown. **Figure 6.7B** shows a false colored SEM image of a metal crossing in EcoFlex (***green***), and two metallization layers (***reddish***) which are separated by a 10 µm thick PP PI layer (***blue***). The bottom electrode is submerged in EcoFlex matrix, while the isolation layer and the top electrodes are located on top of the rubber matrix. **Figure 6.7C** shows a SEM image of a VIA lifted off from the rubber substrate. The VIA remains intact even though the metal tracks are detached from the EcoFlex substrate.

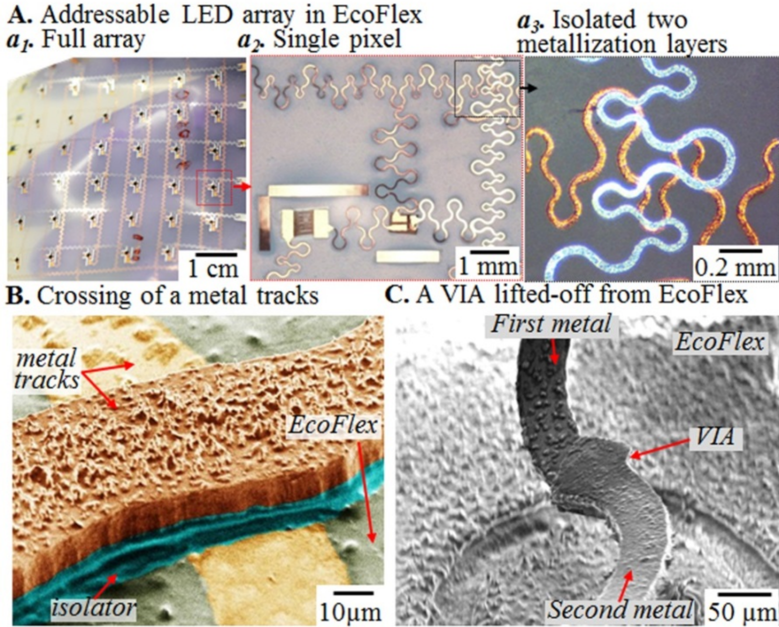

Figure 6.7: Integrated metamorphic optoelectronics in EcoFlex. A. *Integrated active matrix encapsulated in EcoFlex (**a_1**), a single matrix (**a_2**), and crossing of two isolated metallization layers (**a_3**) in EcoFlex.* ***B.*** *False colored SEM image showing different material layers at the crossing (**inset**) and (**C**) a SEM image of a VIA lifted off from EcoFlex substrate.*

The functionality test of the integrated LED arrays is shown in **Figure 6.8**. The full matrix (***a_1***) and a single pixel (***a_2***) are shown in operation. The matrix also responds to the addressing system. As mentioned earlier, an Arduino board is used through a computer to address individual pixels in the array. **Figure 6.8B** demonstrates the anticipated addressing system in a planar array (***b_1***) where LEDs are turned-on in a diagonal array. Air inflation of this array forms a hemisphere without affecting the electrical performance of the device (***b_2***).

6.4. Metamorphic LED Display

Various forms of deformation methods and mechanisms have been demonstrated in previous chapters, which can be also applied to produce metamorphic displays in various geometrical shapes. The basic idea is to use morphological changes to adjust the geometrical shapes and properties. Here, a metamorphic display is shown as a proof of concept.

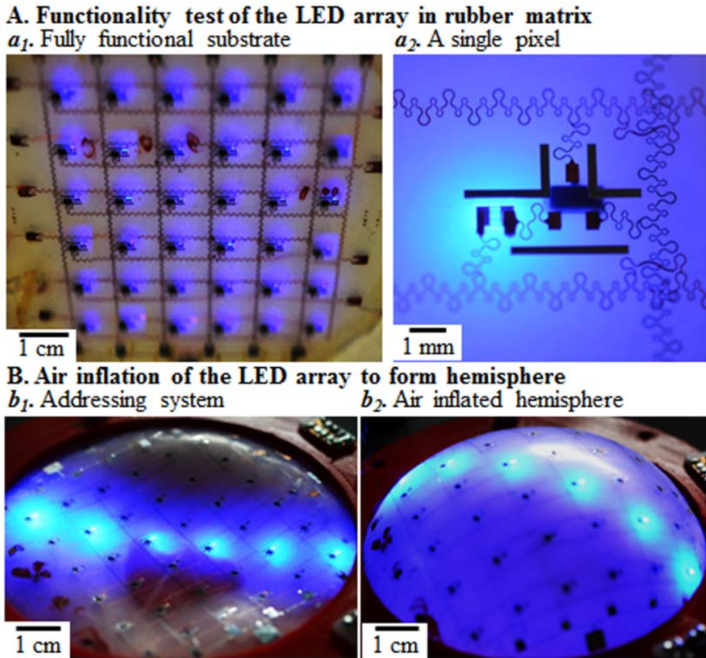

Figure 6.8: Functionality test of the addressable LED arrays in rubber. A. *Fully functional integrated LED active matrix encapsulated in EcoFlex (**a_1**), and a single pixel of the matrix (**a_2**).* ***B.*** *Deformation of the metamorphic LED arrays, the anticipated addressing system in a planar array (**b_1**), and after air inflation to form a partial hemisphere (**b_2**). The array remains functional after inflation.*

Figure 6.9A demonstrates a concept of metamorphic display. In the depicted case an integrated LED matrix is deformed using a 3D printed pyramid shape chaperon (***a***) to morph from a planar shape (***b***) to a cone (***c***). The array is clamped within a circular ring to form air sealing and then deformed using the pyramid chaperon which initially forms a cone. Further vacuum forming of the cone shape array morphs to a pyramid shape (***d***). In principle, the final structure depends on the shape of the 3D printed chaperon. **Figure 6.9B** demonstrates the addressing system of the array. Two sides of the metamorphic pyramid are lighting simultaneously.

In summary, this chapter presented a method to produce multilayer integrated metamorphic printed circuit board (mPCB) with VIAs, which is fully compatible with conventional printed circuit board technology. In principle, this method would allow to realize any electronic devices known today to be stretchable and metamoprhic to take on new 3D shapes and form factors.

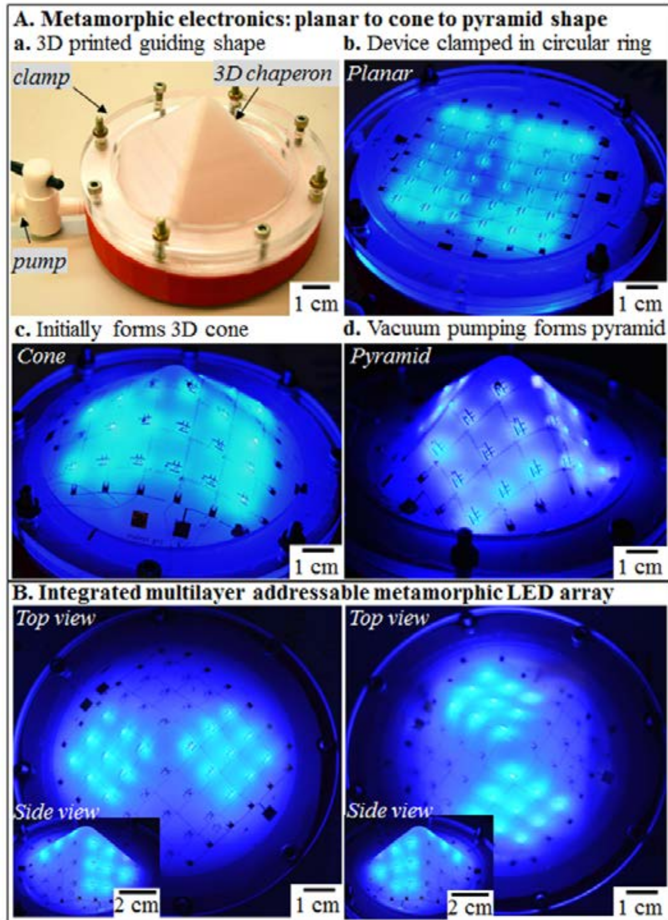

Figure 6.9: Integrated multilayer metamorphic LED arrays. A. *Metamorphic electronics morphing from planar orientation to cone to pyramid shape. A 3D printed pyramid is used as a 3d chaperon (****a_1****) to morph a clamped planar LED matrix (****b****) to a cone (****c****). Further vacuum pumping of the clamped LED matrix morphs to a 3D pyramid as designed in* ***a. B.*** *Demonstrating addressable LED matrix by lighting two sides of the pyramid simultaneously.*

CHAPTER 7

Metamorphic Touchpad

7.1. Reverse Engineering of a Touchpad

7.2. Manufacturing of Stretchable Touchpad

7.2.1. Fabrication of stretchable touchpad

7.2.2. Rubber encapsulation and detachment

7.3. Functionality Tests

7.3.1. Stretchable touchpad in planar orientation

7.3.2. Hemispherical touchpad

Current human-computer interfaces are mostly limited to 2D interfaces. This limits our capacity and experiences to interact in a virtual and 3D world. For example, a 3D touchpad would help a designer to design his graphics in real 3D space or a gamer could experience a true 3D environment while gaming and could interact accordingly. There are a few approaches to realize 3D touchpad [255], where the device uses a 2D touchpad with 3D gestures to sense z direction. The technology uses a 2D surface and virtually creates a 3D space by its motion detectors, which for some applications might be sufficient but certainly not always. However, a true 3D touchpad would revolutionize human-computer interfaces when it comes to the interaction in a 3D space or on a spherical surface.

In this chapter a hemispherical touchpad is demonstrated which is inflated from a stretchable 2D membrane. In short, two stretchable metallization layers have been arranged in two levels separated by a dielectric medium as a checkerboard style.

7.1. Reverse Engineering of a Touchpad

The primary idea is to realize a stretchable touchpad is to replace conventional planar 2D touchpad with metamorphic stretchable touchpad which can be deformed to take 3D shapes. One effective way to achieve this is reverse engineering approach of an existing touchpad.

A commercially bought touchpad is dismounted and studied in depth in order to understand its design, mechanisms and functionality. **Figure 7.1** shows the optical (***A***) and x-ray (***B***) images of the touchpad. The x-ray images show the layers and components in the PCB. As can be seen, the uses a checkerboard pattern and two

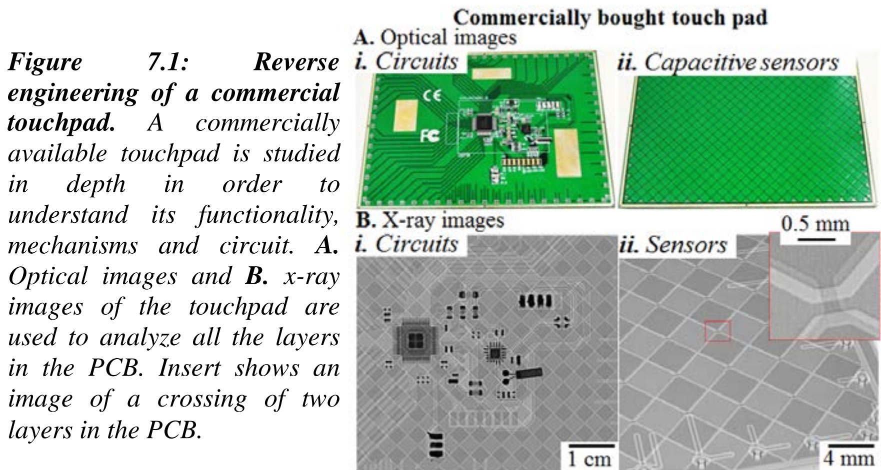

Figure 7.1: Reverse engineering of a commercial touchpad. *A commercially available touchpad is studied in depth in order to understand its functionality, mechanisms and circuit.* ***A.*** *Optical images and* ***B.*** *x-ray images of the touchpad are used to analyze all the layers in the PCB. Insert shows an image of a crossing of two layers in the PCB.*

different metallization layers in 20 × 15 matrix. Each checker in a row is in the same layer and is connected from left to right (***Fig. 7.1B ii***, ***insert***). This particular touch pad follows the projected capacitive principle.

Figure 7.2 schematically shows the principle of a simple capacitor where two conducting plates (***reddish***) with area ***A*** is separated by a distance ***d*** which is filled by a dielectric materials (***blue***). The capacitance of the system is

$$C = k\varepsilon_0(A/d), \qquad \textbf{(eq.7 1)}$$

where $\boldsymbol{A} = \boldsymbol{L}\times\boldsymbol{W}$, $\boldsymbol{k}$ is the dielectric constant of the dielectric material and $\boldsymbol{\varepsilon_0}$ is the permittivity at free space, 8.854×10^{-12} F/m. Thus the capacitance of the system locally depends on the area of the conductive plates, thickness and dielectric constant of the material.

Based on these analyses a stretchable touchpad is designed using meander shape metal tracks (***Fig. 7.3***). Since a closed metal surface is not stretchable, the conducting plates are replaced by densely packed meander metal tracks to be stretchable as shown in **Figure 7.3** (***insert***). As an initial test device a 5 × 5 matrices is designed.

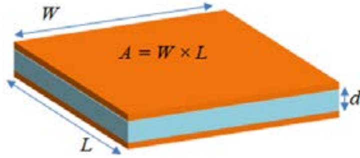

Figure 7.2: Schematic principle of a capacitor. *Two conducting plates with area* ***A*** *are separated by a dielectric medium with thickness of* ***d****. See main body.*

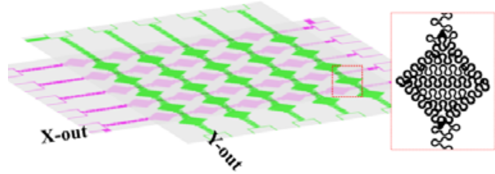

Figure 7.3: Stretchable touchpad design. *Mimic design of a stretchable touchpad inspired by commercial rigid touchpad. Meander shape metal interconnects are designed in two different layers as stretchable conductors which are separated by a thin dielectric layer.*

7.2. Manufacturing of Stretchable Touchpad

7.2.1. Fabrication of Stretchable Touchpad

Fabrication of stretchable touchpad is ideally similar to the process described before in section ***3.1.1***. The process starts on a hard carrier substrate with sacrificial layers.

Figure 7.4A describes the first part of the processing sequence of stretchable touchpad on hard carrier. A cleaned 500 µm thick Si wafer (MicroChemicals, Ulm, Germany) is spin coated with a thick layer of poly(methyl-methacrylate) (**PMMA**) and baked on a hot plate. Subsequently, an 8 µm thick polyimide (**PI** 2611) is spin coated and fully cured in a convection oven at 200 °C for 5 hours under N_2.

A 50 nm/200 nm thick sputter coated layer of Al/Cu has been used as a first metallization layer. The beneath Al layer is later used as a mask to etch the peeling PI layer after the device is released from hard carrier to rubber substrate. The wafer is then patterned for electroplating with photolithography using negative resist and a subsequent standard descumming process (5 minutes, 100 W RF power, 50 SCCM O_2) is performed to remove any residues from the patterned resist. Then a 10 µm thick layer of Cu is electroplated on top of Cu seed layer using Cu 100 electrolyte (nb technologies, Bonn, Germany). Later the resist is stripped using standard remover (NI555 at 80 °C) and a subsequent chemical etching process is carried out to etch the 200 nm Cu seed layer using standard Cu etchant and 50 nm Al in Al etchant (MicroChemicals, Ulm, Germany) (***Fig. 7.4A i***).

As dielectric material initially PI (k = 2.9 [256]) and photopatternable PI (HD 4100, HD Microsystem, Neu-Isenburg, Germany) (k = 3.36 [256]) have been tested. A 20 µm thick PI is spin coated uniformly on top of the first metal tracks. The PI layer covers the entire surface of the substrate; top and sidewalls of the 10 µm tall and 50 µm wide metal tracks (***Fig. 7.4A ii***).

For the second metallization layer a 20 nm/200 nm thick sputter coated seed layer of Ti/Cu is used on top of the plasma activated PI layer. This is patterned by photolithography (***Fig. 8.4A iii***) to electroplate another 10 µm thick layer of Cu (reddish). Later, the unwanted Cu is chemically removed.

7.2.2. Rubber Encapsulation and Detachment

Figure 7.4B describes the rubber encapsulation and final device. Like earlier methods, a castable 3 mm thick and thermo-curable layer of EcoFlex is used as a stretchable encapsulation layer (***Fig. 7.4B iv***). To increase the bond strength between the second metal tracks, PI and the EcoFlex a preceding 5 minutes long O_2 plasma activation step is used. Note that the EcoFlex is not directly in contact with the first metal tracks. The first metal tracks are covered and surrounded with the dielectric PI layer. The EcoFlex forms a strong bond to the oxygen plasma activated PI layer.

A wafer-scale, solvent-free detachment process is used like before to detach the stretchable touchpad from the hard carrier to rubber substrate (not shown in the figure). After detachment, the PI peeling foil is removed using ECR plasma etching (40 SCCM O_2, 10 SCCM CF_4, 100 W RF power, 60 minutes at 0.0025 mbar). This process also removes the dielectric PI layer from everywhere except beneath the

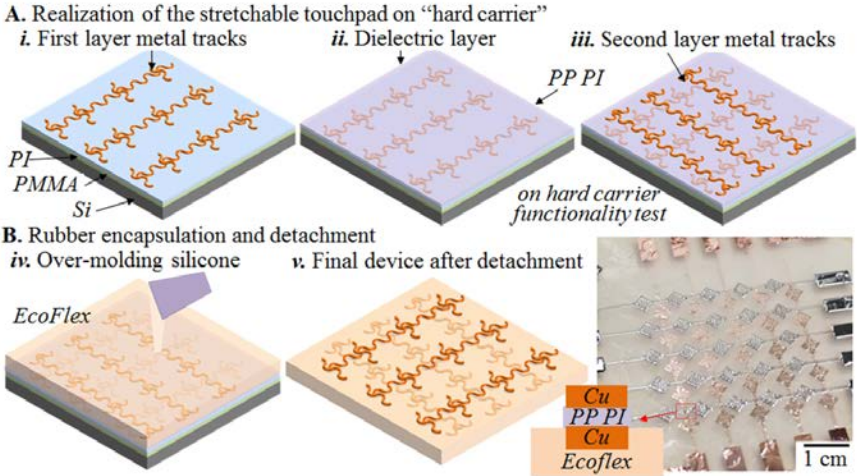

Figure 7.4: Fabrication of stretchable touchpad. A. *"On-hard carrier" fabrication (**i**) PMMA release layer (greenish), PI peeling layer (blue) and metallization layer (orange), (**ii**) thin dielectric layer (purple), and (**iii**) second metallization layer (orange).* ***B.*** *Rubber matrix encapsulation and detachment; (**iv**) over-molding EcoFlex and (**v**) final device after detachment and removing sacrificial PI layer. The peeling process detach in between PMMA-PI interface. The optical image shows the final device in EcoFlex (**right**), and schematic stack of the layers in the final device (**insert**).*

metal tracks (***Fig. 7.4B v***). Right figure shows an optical image (***Fig. 7.4B v, right***) of a final device.

7.3. Functionality Tests

To test the functionality of the stretchable touchpad, the fabricated device is connected to the original touchpad. The connection is made manually using thin isolated Cu cable. The rows and the columns of the fabricated device are connected sequentially to the original touchpad which is connected to a laptop through USB (universal serial bus) connection. During the tests other connected interfaces to the laptop are kept unattended, only the newly fabricated device is under operation.

7.3.1. Stretchable Touchpad in Planar Orientation

Figure 7.5 shows the results of the functionality test of the stretchable touchpad in planar orientation. The first image (***Fig. 7.5A left***) shows the experimental set up of the touchpad and the connection to the computer through the original touchpad. Each row and column has two contact pads in two opposite ends, only one of the

pads is connected to the board and other pad remains floating. The magnified view of the capacitive touch sensors (***Fig. 8.5A right***) shows the conductive electrodes in two different layers within the rubber matrix. The two metallization layers are separated by PI or PP PI (not shown in the figure), the SEM image (***inset***) shows a crossing of two metal tracks in two layers.

Figure 7.5B shows the results of the touchpad in operation. Three images are taken from a video at three different times while the touchpad is in operation. The white spot in the red circles indicates the cursor position at any specific time. The changes in the cursor position are entirely due to the sweeping of a finger on the stretchable touchpad.

The sensing of the touchpad in planar orientation is almost compareable to the original device except that the fabricated touchpad in the rubber matrix seems slightly slower than the original device. This is probably due to the density of the

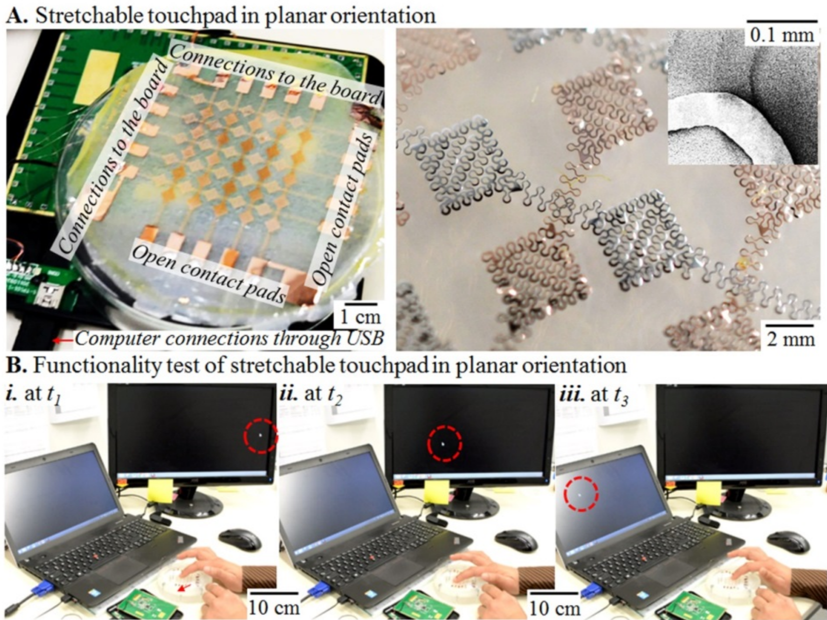

Figure 7.5: Functionality test of the touchpad in planar orientation. A. *Photograph of the fabricated stretchable touchpad connected via thin Cu wires to the original touchpad which is connected to a laptop through USB connection (**left**). The right image shows a magnified view of the capacitive touch sensors in two different layers within rubber matrix, insert shows an SEM image of two metal layers. **B.** Images of the functionality test of the touchpad operating through a laptop. The red circles in three images show the cursor position in different times due to the movement of the finger on the touchpad.*

sensors and the changes in the dielectric material. The stretchable sensor has a lower areal coverage with conductive sensors to empty spaces, and also the area of the conducting plates (***A***) is less than the original device due to the meander shape metal tracks.

7.3.2. Hemispherical Touchpad

The depicted touchpad in EcoFlex substrate is highly stretchable and can be deformed to different geometrical shapes as described previous chapters. This deformation capability of the touchpad is unique in the sense that it can take various 3D shapes out of a 2D plane. To illustrate this concept the stretchable touchpad from the last section is deformed to a 3D hemisphere by air inflation within a clamp.

Figure 7.6A shows the images of the hemispherical touchpad after inflation. The left images show the deformation process, where a planar rubber membrane (***i***) is inflated by air to morph to a hemisphere (***ii***). The membrane is clamped within an 8 cm in diameter circular polymer ring to form a pressure seal and electrical

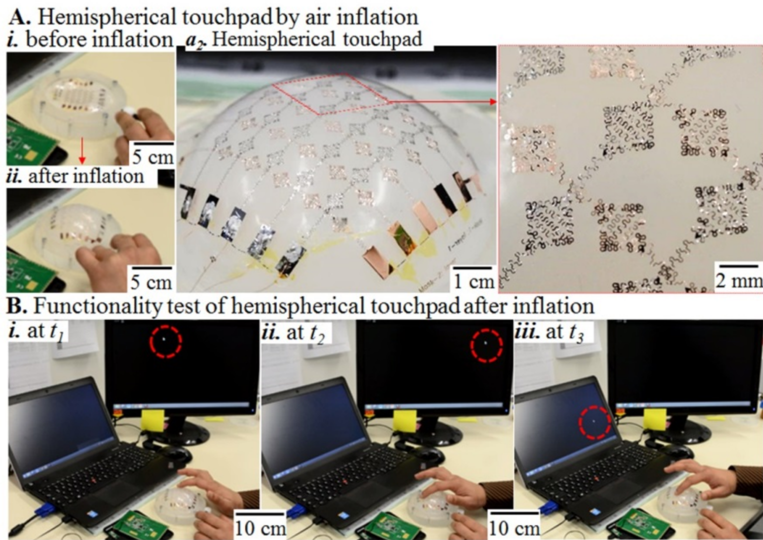

Figure 7.6: Functionality test of the touchpad in hemispherical orientation. A. *Inflation of the stretchable touchpad from planar shape to hemispherical shape (**left**), hemispherical touchpad (**a_2**), and a magnified view of the capacitive touch sensors in two different layers in rubber matrix after inflation (**right**). **B.** Images of the functionality test of the hemispherical touchpad. The cursor in the red circles indicates different position at different times due to the movement of the finger on hemispherical touchpad.*

connections with an opposing surface. A full hemispherical touchpad is shown in **Figure 7.6A, *a_2*** with a magnified view of the stretched conductive plates (***right***).

The functionality test of the sensors in hemispherical orientation is shown in **Figure 7.6B**. The inflated hemispherical touchpad remains functioning similar to the planar shape as shown in the three images which are taken during the operation. Sweeping the bare finger on the sensors can successfully move the cursor over distances.

Since the planar touchpad is inflated to a hemisphere requiring a 200% areal stretching of the substrate and the conductors. The rubber membrane is intrinsically stretchable and increases its area by double due to the inflation. However, the metal tracks are not intrinsically stretchable and only use geometrical design to respond to the applied strain (discussed before). This means the total area of the metal plates and the tracks are nearly same, while the substrate area is doubled. This should change the performance of the hemispherical touchpad dramatically.

However, in practice, the performance of the hemispherical touchpad remains nearly same. This is because the touchpad uses projected capacitive sensing which, in principle, depends on the area of the conductive plates and thickness of the dielectric material (***eq. 7.1***). In the depicted case, the dielectric material is also patterned similar to the meander shape conductors in order to make it equally stretchable, since the used dielectric material is also not intrinsically stretchable. In other words, the dielectric material remains only beneath the top meander shape conductor and the total area of the dielectric material remains also unchanged during the stretching operation. This means the active capacitive sensors in the touchpad remain unchanged, except increased inter-distances of the meander tracks.

The depicted hemispherical touchpad has two metallization layers in two different levels, and top metal track is not embedded in the rubber matrix and only connected to the substrate through dielectric materials. This is a similar arrangement that has been discussed in ***Chapter 6***. As discussed previously, this arrangement leads to a problem during stretching or inflation test. The top metal tracks start to twist and eventually detached from the substrate which leads to short circuits in the touchpad. Additionally, due to the twist during sweeping the finger touches the sensors which also leads to the detachment of the metal tracks and eventually the circuit fails.

A possible solution to this problem could be to encapsulate the sensors using another layer of EcoFlex. This has not been tested yet. However, this might lead to another problem for sensing operation due to the rubber encapsulation, since the sensors use capacitive sensing which might effect by the encapsulation layer.

However, a successful implementation of 3D shaped touchpad would be the best possibility to realize a true 3D touchpad, which would open many new possibilities in the robotics, computer designing, gaming, virtual reality, and so on.

CHAPTER 8

Other Devices

8.1. Wearable Electronics

8.1.1. Body as a primary substrate

8.1.2. Body as a secondary substrate

8.2. Electronics on Fabrics

8.3. Large Area Stretchable Electronics

8.3.1. Large area fabrication

8.3.2. Letter-size stretchable LED arrays

8.1. Wearable Electronics

Wearable electronics have been commercially available for decades. These are the types of electronics that can be mounted on the body; the mounting methods can be different. For example, commercially available wrist watches also falls into the category of wearable electronics. Especially, this type of electronic devices is extensively being used in medical diagnosis or for health monitoring. However, these types of devices are not flexible, not stretchable and not conformable.

In recent years wearable electronics have taken a new dimension. Along with the flexible and stretchable electronics, the wearable electronics also became conformal, which means that the electronic devices can be mounted on the body and the device conforms to the body. This new type of wearable electronics is known as "epidermal electronics" or "e-skin". In this chapter, the term "wearable electronics" refers to the electronic devices that conform to the body.

A number of wearable electronic systems have been demonstrated for last few years. These devices can conform to skin or attached to soft and wavy surfaces, and are able to monitor real-time physiological properties of the body. One of the remarkable demonstrators was epidermal electronics in 2011 by J. Rogers's group, where the group realized a wireless epidermal electronics system that can be mounted directly onto skin with integrated temperature sensors, strain gauges, ECG sensors, EMG sensors, RF coils, RF diode and power coils [50]. A number of similar skin-mountable devices with various types of functionalities have been demonstrated later on. For example, wearable sensors can measure physiological data from body in real time such as blood pressure [81], oxygen saturation [82], breathing rate [83, 84], heartbeat, human body temperature [85, 86], body movement [87, 88] and so on.

During this thesis, a partial attention has been given to realize wearable devices with or without active components on it. The approaches and the results are summarized in this chapter.

The wearable electronic devices can be categorized into two types based on the mounted method of the electronics onto the body. The first category uses the skin or organs as a substrate and the second category uses an intermediate substrate to mount the electronics onto the body.

8.1.1. Body as a Primary Substrate

These types of devices are mounted directly onto the body and require no additional substrate. Since the device uses the body such as skin as primary substrate, the device conforms very uniformly to the mounting surface. The device can be passive where no active components are used rather uses only one type of

electrodes or sensors, or can be active where active components are used with the electrodes or sensors.

i. Passive device

Passive devices usually contain only electrodes for sensing. For example, a single layer metal electrode can be used as temperature sensor just measuring the changes in the resistivity of the electrodes. On the other hand, same metal electrodes can be used as a thermal-pad by passing a low current through the electrodes. As proof of concepts similar devices have been demonstrated here.

Figure 8.1A shows images of a passive device mounted directly onto human skin. The device is fabricated on a hard carrier using PMMA sacrificial layer and transferred to the body using water-soluble tape which is later dissolved in water. Since the device is directly mounted onto the skin, the device conforms to the body

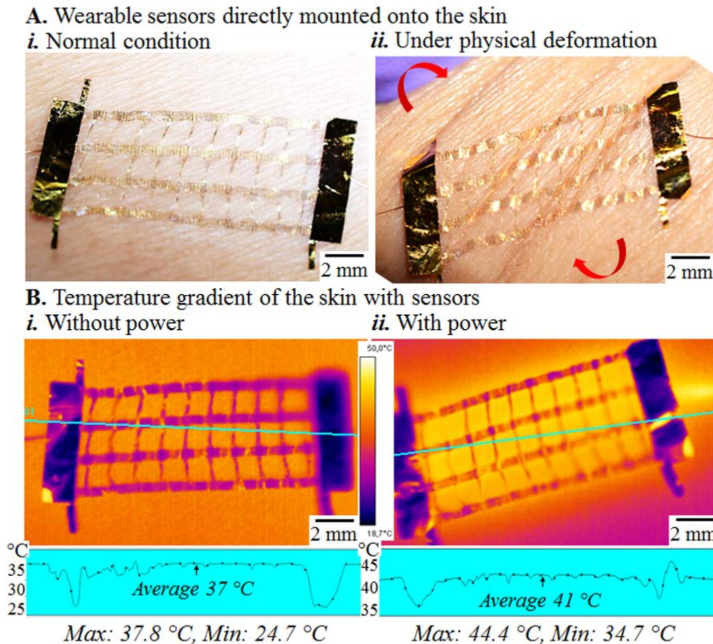

Figure 8.1: Wearable electronics: body as a primary substrate for passive device. ***A.*** *Thin layer of gold electrodes are directly mounted onto skin (**i**), and the mounted device under mechanical deformation (**ii**).* ***B.*** *The device is used as a thermal pad by passing a low current through the electrodes. Without a current (**i**) the device shows a normal body temperature and with current (**ii**) the local temperature of the skin increases.*

(***Fig. 8.1A i***) and follows the distortion of the skin for any mechanical deformation (***Fig. 8.1A ii***).

In the depicted example, 400 nm thick Au electrodes are used as sensors. The device can be used as a thermal patch by passing a low current through the electrodes. **Figure 8.1B** shows the temperature gradient of the sensor mounted onto skin. The images are taken using a thermal camera (FLIR Thermovision A40). Without any power through the sensors, the temperature of the skin remains the normal body temperature nearly 37 °C (***Fig. 8.1B i***) and no temperature gradient is observed. The body temperature is locally increased by passing a low current through the sensors and a temperature gradient can be observed near the mounted patch (***Fig. 8.1B ii***). In this case 0.1 mA current is passed over 2 V potential differences through the device which results an increase of local temperature by 4 °C up to 8 °C.

ii. **Active device**

Active devices usually contain active components to control or perform electrical functionality with electrodes for interconnecting the components. Most of

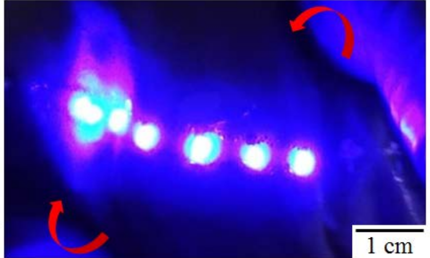

Figure 8.2: Wearable electronics: body as a primary substrate for active device. A. *Electronics with active LEDs and interconnects directly mounted onto the skin. Device is not in operation (*$\boldsymbol{a_1}$*) and in operation (*$\boldsymbol{a_2}$*). The left images (**i**) show the electronics in normal condition and the right images (**ii**) show the device under mechanical stress.*

the demonstrated epidermal electronics which are directly mounted on body are passive and do not contain active components. This is probably due to the difficulties in the processing. Usually the active components are rigid and large in dimensions which make the system less conformal However, there are a few examples where directly body mounted active devices are demonstrated with various functionalities using lab-fabricated active devices [50].

Body mounted active devices would certainly broaden the functionality of this type of devices and also would open new applications. Similar types of body mounted devices have been realized during this thesis using commercially available SMDs.

Figure 8.2A shows images of a LED array mounted directly onto skin as a demonstrator of wearable active device. Similar to the last process, the device fabrication and assembly of the components are done on hard carrier using sacrificial layer and transferred to the body using water-soluble tape which is later dissolved in water. **Figure 8.2A** $\mathbf{a_1}$ shows electronics in off state and in **Figure 8.2A** $\mathbf{a_2}$ electronics in operation. Left figures (***i***) show images of the device in normal condition and the right figures (***ii***) show the conformity of the device to the body during physical deformation.

8.1.2. Body as a Secondary Substrate

These types of devices already have a primary substrate and mounted onto the body as a secondary substrate. Unlike the last cases, the device uses the body as a secondary substrate thus the device conformity depends on the primary substrate. For example, a very thin, flexible and stretchable primary substrate will be more conformal than a thick and non-stretchable substrate.

i. Passive device

Figure 8.3A shows images of wearable sensors mounted on fingertip. The device is fabricated on hard carrier using a PMMA release layer and a thin PI layer (1 µm). The thin PI layer acts as a primary substrate after the device is transferred from the hard carrier using a stamp (water soluble tape or PDMS) onto the body. After mounting the device on the body the metal electrodes become in direct contact with the skin from one side and remains protected from the other side by the PI layer (schematic ***Fig. 8.3A inset***). Since the primary substrate used in this case is a very thin layer of PI, the device shows a very good conformity to the body. The left image in **Figure 8.3A** ***i*** shows the conformal device in normal condition and the right image (***ii***) shows the device under mechanical stress. The device conforms nicely to skin and responses nearly same with the skin during deformation.

However, as mentioned earlier, the conformity of the device to the body greatly depends on the thickness of the primary substrate. **Figure 8.3B** shows images of

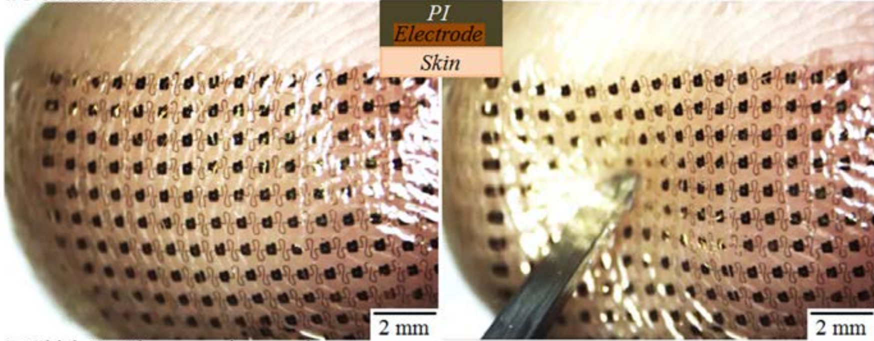

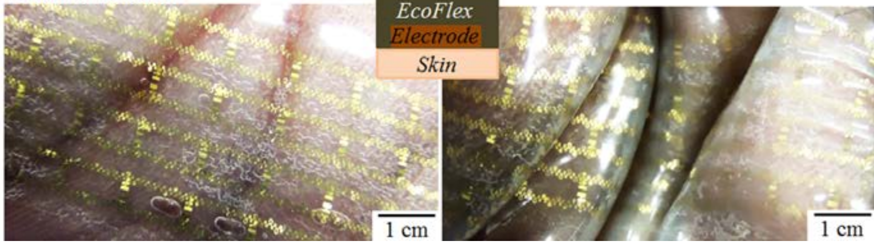

Figure 8.3: Wearable electronics: body as a secondary substrate for passive device. A. *Metal electrodes on a thin PI layer are mounted on fingertip where electrodes are directly in contact with the skin from one side and protected from the other side by a thin PI layer (**inset**). Left image (**i**) shows the device in normal condition and the right image (**ii**) shows the device under mechanical stress.* ***B.*** *Relatively thick EcoFlex membrane is used as a primary substrate for metal tracks which is mounted on hand. Left images (**i**) show the device in normal condition and the right images (**ii**) show the device under deformation.*

passive device on 500 µm thick EcoFlex substrate mounted on hand. The left image (***Fig. 8.3B i***) shows the device in normal condition and the right image (***Fig. 8.3B ii***) shows the device under physical deformation. The conformity of this device is far less than the first device where primary substrate was a very thin PI layer.

ii. **Active device**

Most of the active devices are relatively complex when functionality of the device goes beyond simple sensing, and generally these devices contain several active components to process electrical signals. Such complex active devices are relatively challenging to directly mount on the body (section ***8.1.1. ii***). This requires a primary substrate to assemble the circuit along with the components, and the body is used as a secondary substrate. This also permits the devices to be reused, which is rarely possible when the device is directly mounted on the body.

Figure 8.4 shows an example of a wearable device where EcoFlex substrate is used as a primary substrate and body is used as a secondary substrate. The device has two parts (***Fig 8.4 A***), a processing unit and three sensing units. The processing unit (***a_2***) contains all the active components, SMDs and interconnections. This part is fabricated following the method previously reported in ***section 3.1***. **Figure 8.4A *a_2*** shows the images of the complete device submerged in a rubber matrix from back (***top***) and through EcoFlex (***bottom***).

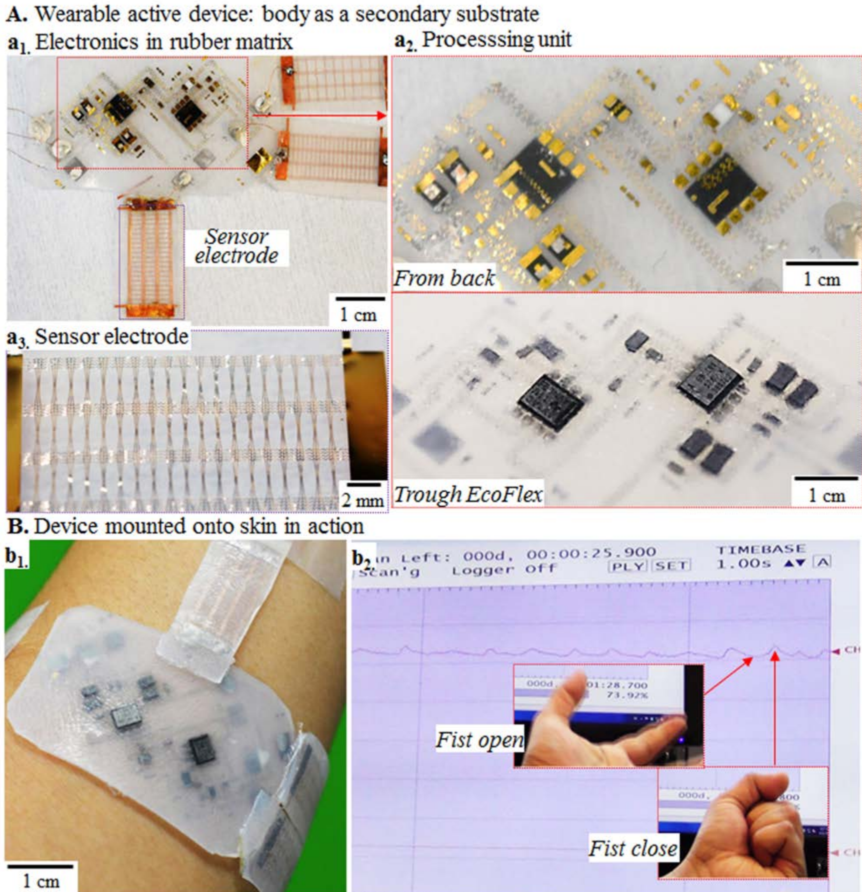

Figure 8.4: Wearable electronics: body as a secondary substrate for active device. A. *Active electronics in rubber matrix (**a_1**) consisting of two parts: a processing unit (**a_2**) and three sensing units (**a_3**).* ***B.*** *The device is mounted on the skin such that the sensing units in direct contact with the skin (**b_1**), the device is used to record the changes in the skin potential during muscle activities in the hand (**b_2**).*

The sensing units use three separate metal electrode meshes (***a_3***) fabricated separately from the processing unit, but in a similar method. The sensor electrodes are connected to the processing unit manually using silver epoxy as shown in **Figure 8.4A** ***a_1***. One of the electrodes is used as a reference sensor and other two electrodes are used to record changes in the body potential locally.

Figure 8.4B shows the image of the active device mounted on the hand in such a manner that the sensor electrodes are directly in contact with the skin. Since, the primary substrate (EcoFlex) is thick, as described in the last section, the conformity of the device is relatively low. Normal adhesive tape is used to have a better conformity of the sensor units to the skin and to stable the device with the body during motion. The device is connected to a computer through RedLab-1608FS (Meilhaus Electronic) via USB connection.

The performance of the device is tested initially to detect the potential changes in the skin during the movement of the hand. The result is shown in **Figure 8.4B** ***b_2***. The recorded signal shows the changes in the body potential when the fist of the device mounted hand is closed and opened subsequently (***inset***). When the fist is closed, an increase in the potential is recorded, and the potential drops when the fist is open. This small change in the body potential is due to the muscle activities.

The demonstrated device is relatively simple in terms of device functionality but shows a unique method to realize wearable electronics. The depicted device uses a single metallization layer which limits the complexity of the electronic circuits. However, a multi-metallization layer method has been demonstrated previously which can be implemented for this type of devices as well. Combining these two methods many more complex wearable devices are possible to realize. Such devices will find its applications in health monitoring, medical diagnosis, sports and other types of wearable electronics.

8.2. Electronics on Fabrics

The importance and the possibilities of electronics in the fiber-based clothing have been discussed previously which also can be considered as wearable electronics. Recently, there has been a great attention in this field along with the development of stretchable electronics.

In principle, this type of devices is easy to fabricate and relatively reliable, since commonly used fibers in the garments industries are not highly stretchable but flexible. So the fabrics itself can be used as a substrate for the electronics.

Figure 8.5 shows a demonstrator of electronics on fabrics. The depicted active device is fabricated on a hard carrier using PMMA sacrificial layer and transferred to the fabric. To transfer the device, a spray coated adhesive layer is used on top of the target fabric. The sacrificial PMMA is partially removed in acetone and is brought in contact to the adhesive coated fabric. The fabric is gently pressed to the device with a thick EcoFlex substrate in order the get a homogeneous contact of the device to the fabric. Later, the fabric is pulled up to release the device from the substrate. As can be seen in the figure, the yield of the transfer process is 100% and reproducible. Going forward it would be possible to realize many complex electronic devices in fabrics.

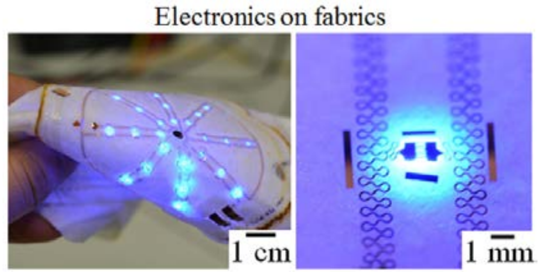

Figure 8.5: Active electronics on fabrics. *Active LED arrays on fabrics.*

8.3. Large Area Stretchable Electronics

To realize a flexible, stretchable and metamorphic electronics world, the manufacturing process requires being compatible with large scale industrial production. In addition, the substrate size has to be dimension increased beyond what is currently possible in the field of stretchable electronics. Considering these facts, the demonstrated devices so far is limited to wafer-scale fabrication which might not be always sufficient for some applications.

In this section, an industry compatible manufacturing process is presented to realize large area stretchable electronics. Similar to the wafer-processing, the large area manufacturing method also uses an on hard carrier fabrication process to enable high-temperature processing, and improve registration, alignment accuracy, and enable the use of automated mounting methods.

8.3.1. Large Area Fabrication

To enable large area stretchable electronics a method has been developed that uses conventional PCB substrate materials. Conventional PCB such as FR4 uses cured glass epoxy as a substrate material. Similar FR4 substrates are also used during this project to realize an industry compatible large area stretchable electronics fabrication process.

Similar to the process used in the wafer-level fabrication, the reported large area fabrication method uses two layers of scrificial materials, PMMA as a release layer and PI as a peeling layer. As metalization layer adhesive copper foils are used since evaporation or sputtering at this scale is not always available. The complete circuit is finally encapsulated using EcoFlex and detached from the carrier substrate.**Figure 8.6** shows the process flow and corresponding photographs of the large area fabrication method that has been develeoped towards the end off this thesis. Conventional bare FR4 (DE104, Isola AG, Düren, Germany) glass epoxy is used as a hard carrier substrate without Cu cladding. The release PMMA and peeling PI layers are applied using a ductor blade coating technique instead of previously used spin coating (***Fig. 8.6 a_1***). The

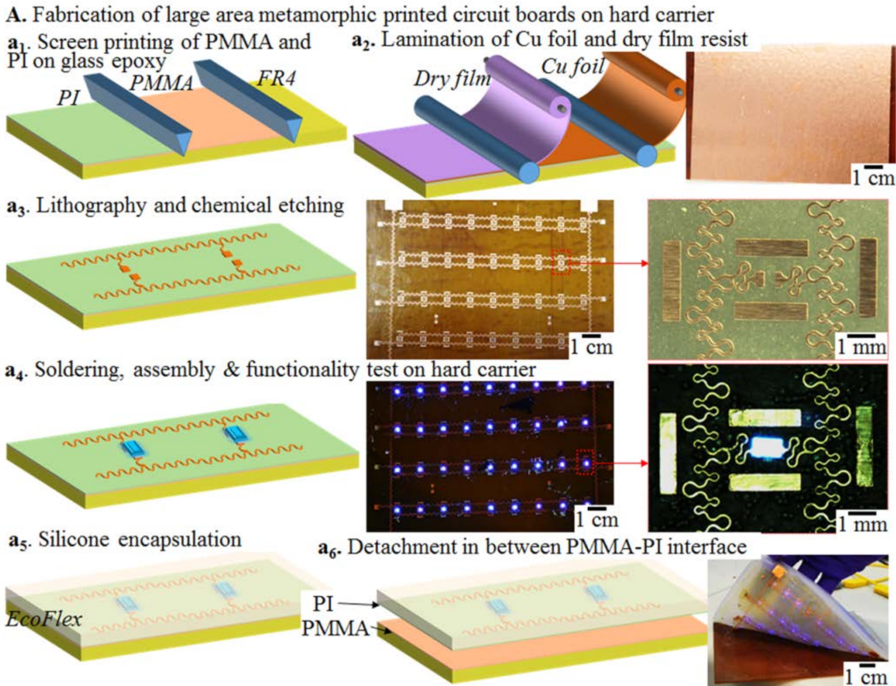

Figure 8.6: Process flow of the large area stretchable printed circuit board. *The method uses conventional glass epoxy (FR4) as a hard carrier substrate and ductor blade for coating the PMMA and PI sacrificial layers (**a_1**). Lamination process is used to laminate metal foil and dry film photoresist (**a_2**). Subsequently the metal foil is patterned by photolithography and chemical etching (**a_3**), later coated with solder bump after another lithography process, and the components are assembled on hard carrier (**a_4**). Right photographs show the corresponding images of the processed substrate and the functionality test on hard carrier (**a_4, right**). Finally, the device is encapsulated by EcoFlex mold (**a_5**) and detached from the carrier substrate (**a_6**). The right image shows a peeling process of the active devices from the carrier substrate (**a_6, right**)*

PI layer is cured in a convection oven at 200 °C for 5 hours under N_2. As a metallization layer adhesive Cu foil is used with different thicknesses. In the depicted case 35 µm thick letter size adhesive Cu foil (Holland Shielding Systems BV) is laminated (***Fig. 8.6*** a_2) instead of the previously used evaportion and electroplating method for wafer-scale fabrication. The large area lithography also uses the lamination of the dry film as a photoresist (a_2). The pattern Cu is chemically removed in a HNO_3 bath, and the remaining resist is subsequently removed in the remover (***Fig. 8.6*** a_3).

Another set of lithographic steps is performed to define the locations of the solder bump based interconnects, which is coated using a dip coating process in a liquid solder bath (Indalloy #117, MP. 47 °C, Indium Corp., NY). The fabrication process is completed after removing the second layer of photoresist.

Similar to the wafer-scale fabrication process, the large area fabrication method is also compatible with various types of chip attachment and assembly methods including solder bump based interconnects, flip-chip die attach, robotic pick-and-place, or engineered self-assembly using molten solder. In the demonstrated case a semi-automated pick-and-place machine is used to assemble the components under a microscope in combination with solder bumps to achieve alignment. In the depicted demonstrator, two terminals chip-scale (L=1 mm, W=0.6 mm, H=0.2 mm) surface mount LEDs (459 nm, Creative LED GMBH, Schaan, Liechtenstein) are used. Specifically, the LEDs are placed onto the solder bumps which are located on the receiving substrate. Reflow of the solder causes the chips to attach and self-align as a result of the reduction of the surface free energy of the solder. The approach enables "on-hard-carrier" functionality tests (***Fig. 8.6*** a_4). The illustrated result shows an array of LEDs (***middle***) and a single LED (***right***) under test.

Figure 8.6 describes the rubber encapsulation (a_5) and detachment process (a_6). A castable 3 mm thick and thermo-curable layer of EcoFlex mold has been used as a stretchable encapsulation layer (a_5) and cured at room temperature overnight. A solvent-free detachment process is used to detach the components and stretchable circuit from the hard carrier (a_6). The detachment process uses the differential interfacial adhesion of the stacked layers to define an interface that can be cleaved. As shown in the right image, the LEDs continue to light up during the detachment process. After detachment, the PI peeling foil is removed using electron cyclotron resonance (ECR) plasma etching (40 SCCM O_2, 10 SCCM CF_4, 100 WRF, 30 minutes at 0.0025 mbar).

8.3.2. Letter-size Stretchable LED arrays

The depicted method is not limited by the technology but by the dimension of the carrier substrate that can be processed using available facilities in the university. Another limiting factor could be the size of the adhesive Cu foil. A letter size stretchable system is presented here. **Figure 8.7** shows images of a LED test arrays

on a letter size hard carrier substrate. Functionality test on the hard carrier is particularly important since this allows finding failure modes and comparing the device performance before and after transferring to the rubber substrate.

Letter-size electronics on hard carrier

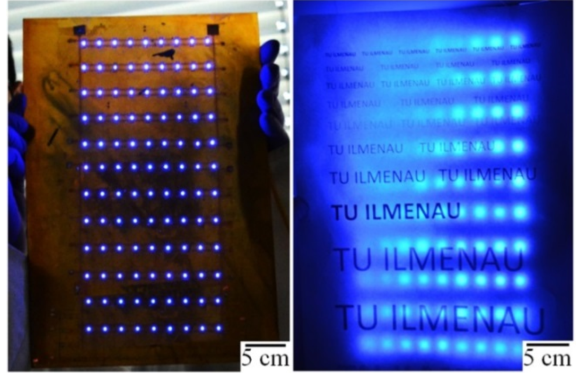

Figure 8.7: Letter size LED arrays on hard carrier. *Device functionality test on the hard carrier before introducing rubber mold.*

There are a few issues that need to be solved and studied further in order to successfully demonstrate the process reliably. For example, current approach using FR4 substrate and coating the sacrificial layers using a ductor blade lead to an inhomogeneous coating of the layers. This is because the available FR4 substrates are not always entirely planer, rather partially bended due to the pre-processing or handling. When the sacrificial layers are coated on this bended surface, the layers become inhomogeneous, which means at some locations the PMMA/PI layers are thick and some other locations the layers are missing or very thin. This generates problems during the detachment process of the device, since the detachment process uses the interfacial delamination in between PMMA and PI layers. Experimentally, it is observed that the detachment process works particularly well in the locations where the sacrificial layers are relatively thick, and faces challenges where sacrificial layers are absent or very thin. At these absent or thin locations of the sacrificial layers, the adhesive Cu foil directly becomes in contact with the carrier substrate and becomes very strongly bonded. The adhesion force between the EcoFlex matrix and the devices (components and metal tracks) is insufficient to remove the strongly bonded Cu tracks from the carrier substrate.

There could be two possible solutions to overcome these issues. The first possibility could be to use a different material such as glass or kapton foil as a carrier substrate. Glass would not bend like FR4 substrate since glass is more rigid. Or, a kapton foil would be flexible enough to overcome the bending issue by the ductor blade. However, these substrates would limit the processing methods. The second possibility could be to laminate different foils as sacrificial layers using adhesive coating where necessary. However, none of these methods were evaluated during this thesis.

Even though the detachment process shows a lower yield than the wafer-scale fabrication process, the method can be used to realize large area stretchable electronics. For example, **Figure 8.8** shows the images of a letter size LED array on a stretchable substrate. The detachment process of this particular sample is assisted by acetone locally where needed. The stretchability test of this device remains for further investigation.

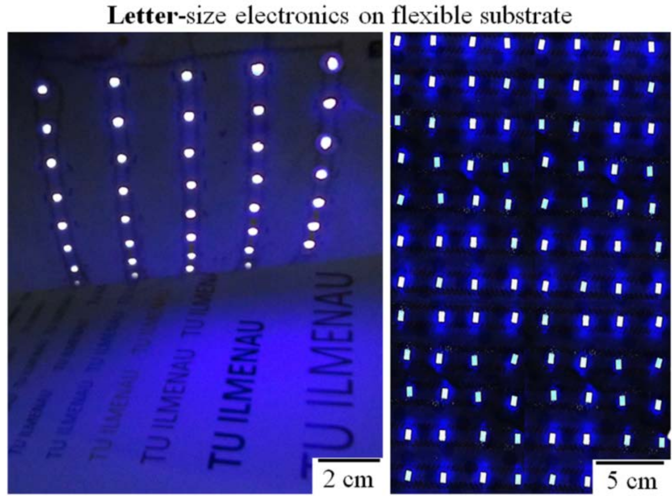

Figure 8.8: Letter size LED arrays on rubber substrate. *Large area LED arrays on rubber substrate under operation.*

CHAPTER 9

Conclusion

9.1. Stretchable to Metamorphic Electronics

9.2. Outcomes of the Thesis

9.2.1. Technology

9.2.2. Design

9.2.3. Functional systems

9.2.4. Metamorphic electronics

9.3. Future Perspectives

9.1. Stretchable to Metamorphic Electronics

Having a pre-defined shape and dimension of current electronic devices will no longer be sufficient for the users in future. The future electronics will be user-friendly; not only by software but also by hardware, *i.e.* the users will shape their electronic devices at will. This is the ultimate vision of metamorphic electronics.

The concept of metamorphic electronics is inspired by natural phenomena but the technology is fundamentally built on stretchable electronics. A successful implementation of metamorphic electronics requires a reliable and highly stretchable electronics technology. Even though the research in stretchable electronics has seen a rapid increase in recent years, the technology is still limited in prototype demonstrations. There are still challenges to commercialize the technology. The main challenge remains related to manufacturing and reliability of the devices and structures. In addition, there are also concerns related to materials, since the technology requires entirely a different materials perspective than the conventional rigid electronics materials.

To commercially manufacture stretchable electronic devices, it is highly important to establish an industry-compatible method to fabricate stretchable electronic systems. In principle, the method should follow similar processing steps like conventional PCB's as this would allow realizing multilayer integrated stretchable printed circuit boards more conveniently than presently reported. In addition to these, the methods should also allow direct use of commercially available pristine SMDs to have access to wide range of available components and devices. This would ease the technology to realize complex and high-performance electronic systems.

Moreover, to enable metamorphic electronics based on stretchable electronics, the devices require to have high stretchability and deformability. Additionally, the deformation mechanisms should be well controlled to achieve desired shapes.

9.2. Outcomes of the Thesis

This thesis aimed to realize a stretchable printed circuit board technology that would replace the rigid carrier of conventional PCB substrate with a stretchable rubber substrate and also would be compatible with industrial manufacturing processes. To fulfill this goal a systematic study was carried out in terms of materials, methods, suitable designs, suitable fabrication and devices. A number of stretchable systems were demonstrated to test and apply the gained knowledge.

Finally, the technology is used to enable the concept of metamorphic electronics which is the electronic device that changes their shape at will.

9.2.1. Technology

Single layer stretchable printed circuit boards

The first step was to develop a method to realize a single layer stretchable printed circuit board that is compatible with common industrial manufacturing practice. The reported and studied approach was different from other reported methods in this field, which apply the metallization to the rubber support and mount the components on top, which also suffer from a lower level of alignment and fixation. Instead, a hard carrier was introduced, which delays the use of the stretchable rubber support to the end of the processing sequence. Like conventional PCB technology, the hard carrier fabrication is important since it enables: alignment and registration, high temperature processing, conventional robotic chip placement or advanced chip placement of microscopic dies using fluidic self-assembly, and “on-hard-carrier” device tests. Moreover, the depicted method enables direct use of commercially available SMDs which is important to easily realize complex electronic devices.

As a substrate, highly stretchable silicone material (EcoFlex) was used which encapsulates the device layer. To transfer the device layer from the hard carrier to the soft elastomeric substrate a single-step, wafer-level detachment process was developed. A solvent-free detachment process was developed, which uses the differential interfacial adhesion in between sacrificial cleaving layers.

Multilayer stretchable printed circuit boards

Most of the electronic systems require more than one metallization layers to interconnect in between the components and to achieve correct functionality. However, most of the demonstrated solutions of stretchable electronic systems at the start of this thesis had limited integration density capabilities due to the use of one interconnection layer between the functional devices. So, it was essential to realize and study methods to enable the fabrication of multilayer printed circuit boards, where different metallization layers are connected through VIAs. Again, a goal was to develop a possible solution which is applicable to industrial scale processing.

This thesis demonstrated and studied a method to realize multilayer stretchable printed circuit boards, where different metallization layers are connected through VIAs. The performance of VIAs with different dimensions and locations has been studied. The VIAs placed beneath a contact pad of a rigid component proof to be more reliable than the VIAs placed at an isolated location in the rubber matrix.

9.2.2. Design

One of the main challenges in the field of stretchable electronics is to design reliable stretchable interconnects. The commonly used designs proofed to be insufficiently reliable for long-term applications or for commercial productions. During this thesis several commonly used meander shape metal tracks have been studied using computer aided simulations. A systematic study of the failure modes of the metal tracks and a deeper understanding of the stress distribution over the metal tracks during stretching has enabled the design of an optimized metal track.

The newly developed meander design is named as "***stress adaptive***" metal track, which varies in width to accommodate produced torque in the metal tracks due to the non-uniform stress distribution over the meander loops during stretching operation. The design rationale of the stress adaptive metal track has been discussed in detail. The stress adaptive design shows a significant improvement in the stress distributions over the metal tracks, and experimentally results a higher level of maximum stretching and higher number of stretch-release cycles comparing with previously reported meander designs.

Additions to the stretchable metal track design, this thesis also introduced a concept of reinforcement bars and 3D reinforcement frames. These structural support structures improved the mechanical reliability. Especially, for large number of components and dense electronic systems the 3D reinforcement frames were relevant long run performance.

9.2.3. Functional Systems

The gained knowledge has been applied to fabricate and demonstrate metamorphic electronic systems. The achievements in this thesis are the several stretchable devices demonstrating electronics, optoelectronics, acoustoelectronics, and sensor arrays using single or multilayer integrated stretchable printed circuit boards.

The first optoelectronic demonstrator contained arrays with packaged SMDs and bare dies integrated LEDs using a single metallization layer within a rubber matrix. The second demonstrator uses lab-fabricated Si μ-transistors with three contact pads. These electronic and optoelectronic demonstrators are rather simple, and use only one type of SMDs as active components. However, the third demonstrator uses different types of SMDs and sensors to realize an integrated stretchable acoustoelectronics system using a single metallization layer. To be specific, the acoustoelectronics system contained bare dies resistors, capacitors and MEMS microphones, in a total of 25 electronic elements and a stretchable network with nearly 100 interconnections to function. The combination of these metrics did go beyond the state of the art in the field of stretchable electronics at the time the results were published.

Subsequently, more complex stretchable metamorphic electronic systems have been demonstrated applying the gained knowledge on how to fabricate two metallization layers with interconnected VIAs. In this fourth demonstrator a fully addressable integrated active matrix is realized using chip scale LEDs and transistors. Each pixel of the matrix can be addressed using a computer through an Arduino board.

Additional demonstrators include stretchable touchpads, wearable electronics and electronics on fabrics. Finally, an attempt has been taken to adapt the wafer-scale process to enable larger scale processing using conventional PCB materials, where preliminary results are achieved.

9.2.4. Metamorphic Electronics

This thesis introduces the pioneering concept of metamorphic electronics. The concept advances the uniformly stretchable electronic systems to gain non-uniform stretchability and to take on new 3D shapes and form factors. Various types of deformation mechanisms have been demonstrated to achieve this, which include inflation and/or deflation of uniform or patterned rubber membranes, 3D guided deformations, and vacuum forming in combination with 3D chaperon. The range of topologies includes hemispherical, spherical, concave/convex, pyramid, tower, bumble bee-eye, and more complex 3D shapes.

The demonstrated metamorphic devices would enable many new types of applications beyond current imaginations. For example, metamorphic LED arrays, which could change its shapes, would enable deformable 3D displays. Additionally, the deformation mechanisms would solve several problems in the field of acoustics. As an example, sound source localization in 3D space has been demonstrated using hemispherical microphone arrays, which proves to be several times better than 2D arrays.

9.3. Future Perspectives

The recent research trends in stretchable electronics clearly indicate that this emerging technology will not be limited to only lab-based prototypes, it will pursue enormous attraction in commercial products as well. Already existing market analysis shows that the stretchable electronics and conformal electronics market will be nearly $1bn within the next ten years [257, 258], and will continue to grow exponentially. Certainly, current global focus and efforts in this field are not sufficient to face the upcoming market challenges and requirements.

Devices which are already demonstrated in stretchable electronics proof that the technology will find many new types of applications and will improve the performance of many existing devices in various manners. Thus, the limitations remain to be technology related. Stretchable electronics continues to be limited when it comes to a large number of interconnects or multilayer designs with highly integrated electronics which cannot be manufactured reliably for long-term performance using the current state-of-the-art.

Additional problems remain materials related. Especially, physical properties of the materials for stretchable substrate and interconnects need to be studied extensively. This is particularly important for largely integrated and highly dense electronic systems. Research related to the thermal, optical and electrical conductivity of these materials during stretching is largely missing.

System-level failures remain one of the main challenges of this technology. For example, the interfacial delamination of the stretchable matrix and the devices leads to failure of the stretchable electronic system. Or, system level reliability is relatively poor for long-term applications or multi-cycle stretch and release operations. Additionally, for highly dense electronic systems the stretchable interconnects in between the components require improvements to accommodate inhomogeneous strain in those regions. This demands more attention to fundamentally understand the failure modes of the system and to seek for permanent solutions.

In the case of the metamorphic electronics, the technology is even more premature since the field is utterly new. This field requires extensive research in terms of technology, materials, designs and methods. Many more deformation mechanisms could be developed which would achieve new and interesting 3D geometrical shapes. However, in the long run this concept of *adaptive shape* of the electronic devices will certainly improve many limitations of existing stretchable electronics and will find many new applications.

In summary, future research will have to focus on the integration of electronic components, increase in the number of possible interconnects and increase in the number of possible metallization layers. Moreover, registration and reliability challenges will have to be addressed as well. However, once fully developed, most electronic system known to mankind could morph to take on new interesting form factors in the future. Many interesting shape adaptive functions could be demonstrated. Imagination is limitless!

References

[1] M. Riordan, *The lost history of the transistor*, IEEE Spectrum, 41, 5, (2004).
[2] S. H. Lavington, *A history of Manchester computers*, NCC Publications, Manchester, (1975).
[3] J. S. Kilby, *Miniature semiconductor integrated circuit*, US3115581, (1963).
[4] M. Caironi, Y. Y. Noh, *Large Area and Flexible Electronics*, Wiley-VCH, Weinheim, (2015).
[5] T. Someya, *Stretchable electronics*, Wiley-VCH, Weinheim, (2013).
[6] J. A. Rogers, T. Someya, Y. Huang, *Materials and Mechanics for Stretchable Electronics*, Science 327, 5973, (2010).
[7] S. Wagner, S. Bauer, *Materials for stretchable electronics*, MRS Bull., 37, 3, (2012).
[8] M. W. Jawitz, *Printed Circuit Board Materials Handbook*, McGraw-Hill, (1997).
[9] D. H. Kim, J. A. Rogers, *Stretchable Electronics: Materials Strategies and Devices*, Adv. Mat. 20, 24, (2008).
[10] S. P. Lacour, S. Wagner, Z. Y. Huang, Z. Suo, *Stretchable gold conductors on elastomeric substrates*, Appl. Phys. Lett., 82, 15, (2003).
[11] N. Bowden, S. Brittain, A. G. Evans, J. W. Hutchinson, G. M. Whitesides, *Spontaneous formation of ordered structures in thin films of metals supported on an elastomeric polymer*, Nature, 393, 6681, (1998).
[12] S. P. Lacour, Z. Huang, Z. Suo, S. Wagner, *Deformable interconnects for conformal integrated circuits*, MRS Proceedings, 736, D4.8, (2002).
[13] S. P. Lacour, J. Jones, Z. Suo, S. Wagner, *Design and performance of thin metal film interconnects for skin-like electronic circuits*, IEEE Electr. Dev. L 25, 4, (2004).
[14] D. S. Gray, J. Tien, C. S. Chen, *High-conductivity elastomeric electronics*, Adv. Mat. 16, 5, (2004).
[15] D. Y. Khang, H. Q. Jiang, Y. Huang, J. A. Rogers, *A stretchable form of single-crystal silicon for high-performance electronics on rubber substrates*, Science, 311, 5758, (2006).
[16] D. H. Kim, J. Z. Song, W. M. Choi, H. S. Kim, R. H. Kim, Z. J. Liu, Y. Y. Huang, K. C. Hwang, Y. W. Zhang, J. A. Rogers, *Materials and noncoplanar mesh designs for integrated circuits with linear elastic responses to extreme mechanical deformations*, Pro. Natl. Acad. Sci. USA, 105, 48, (2008).
[17] T. Q. Trung, N. -E. Lee, *Recent Progress on Stretchable Electronic Devices with Intrinsically Stretchable Components*, Adv. Mat., 29, 3, (2017).
[18] Z. M. Yu, Y. J. Xia, D. H. Du, J. Y. Ouyang, *PEDOT:PSS Films with Metallic Conductivity through a Treatment with Common Organic Solutions of Organic Salts and Their Application as a Transparent Electrode of Polymer Solar Cells*, ACS App. Mat. & Int., 8, 18, (2016).

[19] Y. -Y. Lee, H. -Y. Kang, S. H. Gwon, G. M. Choi, S. -M. Lim, J. -Y. Sun, Y. -C. Joo, *A Strain-Insensitive Stretchable Electronic Conductor: PEDOT:PSS/Acrylamide Organogels*, Adv. Mat., 28, 8, (2016).
[20] D. J. Lipomi, J. A. Lee, M. Vosgueritchian, B. C. K. Tee, J. A. Bolander, Z. Bao, *Electronic Properties of Transparent Conductive Films of PEDOT:PSS on Stretchable Substrates*, Chem. of Mat., 24, 2, (2012).
[21] B. -U. Hwang, J. -H. Lee, T. Q. Trung, E. Roh, D. -I. Kim, S. -W. Kim, N. -E. Lee, *Transparent Stretchable Self-Powered Patchable Sensor Platform with Ultrasensitive Recognition of Human Activities*, ACS Nano, 9, 9, (2015).
[22] F. Xu, Y. Zhu, *Highly Conductive and Stretchable Silver Nanowire Conductors*, Adv. Mat., 24, 37, (2012).
[23] N. Matsuhisa, M. Kaltenbrunner, T. Yokota, H. Jinno, K. Kuribara, T. Sekitani, T. Someya, *Printable elastic conductors with a high conductivity for electronic textile applications*, Nat. Comm., 6, 7461, (2015).
[24] B. W. An, B. G. Hyun, S. -Y. Kim, M. Kim, M. -S. Lee, K. Lee, J. B. Koo, H. Y. Chu, B. -S. Bae, J. -U. Park, *Stretchable and Transparent Electrodes using Hybrid Structures of Graphene–Metal Nanotrough Networks with High Performances and Ultimate Uniformity*, Nano Letters, 14, 11, (2014).
[25] S. Han, S. Hong, J. Ham, J. Yeo, J. Lee, B. Kang, P. Lee, J. Kwon, S. S. Lee, M. -Y. Yang, S. H. Ko, *Fast Plasmonic Laser Nanowelding for a Cu-Nanowire Percolation Network for Flexible Transparent Conductors and Stretchable Electronics*, Adv. Mat., 26, 33, (2014).
[26] T. Sekitani, H. Nakajima, H. Maeda, T. Fukushima, T. Aida, K. Hata, T. Someya, *Stretchable active-matrix organic light-emitting diode display using printable elastic conductors*, Nat. Mat., 8, 6, (2009).
[27] Y. Zhang, C. J. Sheehan, J. Zhai, G. Zou, H. Luo, J. Xiong, Y. T. Zhu, Q. X. Jia, *Polymer-Embedded Carbon Nanotube Ribbons for Stretchable Conductors*, Adv. Mat., 22, 28, (2010).
[28] S. Won, Y. Hwangbo, S. K. Lee, K. S. Kim, K. S. Kim, S. M. Lee, H. J. Lee, J. H. Ahn, J. H. Kim, S. B. Lee, *Double-layer CVD graphene as stretchable transparent electrodes*, Nanoscale, 6, 11, (2014).
[29] H. Ki, J. Jang, Y. Jo, D. -Y. Kim, S. -S. Chee, B. -Y. Oh, C. Song, S. S. Lee, S. Choi, Y. Choi, S. Jeong, M. -H. Ham, *Chemically Driven, Water-Soluble Composites of Carbon Nanotubes and Silver Nanoparticles as Stretchable Conductors*, ACS Macro Letters, 4, 7, (2015).
[30] M. J. Hu, X. B. Cai, Q. Q. Guo, B. Bian, T. Y. Zhang, J. Yang, *Direct Pen Writing of Adhesive Particle-Free Ultrahigh Silver Salt-Loaded Composite Ink for Stretchable Circuits*, ACS Nano, 10, 1, (2016).
[31] Z. Yu, X. Niu, Z. Liu, Q. Pei, *Intrinsically Stretchable Polymer Light-Emitting Devices Using Carbon Nanotube-Polymer Composite Electrodes*, Adv. Mat., 23, 34, (2011).
[32] J. Liang, L. Li, X. Niu, Z. Yu, Q. Pei, *Elastomeric polymer light-emitting devices and displays*, Nat. Photon., 7, 10, (2013).

[33] C. Yan, J. Wang, X. Wang, W. Kang, M. Cui, C. Y. Foo, P. S. Lee, *An Intrinsically Stretchable Nanowire Photodetector with a Fully Embedded Structure*, Adv. Mat., 26, 6, (2014).
[34] D. J. Lipomi, B. C. K. Tee, M. Vosgueritchian, Z. Bao, *Stretchable Organic Solar Cells*, Adv. Mat., 23, 15, (2011).
[35] Y. Huang, M. Zhong, Y. Huang, M. S. Zhu, Z. X. Pei, Z. F. Wang, Q. Xue, X. M. Xie, C. Y. Zhi, *A self-healable and highly stretchable supercapacitor based on a dual crosslinked polyelectrolyte*, Nat. Comm., 6, 10310, (2015).
[36] J. Liang, L. Li, D. Chen, T. Hajagos, Z. Ren, S. -Y. Chou, W. Hu, Q. Pei, *Intrinsically stretchable and transparent thin-film transistors based on printable silver nanowires, carbon nanotubes and an elastomeric dielectric*, Nat. Comm., 6, 7647, (2015).
[37] G. Kettlgruber, M. Kaltenbrunner, C. M. Siket, R. Moser, I. M. Graz, R. Schwodiauer, S. Bauer, *Intrinsically stretchable and rechargeable batteries for self-powered stretchable electronics*, J. Mat. Chem. A, 1, 18, (2013).
[38] J. -H. Lee, K. Y. Lee, M. K. Gupta, T. Y. Kim, D. -Y. Lee, J. Oh, C. Ryu, W. J. Yoo, C. -Y. Kang, S. -J. Yoon, J. -B. Yoo, S. -W. Kim, *Highly Stretchable Piezoelectric-Pyroelectric Hybrid Nanogenerator*, Adv. Mat., 26, 5, (2014).
[39] E. Roh, B. -U. Hwang, D. Kim, B. -Y. Kim, N. -E. Lee, *Stretchable, Transparent, Ultrasensitive, and Patchable Strain Sensor for Human–Machine Interfaces Comprising a Nanohybrid of Carbon Nanotubes and Conductive Elastomers*, ACS Nano, 9, 6, (2015).
[40] T. Q. Trung, S. Ramasundaram, B. -U. Hwang, N. -E. Lee, *An All-Elastomeric Transparent and Stretchable Temperature Sensor for Body-Attachable Wearable Electronics*, Adv. Mat., 28, 3, (2016).
[41] C. Pang, J. H. Koo, A. Nguyen, J. M. Caves, M. -G. Kim, A. Chortos, K. Kim, P. J. Wang, J. B. H. Tok, Z. Bao, *Highly Skin-Conformal Microhairy Sensor for Pulse Signal Amplification*, Adv. Mat., 27, 4, (2015).
[42] C. -L. Choong, M. -B. Shim, B. -S. Lee, S. Jeon, D. -S. Ko, T. -H. Kang, J. Bae, S. H. Lee, K. -E. Byun, J. Im, Y. J. Jeong, C. E. Park, J. -J. Park, U. I. Chung, *Highly Stretchable Resistive Pressure Sensors Using a Conductive Elastomeric Composite on a Micropyramid Array*, Adv. Mat., 26, 21, (2014).
[43] X. Huang, Y. Liu, H. Cheng, W. -J. Shin, J. A. Fan, Z. Liu, C. -J. Lu, G. -W. Kong, K. Chen, D. Patnaik, S. -H. Lee, S. Hage-Ali, Y. Huang, J. A. Rogers, *Materials and Designs for Wireless Epidermal Sensors of Hydration and Strain*, Adv. Func. Mat., 24, 25, (2014).
[44] S. Lim, D. Son, J. Kim, Y. B. Lee, J. -K. Song, S. Choi, D. J. Lee, J. H. Kim, M. Lee, T. Hyeon, D. -H. Kim, *Transparent and Stretchable Interactive Human Machine Interface Based on Patterned Graphene Heterostructures*, Adv. Func. Mat., 25, 3, (2015).
[45] J. Vanfleteren, M. Gonzalez, F. Bossuyt, Y. Y. Hsu, T. Vervust, I. De Wolf, M. Jablonski, *Printed circuit board technology inspired stretchable circuits*, MRS Bull., 37, 3, (2012).

[46] S. -C. Park, S. Biswas, J. Fang, M. Mozafari, T. Stauden, H. O. Jacobs, *Millimeter Thin and Rubber-Like Solid-State Lighting Modules Fabricated Using Roll-to-Roll Fluidic Self-Assembly and Lamination*, Adv. Mat., 27, 24, (2015).
[47] S. Biswas, J. Reiprich, T. Cohrs, T. Stauden, J. Pezoldt, H. O. Jacobs, *Metamorphic hemispherical microphone array for three-dimensional acoustics*, Appl. Phys. Lett., 111, 4, (2017).
[48] J. Lee, J. Wu, M. Shi, J. Yoon, S. -I. Park, M. Li, Z. Liu, Y. Huang, J. A. Rogers, *Stretchable GaAs Photovoltaics with Designs That Enable High Areal Coverage*, Adv. Mat., 23, 8, (2011).
[49] R. -H. Kim, D. -H. Kim, J. Xiao, B. H. Kim, S. -I. Park, B. Panilaitis, R. Ghaffari, J. Yao, M. Li, Z. Liu, V. Malyarchuk, D. G. Kim, A. -P. Le, R. G. Nuzzo, D. L. Kaplan, F. G. Omenetto, Y. Huang, Z. Kang, J. A. Rogers, *Waterproof AlInGaP optoelectronics on stretchable substrates with applications in biomedicine and robotics*, Nat. Mat., 9, 11, (2010).
[50] D. -H. Kim, N. Lu, R. Ma, Y. -S. Kim, R. -H. Kim, S. Wang, J. Wu, S. M. Won, H. Tao, A. Islam, K. J. Yu, T. -i. Kim, R. Chowdhury, M. Ying, L. Xu, M. Li, H. -J. Chung, H. Keum, M. McCormick, P. Liu, Y. -W. Zhang, F. G. Omenetto, Y. Huang, T. Coleman, J. A. Rogers, *Epidermal Electronics*, Science, 333, 6044, (2011).
[51] Y. M. Song, Y. Xie, V. Malyarchuk, J. Xiao, I. Jung, K. -J. Choi, Z. Liu, H. Park, C. Lu, R. -H. Kim, R. Li, K. B. Crozier, Y. Huang, J. A. Rogers, *Digital cameras with designs inspired by the arthropod eye*, Nature, 497, 7447, (2013).
[52] A. M. Gaikwad, A. M. Zamarayeva, J. Rousseau, H. Chu, I. Derin, D. A. Steingart, *Highly Stretchable Alkaline Batteries Based on an Embedded Conductive Fabric*, Adv. Mat., 24, 37, (2012).
[53] S. Xu, Y. H. Zhang, J. Cho, J. Lee, X. Huang, L. Jia, J. A. Fan, Y. W. Su, J. Su, H. G. Zhang, H. Y. Cheng, B. W. Lu, C. J. Yu, C. Chuang, T. I. Kim, T. Song, K. Shigeta, S. Kang, C. Dagdeviren, I. Petrov, P. V. Braun, Y. G. Huang, U. Paik, J. A. Rogers, *Stretchable batteries with self-similar serpentine interconnects and integrated wireless recharging systems*, Nat. Comm., 4, 1543, (2013).
[54] R. C. Webb, A. P. Bonifas, A. Behnaz, Y. Zhang, K. J. Yu, H. Cheng, M. Shi, Z. Bian, Z. Liu, Y. -S. Kim, W. -H. Yeo, J. S. Park, J. Song, Y. Li, Y. Huang, A. M. Gorbach, J. A. Rogers, *Ultrathin conformal devices for precise and continuous thermal characterization of human skin*, Nat. Mat., 12, 10, (2013).
[55] X. Huang, Y. Liu, K. Chen, W. -J. Shin, C. -J. Lu, G. -W. Kong, D. Patnaik, S. -H. Lee, J. F. Cortes, J. A. Rogers, *Stretchable, Wireless Sensors and Functional Substrates for Epidermal Characterization of Sweat*, Small, 10, 15, (2014).
[56] J. Kim, A. Banks, H. Cheng, Z. Xie, S. Xu, K. -I. Jang, J. W. Lee, Z. Liu, P. Gutruf, X. Huang, P. Wei, F. Liu, K. Li, M. Dalal, R. Ghaffari, X. Feng, Y. Huang, S. Gupta, U. Paik, J. A. Rogers, *Epidermal Electronics with Advanced Capabilities in Near-Field Communication*, Small, 11, 8, (2015).
[57] S. I. Park, D. S. Brenner, G. Shin, C. D. Morgan, B. A. Copits, H. U. Chung, M. Y. Pullen, K. N. Noh, S. Davidson, S. J. Oh, J. Yoon, K. -I. Jang, V. K. Samineni, M. Norman, J. G. Grajales-Reyes, S. K. Vogt, S. S. Sundaram, K. M. Wilson, J. S.

Ha, R. Xu, T. Pan, T. -i. Kim, Y. Huang, M. C. Montana, J. P. Golden, M. R. Bruchas, R. W. Gereau Iv, J. A. Rogers, *Soft, stretchable, fully implantable miniaturized optoelectronic systems for wireless optogenetics*, Nat. Biotech., 33, 12, (2015).
[58] S. Biswas, A. Schoeberl, M. Mozafari, J. Pezoldt, T. Stauden, H. O. Jacobs, *Deformable printed circuit boards that enable metamorphic electronics*, NPG Asia Mater., 8, e336, (2016).
[59] S. Biswas, J. Reiprich, T. Cohrs, D. T. Arboleda, A. Schoeberl, M. Mozafari, L. Schlag, T. Stauden, J. Pezoldt, H. O. Jacobs, *3D Metamorphic Stretchable Microphone Arrays*, Adv. Mat. Tech., 2, 10, (2017).
[60] D. H. Kim, J. H. Ahn, W. M. Choi, H. S. Kim, T. H. Kim, J. Z. Song, Y. G. Y. Huang, Z. J. Liu, C. Lu, J. A. Rogers, *Stretchable and foldable silicon integrated circuits*, Science, 320, 5875, (2008).
[61] H. C. Ko, M. P. Stoykovich, J. Z. Song, V. Malyarchuk, W. M. Choi, C. J. Yu, J. B. Geddes, J. L. Xiao, S. D. Wang, Y. G. Huang, J. A. Rogers, *A hemispherical electronic eye camera based on compressible silicon optoelectronics*, Nature, 454, 7205, (2008).
[62] D. H. Kim, Y. S. Kim, J. Wu, Z. J. Liu, J. Z. Song, H. S. Kim, Y. G. Y. Huang, K. C. Hwang, J. A. Rogers, *Ultrathin Silicon Circuits With Strain-isolation Layers and Mesh Layouts for High-Performance Electronics on Fabric, Vinyl, Leather, and Paper*, Adv. Mat., 21, 36, (2009).
[63] S. W. Hwang, H. Tao, D. H. Kim, H. Y. Cheng, J. K. Song, E. Rill, M. A. Brenckle, B. Panilaitis, S. M. Won, Y. S. Kim, Y. M. Song, K. J. Yu, A. Ameen, R. Li, Y. W. Su, M. M. Yang, D. L. Kaplan, M. R. Zakin, M. J. Slepian, Y. G. Huang, F. G. Omenetto, J. A. Rogers, *A Physically Transient Form of Silicon Electronics*, Science, 337, 6102, (2012).
[64] H. Tao, M. A. Brenckle, M. M. Yang, J. D. Zhang, M. K. Liu, S. M. Siebert, R. D. Averitt, M. S. Mannoor, M. C. McAlpine, J. A. Rogers, D. L. Kaplan, F. G. Omenetto, *Silk-Based Conformal, Adhesive, Edible Food Sensors*, Adv. Mat., 24, 8, (2012).
[65] D. H. Kim, R. Ghaffari, N. S. Lu, J. A. Rogers, *Flexible and Stretchable Electronics for Biointegrated Devices*, Ann. Rev. Biomed. Eng., 14, (2012).
[66] W. H. Kang, W. Cao, S. Wagner, B. Morrison, *Stretchable Neural Interfaces* in Stretchable Electronics, Wiley-VCH, pp. 379-399 (2013).
[67] K. S. Topp, B. S. Boyd, *Structure and biomechanics of peripheral nerves: Nerve responses to physical stresses and implications for physical therapist practice*, Phys. Ther., 86, 1, (2006).
[68] S. P. Lacour, S. Benmerah, E. Tarte, J. FitzGerald, J. Serra, S. McMahon, J. Fawcett, O. Graudejus, Z. Yu, B. Morrison, *Flexible and stretchable micro-electrodes for in vitro and in vivo neural interfaces*, Med. Bio. Eng. Com., 48, 10, (2010).
[69] Z. Yu, O. Graudejus, C. Tsay, S. P. Lacour, S. Wagner, B. Morrison, *Monitoring Hippocampus Electrical Activity In Vitro on an Elastically Deformable Microelectrode Array*, J. Neur., 26, 7, (2009).

[70] J. Kitzmiller, D. Beversdorf, D. Hansford, *Fabrication and testing of microelectrodes for small-field cortical surface recordings*, Biomed. Micro., 8, 1, (2006).
[71] K. W. Meacham, R. J. Giuly, L. Guo, S. Hochman, S. P. DeWeerth, *A lithographically-patterned, elastic multi-electrode array for surface stimulation of the spinal cord*, Biomed. Micro., 10, 2, (2008).
[72] D. H. Kim, N. S. Lu, R. Ghaffari, Y. S. Kim, S. P. Lee, L. Z. Xu, J. A. Wu, R. H. Kim, J. Z. Song, Z. J. Liu, J. Viventi, B. de Graff, B. Elolampi, M. Mansour, M. J. Slepian, S. Hwang, J. D. Moss, S. M. Won, Y. G. Huang, B. Litt, J. A. Rogers, *Materials for multifunctional balloon catheters with capabilities in cardiac electrophysiological mapping and ablation therapy*, Nat. Mat., 10, 4, (2011).
[73] I. R. Minev, P. Musienko, A. Hirsch, Q. Barraud, N. Wenger, E. M. Moraud, J. Gandar, M. Capogrosso, T. Milekovic, L. Asboth, R. F. Torres, N. Vachicouras, Q. H. Liu, N. Pavlova, S. Duis, A. Larmagnac, J. Voros, S. Micera, Z. G. Suo, G. Courtine, S. P. Lacour, *Electronic dura mater for long-term multimodal neural interfaces*, Science, 347, 6218, (2015).
[74] D. Khodagholy, J. N. Gelinas, T. Thesen, W. Doyle, O. Devinsky, G. G. Malliaras, G. Buzsaki, *NeuroGrid: recording action potentials from the surface of the brain*, Nat. Neurosci., 18, 2, (2015).
[75] D. Qi, Z. Liu, M. Yu, Y. Liu, Y. Tang, J. Lv, Y. Li, J. Wei, B. Liedberg, Z. Yu, X. Chen, *Highly Stretchable Gold Nanobelts with Sinusoidal Structures for Recording Electrocorticograms*, Adv. Mat., 27, 20, (2015).
[76] S. J. Kim, H. R. Cho, K. W. Cho, S. T. Qiao, J. S. Rhim, M. Soh, T. Kim, M. K. Choi, C. Choi, I. Park, N. S. Hwang, T. Hyeon, S. H. Choi, N. S. Lu, D.H. Kim, *Multifunctional Cell-Culture Platform for Aligned Cell Sheet Monitoring, Transfer Printing, and Therapy*, ACS Nano., 9, 3, (2015).
[77] S. Y. Park, J. Park, S. H. Sim, M. G. Sung, K. S. Kim, B. H. Hong, S. Hong, *Enhanced Differentiation of Human Neural Stem Cells into Neurons on Graphene*, Adv. Mat., 23, 36, (2011).
[78] B. Tian, J. Liu, T. Dvir, L. Jin, J.H. Tsui, Q. Qing, Z. Suo, R. Langer, D. S. Kohane, C. M. Lieber, *Macroporous nanowire nanoelectronic scaffolds for synthetic tissues*, Nat. Mat., 11, 11, (2012).
[79] J. Liu, T. -M. Fu, Z. Cheng, G. Hong, T. Zhou, L. Jin, M. Duvvuri, Z. Jiang, P. Kruskal, C. Xie, Z. Suo, Y. Fang, C. M. Lieber, *Syringe-injectable electronics*, Nat. Nano., 10, 7, (2015).
[80] D. Son, J. Lee, D. J. Lee, R. Ghaffari, S. Yun, S. J. Kim, J. E. Lee, H. R. Cho, S. Yoon, S. Yang, S. Lee, S. Qiao, D. Ling, S. Shin, J. -K. Song, J. Kim, T. Kim, H. Lee, J. Kim, M. Soh, N. Lee, C. S. Hwang, S. Nam, N. Lu, T. Hyeon, S. H. Choi, D. -H. Kim, *Bioresorbable Electronic Stent Integrated with Therapeutic Nanoparticles for Endovascular Diseases*, ACS Nano, 9, 6, (2015).
[81] P. Bingger, M. Zens, P. Woias, *Highly flexible capacitive strain gauge for continuous long-term blood pressure monitoring*, Biomed. Micro., 14, 3, (2012).
[82] M. M. Rodgers, V. M. Pai, R. S. Conroy, *Recent Advances in Wearable Sensors for Health Monitoring*, IEEE Sens. J., 15, 6, (2015).

[83] S. Gong, W. Schwalb, Y. W. Wang, Y. Chen, Y. Tang, J. Si, B. Shirinzadeh, W. L. Cheng, *A wearable and highly sensitive pressure sensor with ultrathin gold nanowires*, Nat. Comm., 5, 3132, (2014).
[84] M. Li, H. Li, W. Zhong, Q. Zhao, D. Wang, *Stretchable Conductive Polypyrrole/Polyurethane (PPy/PU) Strain Sensor with Netlike Microcracks for Human Breath Detection*, ACS App. Mat. & Int., 6, 2, (2014).
[85] R. C. Webb, A. P. Bonifas, A. Behnaz, Y. Zhang, K. J. Yu, H. Cheng, M. Shi, Z. Bian, Z. Liu, Y. -S. Kim, W. -H. Yeo, J. S. Park, J. Song, Y. Li, Y. Huang, A. M. Gorbach, J. A. Rogers, *Ultrathin conformal devices for precise and continuous thermal characterization of human skin*, Nat. Mat., 12, 10, (2013).
[86] S. Harada, K. Kanao, Y. Yamamoto, T. Arie, S. Akita, K. Takei, *Fully Printed Flexible Fingerprint-like Three-Axis Tactile and Slip Force and Temperature Sensors for Artificial Skin*, ACS Nano, 8, 12, (2014).
[87] T. Yamada, Y. Hayamizu, Y. Yamamoto, Y. Yomogida, A. Izadi-Najafabadi, D. N. Futaba, K. Hata, *A stretchable carbon nanotube strain sensor for human-motion detection*, Nat. Nano., 6, 5, (2011).
[88] Y. Wang, L. Wang, T. Yang, X. Li, X. Zang, M. Zhu, K. Wang, D. Wu, H. Zhu, *Wearable and Highly Sensitive Graphene Strain Sensors for Human Motion Monitoring*, Adv. Func. Mat., 24, 29, (2014).
[89] K. Cherenack, L. van Pieterson, *Smart textiles: Challenges and opportunities*, J. Appl. Phys., 112, 9, (2012).
[90] S. D. Guler, M. Gannon, K. Sicchio, *A Brief History of Wearables*, in: S.D. Guler, M. Gannon, K. Sicchio (Eds.), *Crafting Wearables: Blending Technology with Fashion*, Apress, Berkeley, CA, 2016, pp. 3-10, (2016).
[91] W. Zeng, L. Shu, Q. Li, S. Chen, F. Wang, X.-M. Tao, *Fiber-Based Wearable Electronics: A Review of Materials, Fabrication, Devices, and Applications*, Adv. Mat., 26, 31, (2014).
[92] L. M. Castano, A. B. Flatau, *Smart fabric sensors and e-textile technologies: a review*, Smart Mat. Struct., 23, 5, (2014).
[93] M. Hamedi, R. Forchheimer, O. Inganas, *Towards woven logic from organic electronic fibres*, Nat. Mat., 6, 5, (2007).
[94] M. Maccioni, E. Orgiu, P. Cosseddu, S. Locci, A. Bonfiglio, *Towards the textile transistor: Assembly and characterization of an organic field effect transistor with a cylindrical geometry*, Appl. Phys. Lett., 89, 14, (2006).
[95] R. Salvado, C. Loss, R. Goncalves, P. Pinho, *Textile Materials for the Design of Wearable Antennas: A Survey*, Sensors, 12, 11, (2012).
[96] I. Locher, M. Klemm, T. Kirstein, G. Troster, *Design and characterization of purely textile patch antennas*, IEEE T. Adv. Pack., 29, 4, (2006).
[97] L. M. Castano, A. B. Flatau, *Smart Textile Transducers: Design, Techniques, and Applications*, in: M. Hosseini, A.S.H. Makhlouf (Eds.), *Industrial Applications for Intelligent Polymers and Coatings*, Springer, Cham, 2016, pp. 121-146, (2016).
[98] J. A. Rogers, Y. Huang, *A curvy, stretchy future for electronics*, Proc. of the Nat. Aca. of Sci., 106, 27, (2009).

[99] D. Cottet, J. Grzyb, T. Kirstein, G. Troster, *Electrical characterization of textile transmission lines*, IEEE T. Adv. Pack., 26, 2, (2003).
[100] S. Danto, Z. Ruff, Z. Wang, J. D. Joannopoulos, Y. Fink, *Ovonic Memory Switching in Multimaterial Fibers*, Adv. Func. Mat., 21, 6, (2011).
[101] R. Jalili, J. M. Razal, P. C. Innis, G. G. Wallace, *One-Step Wet-Spinning Process of Poly(3,4-ethylenedioxythiophene):Poly(styrenesulfonate) Fibers and the Origin of Higher Electrical Conductivity*, Adv. Func. Mat., 21, 17, (2011).
[102] C. Pang, G. -Y. Lee, T. -i. Kim, S. M. Kim, H. N. Kim, S. -H. Ahn, K. -Y. Suh, *A flexible and highly sensitive strain-gauge sensor using reversible interlocking of nanofibres*, Nat. Mat., 11, 9, (2012).
[103] M. Rothmaier, M. P. Luong, F. Clemens, *Textile pressure sensor made of flexible plastic optical fibers*, Sensors, 8, 7, (2008).
[104] S. Jayaraman, S. Park, *Fabric-based sensor for monitoring vital signs*, US6970731, (2005).
[105] R. Paradiso, G. Loriga, N. Taccini, *A wearable health care system based on knitted integrated sensors*, IEEE Trans. on Info. Tech. in Biomed., 9, 3, (2005).
[106] J. Zhong, Y. Zhang, Q. Zhong, Q. Hu, B. Hu, Z. L. Wang, J. Zhou, *Fiber-Based Generator for Wearable Electronics and Mobile Medication*, ACS Nano, 8, 6, (2014).
[107] S. Lam Po Tang, *Recent developments in flexible wearable electronics for monitoring applications*, Trans. of the Inst. of Meas. and Cont., 29, 3-4, (2007).
[108] W. Zeng, X. -M. Tao, S. Chen, S. Shang, H. L. W. Chan, S. H. Choy, *Highly durable all-fiber nanogenerator for mechanical energy harvesting*, Ene. & Env. Sci., 6, 9, (2013).
[109] M. R. Lee, R. D. Eckert, K. Forberich, G. Dennler, C. J. Brabec, R. A. Gaudiana, *Solar Power Wires Based on Organic Photovoltaic Materials*, Science, 324, 5924, (2009).
[110] L. Hu, M. Pasta, F. La Mantia, L. Cui, S. Jeong, H. D. Deshazer, J. W. Choi, S. M. Han, Y. Cui, *Stretchable, Porous, and Conductive Energy Textiles*, Nano Letters, 10, 2, (2010).
[111] A. Lymberis, R. Paradiso, *Smart fabrics and interactive textile enabling wearable personal applications: R&D state of the art and future challenges*, 30th Ann. Int. Conf. of the IEEE Eng. in Med. and Bio. Soc., Vancouver, BC, Canada, (2008).
[112] W. Weng, P. Chen, S. He, X. Sun, H. Peng, *Smart Electronic Textiles*, Ang. Chem. Int. Ed., 55, 21, (2016).
[113] H. Yousef, M. Boukallel, K. Althoefer, *Tactile sensing for dexterous in-hand manipulation in robotics—A review*, Sen. and Act. A: Physical, 167, 2, (2011).
[114] J. Tegin, J. Wikander, *Tactile sensing in intelligent robotic manipulation – a review*, Ind. Robot: An Int. J., 32, 1, (2005).
[115] N. S. Lu, D. H. Kim, *Flexible and Stretchable Electronics Paving the Way for Soft Robotics*, Soft Robot, 1, 1, (2014).
[116] C. Majidi, *Soft Robotics: A Perspective-Current Trends and Prospects for the Future*, Soft Robot, 1, 1, (2014).

[117] D. Rus, M.T. Tolley, *Design, fabrication and control of soft robots*, Nature, 521, 7553, (2015).
[118] S. Bauer, S. Bauer-Gogonea, I. Graz, M. Kaltenbrunner, C. Keplinger, R. Schwödiauer, *25th Anniversary Article: A Soft Future: From Robots and Sensor Skin to Energy Harvesters*, Adv. Mat., 26, 1, (2014).
[119] S. O'Sullivan, R. Nagle, J. A. McEwen, V. Casey, *Elastomer rubbers as deflection elements in pressure sensors: investigation of properties using a custom designed programmable elastomer test rig*, J Phy. D Appl. Phys., 36, 15, (2003).
[120] C. Pailler-Mattei, S. Bec, H. Zahouani, *In vivo measurements of the elastic mechanical properties of human skin by indentation tests*, Med. Eng. Phys., 30, 5, (2008).
[121] B. C. K. Tee, S. C. B. Mannsfeld, Z. Bao, *Elastomer-Based Pressure and Strain Sensors* in Stretchable Electronics, Wiley-VCH, pp. 325-353, (2013).
[122] D. P. J. Cotton, I. M. Graz, S. P. Lacour, *A Multifunctional Capacitive Sensor for Stretchable Electronic Skins*, IEEE Sens. J., 9, 12, (2009).
[123] A. Kulkarni, H. Kim, J. Choi, T. Kim, *A novel approach to use of elastomer for monitoring of pressure using plastic optical fiber*, Rev. Sci. Inst., 81, 4, (2010).
[124] M. Amjadi, K. -U. Kyung, I. Park, M. Sitti, *Stretchable, Skin-Mountable, and Wearable Strain Sensors and Their Potential Applications: A Review*, Adv. Func. Mat., 26, 11, (2016).
[125] M. Ramuz, B. C. K. Tee, J. B. H. Tok, Z. Bao, *Transparent, Optical, Pressure-Sensitive Artificial Skin for Large-Area Stretchable Electronics*, Adv. Mat., 24, 24, (2012).
[126] S. C. B. Mannsfeld, B. C. K. Tee, R. M. Stoltenberg, C. V. H. H. Chen, S. Barman, B. V. O. Muir, A. N. Sokolov, C. Reese, Z. Bao, *Highly sensitive flexible pressure sensors with microstructured rubber dielectric layers*, Nat. Mat., 9, 10, (2010).
[127] T. Sekitani, Y. Noguchi, K. Hata, T. Fukushima, T. Aida, T. Someya, *A Rubberlike Stretchable Active Matrix Using Elastic Conductors*, Science, 321, 5895, (2008).
[128] C. J. Yu, Z. Y. Wang, H. Y. Yu, H. Q. Jiang, *A stretchable temperature sensor based on elastically buckled thin film devices on elastomeric substrates*, Appl. Phys. Lett., 95, 14, (2009).
[129] M. G. Chung, D. H. Kim, H. M. Lee, T. Kim, J. H. Choi, D. k. Seo, J. -B. Yoo, S. -H. Hong, T. J. Kang, Y. H. Kim, *Highly sensitive NO2 gas sensor based on ozone treated graphene*, Sen. and Act. B: Che., 166, (2012).
[130] J. Yoon, S. Y. Hong, Y. Lim, S. -J. Lee, G. Zi, J. S. Ha, *Design and Fabrication of Novel Stretchable Device Arrays on a Deformable Polymer Substrate with Embedded Liquid-Metal Interconnections*, Adv. Mat., 26, 38, (2014).
[131] X. Liao, Q. Liao, Z. Zhang, X. Yan, Q. Liang, Q. Wang, M. Li, Y. Zhang, *A Highly Stretchable ZnO@Fiber-Based Multifunctional Nanosensor for Strain/Temperature/UV Detection*, Adv. Func. Mat., 26, 18, (2016).
[132] D. Kim, G. Shin, J. Yoon, D. Jang, S.J. Lee, G. Zi, J.S. Ha, *High performance stretchable UV sensor arrays of SnO2 nanowires*, Nanotechnology, 24, 31, (2013).

[133] T. Sekitani, U. Zschieschang, H. Klauk, T. Someya, *Flexible organic transistors and circuits with extreme bending stability*, Nat. Mat., 9, 12, (2010).
[134] G. Shuxiang, T. Fukuda, K. Asaka, *A new type of fish-like underwater microrobot*, IEEE/ASME Tran. on Mec., 8, 1, (2003).
[135] X. Feng, B. D. Yang, Y. Liu, Y. Wang, C. Dagdeviren, Z. Liu, A. Carlson, J. Li, Y. Huang, J. A. Rogers, *Stretchable Ferroelectric Nanoribbons with Wavy Configurations on Elastomeric Substrates*, ACS Nano, 5, 4, (2011).
[136] S. Rosset, H. R. Shea, *Flexible and stretchable electrodes for dielectric elastomer actuators*, Appl. Phy. A, 110, 2, (2013).
[137] P. Mostafalu, A. S. Nezhad, M. Nikkhah, M. Akbari, *Flexible Electronic Devices for Biomedical Applications*, in: D. Zhang, B. Wei (Eds.), Advanced Mechatronics and MEMS Devices II, Springer, Cham, pp. 341-366 (2017).
[138] J. M. Cruz-Hernandez, V. Hayward, *Electro-mechanical transducer suitable for tactile display and article conveyance*, US6693516, (2002).
[139] F. Carpi, G. Frediani, S. Turco, D. De Rossi, *Bioinspired Tunable Lens with Muscle-Like Electroactive Elastomers*, Adv. Func. Mat., 21, 21, (2011).
[140] K. Xie, B. Wei, *Materials and Structures for Stretchable Energy Storage and Conversion Devices*, Adv. Mat., 26, 22, (2014).
[141] D. J. Lipomi, Z. A. Bao, *Stretchable, elastic materials and devices for solar energy conversion*, Ene. & Env. Sci., 4, 9, (2011).
[142] T. Sekitani, T. Someya, *Stretchable, Large-area Organic Electronics*, Adv. Mat., 22, 20, (2010).
[143] S. W. Jin, J. Park, S. Y. Hong, H. Park, Y. R. Jeong, J. Park, S. S. Lee, J.S. Ha, *Stretchable Loudspeaker using Liquid Metal Microchannel*, Sci. Rep.-Uk, 5, (2015).
[144] L. Cai, S. M. Zhang, J. S. Miao, Z. B. Yu, C. Wang, *Fully Printed Stretchable Thin-Film Transistors and Integrated Logic Circuits*, ACS Nano, 10, 12, (2016).
[145] Z. Y. Wang, W. K. Zhang, X. L. Li, L. Z. Gao, *Recent progress in flexible energy storage materials for lithium-ion batteries and electrochemical capacitors: A review*, J. Mat. Res., 31, 12, (2016).
[146] D. -H. Kim, J. Xiao, J. Song, Y. Huang, J. A. Rogers, *Stretchable, Curvilinear Electronics Based on Inorganic Materials*, Adv. Mat., 22, 19, (2010).
[147] K. -Y. Chun, Y. Oh, J. Rho, J. -H. Ahn, Y. -J. Kim, H. R. Choi, S. Baik, *Highly conductive, printable and stretchable composite films of carbon nanotubes and silver*, Nat. Nano., 5, 12, (2010).
[148] J. A. Rogers, R. Ghaffari, D. H. Kim, *Stretchable Bioelectronics for Medical Devices and Systems*, Springer, (2016).
[149] X. W. Yu, B. K. Mahajan, W. Shou, H. Pan, *Materials, Mechanics, and Patterning Techniques for Elastomer-Based Stretchable Conductors*, Micromachines, 8, 1, (2017).
[150] C. Kittel, *Introduciton to Solid State Physics*, 7TH ED, John Wiley & Sons, Inc., (2007).
[151] Z. M. Song, X. Wang, C. Lv, Y. H. An, M. B. Liang, T. Ma, D. He, Y. J. Zheng, S. Q. Huang, H. Y. Yu, H. Q. Jiang, *Kirigami-based stretchable lithium-ion batteries*, Sci. Rep.-Uk, 5, (2015).

[152] Z. M. Song, T. Ma, R. Tang, Q. Cheng, X. Wang, D. Krishnaraju, R. Panat, C. K. Chan, H. Y. Yu, H. Q. Jiang, *Origami lithium-ion batteries*, Nat. Comm., 5, 3140, (2014).
[153] P. Z. Hanakata, Z. Qi, D. K. Campbell, H. S. Park, *Highly stretchable MoS2 kirigami*, Nanoscale, 8, 1, (2016).
[154] W. S. Wong, A. Salleo, *Flexible Electronics: Materials and Applications*, Springer, USA, (2009).
[155] M. Adler, R. Bieringer, T. Schauber, J. Günther, *Materials for Stretchable Electronics Compliant with Printed Circuit Board Fabrication* in Stretchable Electronics, Wiley-VCH, pp. 161-185, (2013).
[156] S. P. Lacour, *Stretchable Thin-Film Electronics* in Stretchable Electronics, Wiley-VCH, pp. 81-109, (2013).
[157] Y. S. Lee, S. M. Yang, D. Y. Park, W. J. Lee, J. Y. Park, S. H. Choa, *Characteristics of Mechanical Behavior and Environmental Reliability of Ultra-Stretchable Ecoflex Substrates*, Nanosci. Nanotech. Let., 9, 8, (2017).
[158] L. Ventrelli, L. Beccai, V. Mattoli, A. Menciassi, P. Dario, *Development of a stretchable skin-like tactile sensor based on polymeric composites*, IEEE Int. Conf. on Robotics and Biomimetics (ROBIO), Guilin, China, pp. 123-128, (2009).
[159] S. Y. Hong, J. Y. Yoon, S. W. Jin, Y. I. Lim, S. J. Lee, G. S. Zi, J. S. Ha, *High-Density, Stretchable, All-Solid-State Microsupercapacitor Arrays*, ACS Nano, 8, 12, (2014).
[160] S. Ryu, P. Lee, J. B. Chou, R. Z. Xu, R. Zhao, A. J. Hart, S. G. Kim, *Extremely Elastic Wearable Carbon Nanotube Fiber Strain Sensor for Monitoring of Human Motion*, ACS Nano, 9, 6, (2015).
[161] X. Huang, H. Cheng, K. Chen, Y. Zhang, Y. Zhang, Y. Liu, C. Zhu, S. c. Ouyang, G. W. Kong, C. Yu, Y. Huang, J.A. Rogers, *Epidermal Impedance Sensing Sheets for Precision Hydration Assessment and Spatial Mapping*, IEEE Tran. on Biomed. Eng., 60, 10, (2013).
[162] L. Cai, L. Song, P. Luan, Q. Zhang, N. Zhang, Q. Gao, D. Zhao, X. Zhang, M. Tu, F. Yang, W. Zhou, Q. Fan, J. Luo, W. Zhou, P. M. Ajayan, S. Xie, *Super-stretchable, Transparent Carbon Nanotube-Based Capacitive Strain Sensors for Human Motion Detection*, Sci. Rep., 3, 3048, (2013).
[163] T. S. Hansen, K. West, O. Hassager, N. B. Larsen, *Highly Stretchable and Conductive Polymer Material Made from Poly(3,4-ethylenedioxythiophene) and Polyurethane Elastomers*, Adv. Func. Mat., 17, 16, (2007).
[164] M. Z. Seyedin, J. M. Razal, P. C. Innis, G. G. Wallace, *Strain-Responsive Polyurethane/PEDOT:PSS Elastomeric Composite Fibers with High Electrical Conductivity*, Adv. Func. Mat., 24, 20, (2014).
[165] H. Weili, N. Xiaofan, L. Lu, Y. Sungryul, Y. Zhibin, P. Qibing, *Intrinsically stretchable transparent electrodes based on silver-nanowire–crosslinked-polyacrylate composites*, Nanotechnology, 23, 34, (2012).
[166] A. Vohra, H. L. Filiatrault, S. D. Amyotte, R. S. Carmichael, N. D. Suhan, C. Siegers, L. Ferrari, G. J. E. Davidson, T. B. Carmichael, *Reinventing Butyl Rubber for Stretchable Electronics*, Adv. Func. Mat., 26, 29, (2016).

[167] Z. Ma, B. Su, S. Gong, Y. Wang, L. W. Yap, G. P. Simon, W. Cheng, *Liquid-Wetting-Solid Strategy To Fabricate Stretchable Sensors for Human-Motion Detection*, ACS Sensors, 1, 3, (2016).
[168] Y. L. Park, B. R. Chen, R. J. Wood, *Design and Fabrication of Soft Artificial Skin Using Embedded Microchannels and Liquid Conductors*, IEEE Sens. J., 12, 8, (2012).
[169] W. Wu, *Inorganic nanomaterials for printed electronics: a review*, Nanoscale, 9, 22, (2017).
[170] J. S. Noh, *Conductive Elastomers for Stretchable Electronics, Sensors and Energy Harvesters*, Polymers, 8, 4, (2016).
[171] M. A. H. Khondoker, D. Sameoto, *Fabrication methods and applications of microstructured gallium based liquid metal alloys*, Smart Mat. Stru., 25, 9, (2016).
[172] P. Lee, J. Ham, J. Lee, S. Hong, S. Han, Y. D. Suh, S. E. Lee, J. Yeo, S. S. Lee, D. Lee, S. H. Ko, *Highly Stretchable or Transparent Conductor Fabrication by a Hierarchical Multiscale Hybrid Nanocomposite*, Adv. Func. Mat., 24, 36, (2014).
[173] Y. G. Sun, V. Kumar, I. Adesida, J. A. Rogers, *Buckled and wavy ribbons of GaAs for high-performance electronics on elastomeric substrates*, Adv. Mat., 18, 21, (2006).
[174] Y. G. Sun, W. M. Choi, H. Q. Jiang, Y. G. Y. Huang, J. A. Rogers, *Controlled buckling of semiconductor nanoribbons for stretchable electronics*, Nat. Nano., 1, 3, (2006).
[175] M. D. Dickey, *Stretchable and Soft Electronics using Liquid Metals*, Adv. Mat., 29, 27, (2017).
[176] A. C. Siegel, D. A. Bruzewicz, D. B. Weibel, G. M. Whitesides, *Microsolidics: Fabrication of three-dimensional metallic microstructures in poly(dimethylsiloxane)*, Adv. Mat., 19, 5, (2007).
[177] M. D. Dickey, R. C. Chiechi, R. J. Larsen, E. A. Weiss, D. A. Weitz, G. M. Whitesides, *Eutectic Gallium-Indium (EGaIn): A Liquid Metal Alloy for the Formation of Stable Structures in Microchannels at Room Temperature*, Adv. Func. Mat., 18, 7, (2008).
[178] M. Kubo, X. F. Li, C. Kim, M. Hashimoto, B. J. Wiley, D. Ham, G. M. Whitesides, *Stretchable Microfluidic Radiofrequency Antennas*, Adv. Mat., 22, 25, (2010).
[179] J. H. So, J. Thelen, A. Qusba, G. J. Hayes, G. Lazzi, M. D. Dickey, *Reversibly Deformable and Mechanically Tunable Fluidic Antennas*, Adv. Func. Mat., 19, 22, (2009).
[180] S. Cheng, Z. G. Wu, *A Microfluidic, Reversibly Stretchable, Large-Area Wireless Strain Sensor*, Adv. Func. Mat., 21, 12, (2011).
[181] N. Lazarus, C. D. Meyer, S. S. Bedair, H. Nochetto, I. M. Kierzewski, *Multilayer liquid metal stretchable inductors*, Smart Mat. Struc., 23, 8, (2014).
[182] A. Hirsch, H. O. Michaud, A. P. Gerratt, S. de Mulatier, S. P. Lacour, *Intrinsically Stretchable Biphasic (Solid-Liquid) Thin Metal Films*, Adv. Mat., 28, 22, (2016).

[183] P. Li, K. Sun, J. Ouyang, *Stretchable and Conductive Polymer Films Prepared by Solution Blending*, ACS Appl. Mat. & Int., 7, 33, (2015).
[184] C. Zhao, C. Wang, Z. Yue, K. Shu, G. G. Wallace, *Intrinsically Stretchable Supercapacitors Composed of Polypyrrole Electrodes and Highly Stretchable Gel Electrolyte*, ACS Appl. Mat. & Int., 5, 18, (2013).
[185] M. Y. Wu, J. Zhao, N. J. Curley, T. H. Chang, Z. Q. Ma, M. S. Arnold, *Biaxially stretchable carbon nanotube transistors*, J. Appl. Phys., 122, 12, (2017).
[186] T. Sekitani, H. Nakajima, H. Maeda, T. Fukushima, T. Aida, K. Hata, T. Someya, *Stretchable active-matrix organic light-emitting diode display using printable elastic conductors*, Nat. Mat., 8, 6, (2009).
[187] C. Yan, S. -K. Lee, H. Jang, J. -H. Ahn, *Graphene for Stretchable Electronics* in Stretchable Electronics, Wiley-VCH, pp. 41-80, (2013).
[188] S. J. Kim, K. Choi, B. Lee, Y. Kim, B.H. Hong, *Materials for Flexible, Stretchable Electronics: Graphene and 2D Materials*, Ann. Rev. Mat. Res., 45, (2015).
[189] K. S. Kim, Y. Zhao, H. Jang, S. Y. Lee, J. M. Kim, K. S. Kim, J. H. Ahn, P. Kim, J. Y. Choi, B. H. Hong, *Large-scale pattern growth of graphene films for stretchable transparent electrodes*, Nature, 457, 7230, (2009).
[190] D. Wang, H. Li, M. Li, H. Jiang, M. Xia, Z. Zhou, *Stretchable conductive polyurethane elastomer in situ polymerized with multi-walled carbon nanotubes*, J. of Mat. Chem. C, 1, 15, (2013).
[191] C. Müller, S. Goffri, D. W. Breiby, J. W. Andreasen, H. D. Chanzy, R. A. J. Janssen, M. M. Nielsen, C. P. Radano, H. Sirringhaus, P. Smith, N. Stingelin-Stutzmann, *Tough, Semiconducting Polyethylene-poly(3-hexylthiophene) Diblock Copolymers*, Adv. Func. Mat., 17, 15, (2007).
[192] R. Peng, B. Pang, D. Q. Hu, M. J. Chen, G. B. Zhang, X. H. Wang, H. B. Lu, K. Cho, L. Z. Qiu, *An ABA triblock copolymer strategy for intrinsically stretchable semiconductors*, J. of Mat. Chem. C, 3, 15, (2015).
[193] M. Shin, J. Y. Oh, K. -E. Byun, Y. -J. Lee, B. Kim, H. -K. Baik, J .-J. Park, U. Jeong, *Polythiophene Nanofibril Bundles Surface-Embedded in Elastomer: A Route to a Highly Stretchable Active Channel Layer*, Adv. Mat., 27, 7, (2015).
[194] E. Song, B. Kang, H. H. Choi, D. H. Sin, H. Lee, W. H. Lee, K. Cho, *Stretchable and Transparent Organic Semiconducting Thin Film with Conjugated Polymer Nanowires Embedded in an Elastomeric Matrix*, Adv. Elec. Mat., 2, 1, (2016).
[195] A. Chortos, J. Lim, J. W. F. To, M. Vosgueritchian, T. J. Dusseault, T. -H. Kim, S. Hwang, Z. Bao, *Highly Stretchable Transistors Using a Microcracked Organic Semiconductor*, Adv. Mat., 26, 25, (2014).
[196] K. Oh, J. Y. Lee, S. -S. Lee, M. Park, D. Kim, H. Kim, *Highly stretchable dielectric nanocomposites based on single-walled carbon nanotube/ionic liquid gels*, Com. Sci. and Tech., 83, (2013).
[197] M. D. Bartlett, A. Fassler, N. Kazem, E. J. Markvicka, P. Mandal, C. Majidi, *Stretchable, High-k Dielectric Elastomers through Liquid-Metal Inclusions*, Adv. Mat., 28, 19, (2016).

[198] D. -H. Kim, N. Lu, J. A. Rogers, *Stretchable Electronic and Optoelectronic Devices Using Single-Crystal Inorganic Semiconductor Materials* in Stretchable Electronics, Wiley-VCH, pp. 235-269, (2012).
[199] A. J. Baca, M. A. Meitl, H. C. Ko, S. Mack, H. S. Kim, J. Dong, P. M. Ferreira, J. A. Rogers, *Printable Single-Crystal Silicon Micro/Nanoscale Ribbons, Platelets and Bars Generated from Bulk Wafers*, Adv. Func. Mat., 17, 16, (2007).
[200] W. M. Choi, J. Song, D. -Y. Khang, H. Jiang, Y. Y. Huang, J. A. Rogers, *Biaxially Stretchable "Wavy" Silicon Nanomembranes*, Nano Letters, 7, 6, (2007).
[201] S. I. Park, Y. J. Xiong, R. H. Kim, P. Elvikis, M. Meitl, D. H. Kim, J. Wu, J. Yoon, C. J. Yu, Z. J. Liu, Y. G. Huang, K. Hwang, P. Ferreira, X. L. Li, K. Choquette, J. A. Rogers, *Printed Assemblies of Inorganic Light-Emitting Diodes for Deformable and Semitransparent Displays*, Science, 325, 5943, (2009).
[202] Y. G. Sun, E. Menard, J. A. Rogers, H. S. Kim, S. Kim, G. Chen, I. Adesida, R. Dettmer, R. Cortez, A. Tewksbury, *Gigahertz operation in flexible transistors on plastic substrates*, Appl. Phys. Lett., 88, 18, (2006).
[203] J. -H. Ahn, H. -S. Kim, K. J. Lee, S. Jeon, S. J. Kang, Y. Sun, R. G. Nuzzo, J. A. Rogers, *Heterogeneous Three-Dimensional Electronics by Use of Printed Semiconductor Nanomaterials*, Science, 314, 5806, (2006).
[204] K. J. Lee, M. A. Meitl, J. H. Ahn, J. A. Rogers, R. G. Nuzzo, V. Kumar, I. Adesida, *Bendable GaN high electron mobility transistors on plastic substrates*, J. Appl. Phys., 100, 12, (2006).
[205] Y. Sun, D. Y. Khang, F. Hua, K. Hurley, R. G. Nuzzo, J. A. Rogers, *Photolithographic Route to the Fabrication of Micro/Nanowires of III–V Semiconductors*, Adv. Func. Mat., 15, 1, (2005).
[206] T. -H. Kim, W. M. Choi, D. -H. Kim, M. A. Meitl, E. Menard, H. Jiang, J. A. Carlisle, J. A. Rogers, *Printable, Flexible, and Stretchable Forms of Ultrananocrystalline Diamond with Applications in Thermal Management*, Adv. Mat., 20, 11, (2008).
[207] D. -Y. Khang, J. Xiao, C. Kocabas, S. MacLaren, T. Banks, H. Jiang, Y. Y. Huang, J. A. Rogers, *Molecular Scale Buckling Mechanics in Individual Aligned Single-Wall Carbon Nanotubes on Elastomeric Substrates*, Nano Letters, 8, 1, (2008).
[208] M. J. Schultz, X. Zhang, S. Unarunotai, D. -Y. Khang, Q. Cao, C. Wang, C. Lei, S. MacLaren, J. A. N. T. Soares, I. Petrov, J. S. Moore, J. A. Rogers, *Synthesis of linked carbon monolayers: Films, balloons, tubes, and pleated sheets*, Proc. of the Nat. Aca. of Sci., 105, 21, (2008).
[209] S. Xu, Y. H. Zhang, L. Jia, K. E. Mathewson, K. I. Jang, J. Kim, H. R. Fu, X. Huang, P. Chava, R. H. Wang, S. Bhole, L. Z. Wang, Y. J. Na, Y. Guan, M. Flavin, Z. S. Han, Y. G. Huang, J. A. Rogers, *Soft Microfluidic Assemblies of Sensors, Circuits, and Radios for the Skin*, Science, 344, 6179, (2014).
[210] F. Bossuyt, T. Vervust, J. Vanfleteren, *Stretchable Electronics Technology for Large Area Applications: Fabrication and Mechanical Characterization*, IEEE T. Comp. Pack. Man., 3, 2, (2013).

[211] J. Kim, G. A. Salvatore, H. Araki, A. M. Chiarelli, Z. Xie, A. Banks, X. Sheng, Y. Liu, J. W. Lee, K. -I. Jang, S. Y. Heo, K. Cho, H. Luo, B. Zimmerman, J. Kim, L. Yan, X. Feng, S. Xu, M. Fabiani, G. Gratton, Y. Huang, U. Paik, J. A. Rogers, *Battery-free, stretchable optoelectronic systems for wireless optical characterization of the skin*, Sci. Adv., 2, 8, (2016).
[212] X. Wang, H. Hu, Y. Shen, X. Zhou, Z. Zheng, *Stretchable Conductors with Ultrahigh Tensile Strain and Stable Metallic Conductance Enabled by Prestrained Polyelectrolyte Nanoplatforms*, Adv. Mat., 23, 27, (2011).
[213] X. Liu, X. Zhou, Y. Li, Z. Zheng, *Surface-Grafted Polymer-Assisted Electroless Deposition of Metals for Flexible and Stretchable Electronics*, Chem. – An Asi. J., 7, 5 (2012).
[214] Y. N. Xia, G. M. Whitesides, *Soft lithography*, Ang. Chem. Int. Edit., 37, 5, (1998).
[215] S. Cheng, A. Rydberg, K. Hjort, Z. G. Wu, *Liquid metal stretchable unbalanced loop antenna*, Appl. Phys. Lett., 94, 14, (2009).
[216] S. H. Jeong, A. Hagman, K. Hjort, M. Jobs, J. Sundqvist, Z. G. Wu, *Liquid alloy printing of microfluidic stretchable electronics*, Lab. Chip, 12, 22, (2012).
[217] J. X. Wang, C. Y. Yan, K. J. Chee, P. S. Lee, *Highly Stretchable and Self-Deformable Alternating Current Electroluminescent Devices*, Adv. Mat., 27, 18, (2015).
[218] C. S. Boland, U. Khan, C. Backes, A. O'Neill, J. McCauley, S. Duane, R. Shanker, Y. Liu, I. Jurewicz, A. B. Dalton, J. N. Coleman, *Sensitive, High-Strain, High-Rate Bodily Motion Sensors Based on Graphene-Rubber Composites*, ACS Nano, 8, 9, (2014).
[219] J. W. Jeong, M. K. Kim, H. Y. Cheng, W. H. Yeo, X. Huang, Y. H. Liu, Y. H. Zhang, Y. G. Huang, J. A. Rogers, *Capacitive Epidermal Electronics for Electrically Safe, Long-Term Electrophysiological Measurements*, Adv. Healthc. Mat., 3, 5, (2014).
[220] A. Carlson, A. M. Bowen, Y. G. Huang, R. G. Nuzzo, J. A. Rogers, *Transfer Printing Techniques for Materials Assembly and Micro/Nanodevice Fabrication*, Adv. Mat., 24, 39, (2012).
[221] J. Zaumseil, M. A. Meitl, J. W. P. Hsu, B. R. Acharya, K. W. Baldwin, Y. L. Loo, J. A. Rogers, *Three-dimensional and multilayer nanostructures formed by nanotransfer printing*, Nano Letters, 3, 9, (2003).
[222] W. R. Childs, R. G. Nuzzo, *Decal transfer microlithography: A new soft-lithographic patterning method*, J. Am. Chem. Soc., 124, 45, (2002).
[223] W. R. Childs, M. J. Motala, K. J. Lee, R. G. Nuzzo, *Masterless Soft Lithography: Patterning UV/Ozone−Induced Adhesion on Poly(dimethylsiloxane) Surfaces*, Langmuir, 21, 22, (2005).
[224] J. K. Kim, J. W. Park, H. Yang, M. Choi, J. H. Choi, K. Y. Suh, *Low-pressure detachment nanolithography*, Nanotechnology, 17, 4, (2006).
[225] Z. Wang, J. Zhang, R. Xing, J. F. Yuan, D. H. Yan, Y. C. Han, *Micropatterning of organic semiconductor microcrystalline materials and OFET fabrication by "hot lift off"*, J. Am. Chem. Soc., 125, 50, (2003).

[226] K. J. Lee, M. J. Motala, M. A. Meitl, W. R. Childs, E. Menard, A. K. Shim, J. A. Rogers, R. G. Nuzzo, *Large-area, selective transfer of microstructured silicon: A printing-based approach to high-performance thin-film transistors supported on flexible substrates*, Adv. Mat., 17, 19, (2005).
[227] S. Biswas, M. Mozafari, T. Stauden, H. O. Jacobs, *Surface Tension Directed Fluidic Self-Assembly of Semiconductor Chips across Length Scales and Material Boundaries*, Micromachines, 7, 4, (2016).
[228] S. C. Park, J. Fang, S. Biswas, M. Mozafari, T. Stauden, H. O. Jacobs, *A First Implementation of an Automated Reel-to-Reel Fluidic Self-Assembly Machine*, Adv. Mat., 26, 34, (2014).
[229] S. C. Park, J. Fang, S. Biswas, M. Mozafari, T. Stauden, H. O. Jacobs, *Approaching Roll-to-Roll Fluidic Self-Assembly: Relevant Parameters, Machine Design, and Applications*, J. Micro. S., 24, 6, (2015).
[230] M. A. Skylar-Scott, S. Gunasekaran, J. A. Lewis, *Laser-assisted direct ink writing of planar and 3D metal architectures*, P. Nat. Aca. Sci. USA, 113, 22, (2016).
[231] M. Vatani, Y. F. Lu, K. S. Lee, H. C. Kim, J. W. Choi, *Direct-Write Stretchable Sensors Using Single-Walled Carbon Nanotube/Polymer Matrix*, J. Elec. Pack., 135, 1, (2013).
[232] E. Tekin, P. J. Smith, U. S. Schubert, *Inkjet printing as a deposition and patterning tool for polymers and inorganic particles*, Soft Matter, 4, 4, (2008).
[233] M. Singh, H. M. Haverinen, P. Dhagat, G. E. Jabbour, *Inkjet Printing-Process and Its Applications*, Adv. Mat., 22, 6, (2010).
[234] H. Sirringhaus, T. Kawase, R. H. Friend, T. Shimoda, M. Inbasekaran, W. Wu, E. P. Woo, *High-resolution inkjet printing of all-polymer transistor circuits*, Science, 290, 5499, (2000).
[235] J. T. Muth, D. M. Vogt, R. L. Truby, Y. Menguc, D. B. Kolesky, R. J. Wood, J. A. Lewis, *Embedded 3D Printing of Strain Sensors within Highly Stretchable Elastomers*, Adv. Mat., 26, 36, (2014).
[236] S. J. Leigh, R. J. Bradley, C. P. Purssell, D. R. Billson, D. A. Hutchins, *A Simple, Low-Cost Conductive Composite Material for 3D Printing of Electronic Sensors*, Plos. One., 7, 11, (2012).
[237] R. K. Kramer, C. Majidi, R. J. Wood, *Masked Deposition of Gallium-Indium Alloys for Liquid-Embedded Elastomer Conductors*, Adv. Func. Mat., 23, 42, (2013).
[238] A. J. Bandodkar, R. Nunez-Flores, W. Z. Jia, J. Wang, *All-Printed Stretchable Electrochemical Devices*, Adv. Mat., 27, 19, (2015).
[239] D. Brosteaux, F. Axisa, M. Gonzalez, J. Vanfleteren, *Design and fabrication of elastic interconnections for stretchable electronic circuits*, IEEE Electr. Device. L., 28, 7, (2007).
[240] M. Gonzalez, F. Axisa, M. V. BuIcke, D. Brosteaux, B. Vandevelde, J. Vanfleteren, *Design of metal interconnects for stretchable electronic circuits*, Micro. Rel., 48, 6, (2008).

[241] M. Gonzalez, Y. -Y. Hsu, J. Vanfleteren, *Modeling of Printed Circuit Board Inspired Stretchable Electronic Systems* in Stretchable Electronics, Wiley-VCH, pp. 141-159, (2013).
[242] http://www.matweb.com. (accessed 31.10.2017).
[243] Solvent-free, wafer scale transfer process: *https://www.youtube.com/watch?v=wp-jzKErFYg*.
[244] Inflation of a hemisphere: *https://www.youtube.com/watch?v=w15XHG2SqoU.*
[245] Inflation of a sphere: *https://www.youtube.com/watch?v=kskWzuvVPp8*.
[246] B. Rafaely, *The spherical-shell microphone array*, IEEE T. Audio Speech, 16, 4, (2008).
[247] M. Park, B. Rafaely, *Sound-field analysis by plane-wave decomposition using spherical microphone array*, J. Aco. Soc. Am., 118, 5, (2005).
[248] M. A. Poletti, *Three-dimensional surround sound systems based on spherical harmonics*, J. Audio Eng. Soc., 53, 11, (2005).
[249] B. Rafaely, *Analysis and design of spherical microphone arrays*, IEEE T. Speech Audi P., 13, 1, (2005).
[250] Z. Y. Li, R. Duraiswami, *Flexible and optimal design of spherical microphone arrays for beamforming*, IEEE T. Audio Speech, 15, 2, (2007).
[251] http://www.mouser.com. (accessed 15.10.2017).
[252] J. Huang, N. Ohnishi, N. Sugie, *Spatial localization of sound sources: azimuth and elevation estimation*, IEEE Instrum. Meas. Technol. Conf., IEEE, St. Paul, MN, USA, (1998).
[253] B. Y. Lim, J. Yoon, J. Yun, D. Kim, S. Y. Hong, S. J. Lee, G. Zi, J. S. Ha, *Biaxially Stretchable, Integrated Array of High Performance Microsupercapacitors*, ACS Nano, 8, 11, (2014).
[254] L. A. Guo, S. P. DeWeerth, *High-Density Stretchable Electronics: Toward an Integrated Multilayer Composite*, Adv. Mat., 22, 36, (2010).
[255] http://www.microchip.com, (accessed 11.11.2017).
[256] http://www.hdmicrosystems.com, (accessed 10.11.2017).
[257] https://www.idtechex.com, (accessed 24.11.2017).
[258] https://www.marketsandmarkets.com, (accessed 25.11.2017).